Report of Investigations 2015-5

TSUNAMI INUNDATION MAPS OF FOX ISLANDS COMMUNITIES, INCLUDING DUTCH HARBOR AND AKUTAN, ALASKA

D.J. Nicolsky, E.N. Suleimani, J.T. Freymueller, and R.D. Koehler

Published by

STATE OF ALASKA
DEPARTMENT OF NATURAL RESOURCES

DIVISION OF GEOLOGICAL & GEOPHYSICAL SURVEYS

2015

TSUNAMI INUNDATION MAPS OF FOX ISLANDS COMMUNITIES INCLUDING DUTCH HARBOR AND AKUTAN, ALASKA

D.J. Nicolsky, E.N. Suleimani, J.T. Freymueller, and R.D. Koehler

Report of Investigations 2015-5

State of Alaska
Department of Natural Resources
Division of Geological & Geophysical Surveys

STATE OF ALASKA
Bill Walker, *Governor*

DEPARTMENT OF NATURAL RESOURCES
Mark D. Myers, Ph.D., *Commissioner*

DIVISION OF GEOLOGICAL & GEOPHYSICAL SURVEYS
Steve Masterman, *State Geologist and Director*

Publications produced by the Division of Geological & Geophysical Surveys (DGGS) are available for free download from the DGGS website (www.dggs.alaska.gov). Publications on hard-copy or digital media can be examined or purchased in the Fairbanks office:

Alaska Division of Geological & Geophysical Surveys
3354 College Rd., Fairbanks, Alaska 99709-3707
Phone: (907) 451-5010 Fax (907) 451-5050
dggspubs@alaska.gov
www.dggs.alaska.gov

Alaska State Library
State Office Building, 8th Floor
333 Willoughby Avenue
Juneau, Alaska 99811-0571

Alaska Resource Library & Information Services (ARLIS)
3150 C Street, Suite 100
Anchorage, Alaska 99503-3982

Elmer E. Rasmuson Library
University of Alaska Fairbanks
Fairbanks, Alaska 99775-1005

University of Alaska Anchorage Library
3211 Providence Drive
Anchorage, Alaska 99508-4614

CONTENTS

FIGURES

TABLES

APPENDICES

APPENDICES TABLES

SHEETS

TSUNAMI INUNDATION MAPS OF FOX ISLANDS COMMUNITIES INCLUDING DUTCH HARBOR AND AKUTAN, ALASKA

D.J. Nicolsky[1], E.N. Suleimani[1], J.T. Freymueller[1], and R.D. Koehler[2]

Abstract

Potential tsunami hazards for the Fox Islands communities of Unalaska/Dutch Harbor and Akutan were evaluated by numerically modeling the extent of inundation from tsunami waves generated by hypothetical earthquake sources and taking into account historical observations. Worst-case hypothetical scenarios are defined by analyzing results of a sensitivity study of the tsunami dynamics related to various slip distributions along the Aleutian megathrust. The worst-case scenarios for Unalaska and Akutan are thought to be thrust earthquakes in the Fox Islands region with magnitudes ranging from M_W 8.8 to M_W 9.1 that have their greatest slip at 30–40 km (18–25 mi) depth. We also consider Tohoku-type ruptures and an outer-rise rupture in the area of the Fox Islands. Results presented here are intended to provide guidance to local emergency management agencies in tsunami inundation assessment, evacuation planning, and public education to mitigate future tsunami hazards.

INTRODUCTION

Subduction of the Pacific plate under the North American plate has resulted in numerous great earthquakes and has the highest potential to generate tsunamis in Alaska (Dunbar and Weaver, 2008). The Aleutian megathrust (fig. 1), the fault formed by the Pacific–North American plate interface, is the most seismically active tsunamigenic fault zone in the U.S. The latest sequence of great earthquakes along the Aleutian megathrust began in 1938 with a M_W 8.3 earthquake west of Kodiak Island (Estabrook and others, 1994; fig. 2, Davis and others, 1981). Four subsequent events, the 1946 M_W 8.6 Aleutian (Lopez and Okal, 2006), the 1957 M_W 8.6 Andreanof Island (Johnson and Satake, 1993), the 1964 M_W 9.2 Alaska (Kanamori, 1970), and the 1965 M_W 8.7

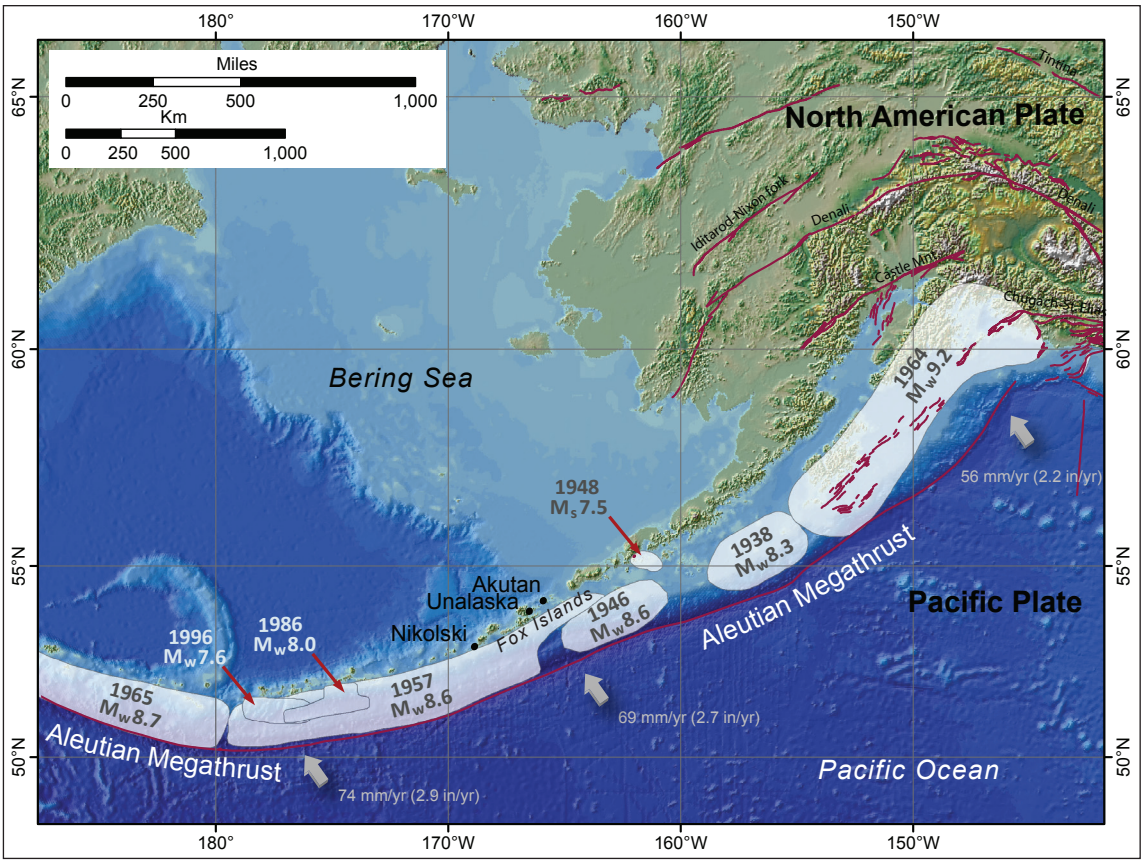

Figure 1. Map of south-central Alaska and the Alaska Peninsula, identifying major active or potentially active faults (dark purple lines) and the rupture zones of the 1938, 1946, 1948, 1957, 1964, and 1965 earthquakes (light shaded areas).

[1]Alaska Earthquake Center, Geophysical Institute, University of Alaska, P.O. Box 757320, Fairbanks, AK 99775-7320; djnicolsky@alaska.edu
[2]Alaska Division of Geological & Geophysical Surveys, 3354 College Rd., Fairbanks, AK 99709-3707; now at Nevada Bureau of Mines and Geology, Mackay School of Earth Science and Engineering, University of Nevada, Reno, 1664 North Virginia Street, MS 178, Reno, NV 89557

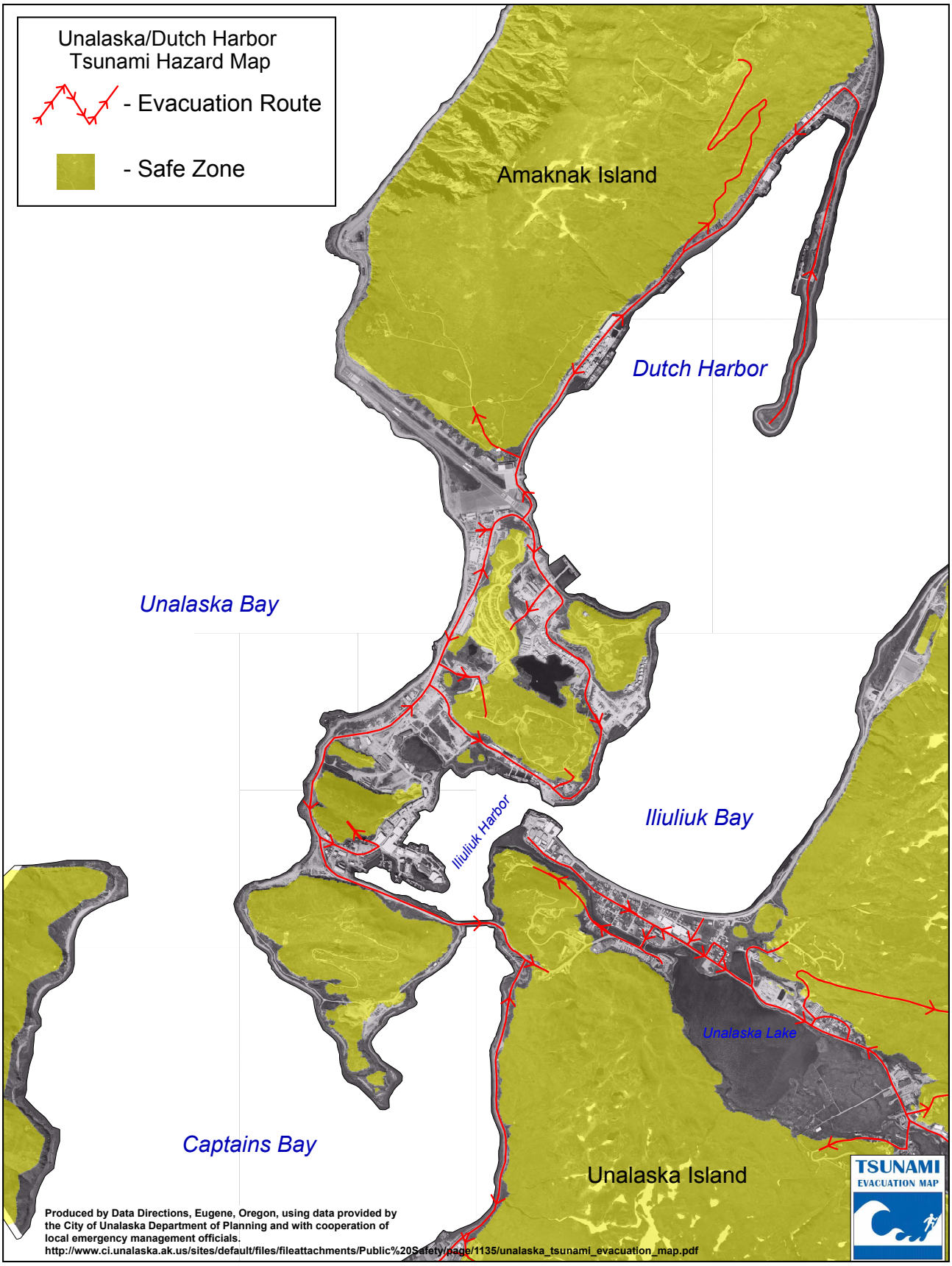

Figure 2. A. Tsunami hazard map for Unalaska, produced by Data Directions, Eugene, Oregon, using data provided by the City of Unalaska Department of Planning and with cooperation of local emergency management officials. The map is intended for emergency response reference purposes only and should not be used for site-specific planning. The Unalaska/Dutch Harbor Tsunami Safe Zone is defined as areas above 15.25 m (50 ft) in elevation (Department of Public Safety, Unalaska, http://www.ci.unalaska.ak.us/publicsafety/page/emergency-preparedness).

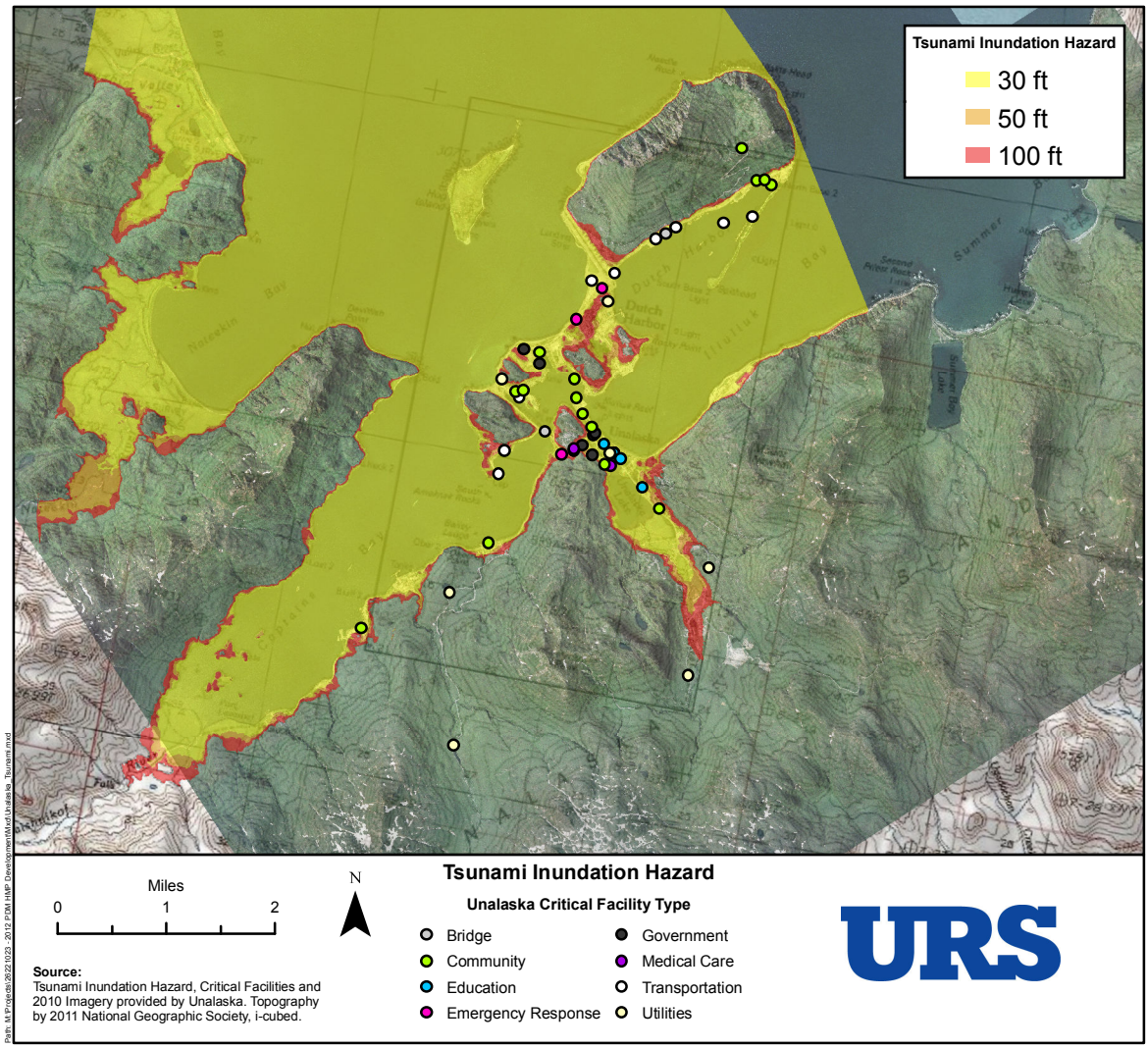

Figure 2. B. Tsunami-hazard inundation map for Unalaska, developed by United Research Services (URS) in Simmons and Nelsen (2013).

Rat Island (Wu and Kanamori, 1973) earthquakes, ruptured almost the entire length of the megathrust (fig. 2, Davis and others, 1981). Tsunamis generated by these great earthquakes reached Alaska coastal communities within minutes after the earthquakes and resulted in widespread damage and loss of life (National Centers for Environmental Information/World Data Service [NCEI/WDS]). Saving lives and property depends on community preparedness, which further depends on estimating potential flooding of the coastal zone in the event of a local or distant tsunami.

On March 9, 1957, the central Aleutian Islands were struck by a M_W 8.6 megathrust earthquake, which initiated near the Andreanof Islands and ruptured from Amchitka Pass to Unimak Island. This earthquake generated a destructive tsunami in Alaska (Lander, 1996). The tsunami also impacted Hawai'i and caused minor damage in San Diego Bay, California, before traveling to such distant countries as Chile, El Salvador, Japan, French Polynesia, and other areas of the Pacific (NCEI/WDS). Despite the fact that a major tsunami impacted the Pacific side of the Fox Islands (Witter and others, 2013), the impact of this tsunami to Dutch Harbor was rather small. The maximum wave height at Dutch Harbor was 0.68 m (2.23 ft) (Lander, 1996) and the extent of runup in Akutan remains unknown. In addition to the major tectonic tsunami generated by ocean-floor displacement between the trench and coastline, the previously dormant Mount Vsevidof (on Umnak Island) erupted (Lander, 1996). We emphasize that an erupting volcano in the area of potential inundation can hinder post-tsunami relief efforts and should be considered in future multi-hazard scenarios. However, hazards associated with volcanic eruptions are beyond the scope of this study.

The city of Unalaska and the village of Akutan did not experience significant waves during previous historic tsunami events. However, the potential occurrence of damaging tsunamis at both locations must be evaluated to develop inundation and tsunami evacuation maps, as future earthquakes in the area could have different patterns of energy release and different effects. Recently the Data Directions Consulting Group (DDCG) defined the Tsunami Safe Zone as the area above 15 m (50 ft) elevation (Department of Public Safety, Unalaska, Tsunami Inundation Zones and Evacuation

Routes, http://www.ci.unalaska.ak.us/publicsafety/page/emergency-preparedness). The Tsunami Safe Zone and evacuation routes developed by DDCG for Unalaska including the port of Dutch Harbor are shown in figure 2a. We note that selection of a particular elevation, such as 15 m (50 ft) above sea level, only has merit if basic considerations of the tsunami hazard in the area of concern have been evaluated and accounted for in the analysis. A tsunami impact assessment for Unalaska by Wei (2008) considered a variety of local and distant sources and found that the Tsunami Safe Zone determined previously for Unalaska was a conservative estimate. A recent Hazard Mitigation Plan by Simmons and Nelsen (2013) suggests that the Tsunami Hazard Zone extends up to 33 m (100 ft) elevation (fig. 2b). In this work we provide an independent analysis of the tsunami hazard in Unalaska and Akutan and evaluate the existing tsunami inundation maps.

Our development of the tsunami inundation map for a community consists of several stages. First we develop hypothetical tsunami scenarios on the basis of credible potential tsunamigenic earthquakes and submarine landslides. Then we perform model simulations for each of these scenarios and compare the results with historical tsunami observations, if available. Finally we develop a "worst case" inundation line that encompasses the maximum extent of flooding based on model simulation of all credible source scenarios and historical observations. The worst case inundation line becomes a basis for local tsunami hazard planning and development of evacuation maps.

The Unalaska and Akutan tsunami inundation maps described in this report are the products of collaborative efforts between state and federal agencies[3] to produce inundation maps for many of Alaska's coastal communities. In this report we generally provide both metric and imperial units of measure. If it is necessary to quote existing data we state the data in the original units of measure and also in the other system. Recall that one foot (1 ft) is approximately 0.305 meters (0.305 m), and one mile (1 mi) is approximately 1.609 kilometers (1.609 km).

This report is intended for use by scientists, engineers, and planners interested in applying modeling based on historic events to develop tsunami inundation and evacuation maps. Digital data and documentation provided with the report enable technical users to explore the range of tsunami inundation expected for future events.

PROJECT BACKGROUND: REGIONAL AND HISTORICAL CONTEXT

SETTING

The city of Unalaska is located at 53°53′ N, 166°32′ W, or about 1,290 km (800 mi) west of Anchorage, and 3,140 km (1,950 mi) northwest of Seattle (figs. 1 and 3). The 2010 U.S. Census recorded the city population as 4,376. Settlements on Unalaska and Amaknak islands have a history dating back thousands of years (McCartney, 1984). In the early 18th century, at the time of Russian contact, Knecht and Davis (2005) estimate as many as six permanent and several seasonal village settlements in Unalaska Bay, including several on Amaknak Island. Later, in the 1750s, Russian explorers began trading fur with local villages and established a permanent trading post in Unalaska in 1778. The United States acquired Alaska in 1867 and declared Unalaska to be its territory. During World War II various federal agencies fortified the island, established an operating naval base, and greatly expanded the pre-existing infrastructure. In the 1950s the city of Unalaska and its neighboring port of Dutch Harbor became a major commercial fishing center. For many years Dutch Harbor was ranked the largest U.S. fishing port by volume and dollar value of seafood catch; it remains a critical element of Alaska's economy. Every summer Dutch Harbor is the terminus port for the Alaska Marine Highway System and is an important resupply port for many marine vessels traveling in the northern Pacific Ocean.

The Native Village of Akutan, on Akutan Island (figs. 1 and 3; 54°08′ N, 165°46′ W), is a coastal Unangan village with a year-round population of 75 and is a federally recognized tribe under the Alaska Native Claims Settlement Act (Alaska Division of Community and Regional Affairs [DCRA], 2015). The village of Akutan was established as a trading port and local storage facility for the trading company based on Unalaska Island. Although Akutan has no major roads or airports, the Trident Seafoods plant occupies significant acreage next to the village. During the active fish-processing season the population in Akutan and Trident Seafoods can multiply by several times and reach more than 1,000 people. Boats are the primary means of local transportation in the area; the Alaska Marine Highway provides regular service to and from Dutch Harbor and False Pass. As in Dutch Harbor, much of the economic activity and infrastructure is on or near the coast and harbors, both potential inundation areas. Recently a new airport for Akutan was built on nearby Akun Island, east of Akutan (shown in fig. 3) and a new boat harbor is being constructed near the village.

SEISMIC AND TSUNAMI HISTORY

Unalaska and Akutan islands are part of the arcuate chain of Aleutian Islands near the area where the Pacific and North American plates converge and form the Alaska–Aleutian Subduction Zone (AASZ). The rate of plate convergence near Unalaska and Akutan Islands is approximately 66–69 mm (2.6–2.7 in) per year (DeMets and others, 1990; Page and others, 1991; Argus and others, 2010) and this segment of the megathrust has produced some of the great earthquakes in the world, such as the M_W 8.6 Andreanof Island Earthquake of 1957. The aftershock area of this event stretches 360 km (223 mi) west and 850 km (528 mi) east of the epicenter

[3]To help mitigate the hazard that earthquakes and tsunamis pose to Alaska coastal communities, the Alaska Tsunami Mapping Team (ATMT) was created. It consists of personnel from the Geophysical Institute at the University of Alaska Fairbanks and from the State of Alaska Division of Geological & Geophysical Surveys. The ATMT participates in the National Tsunami Hazard Mitigation Program by evaluating and mapping potential inundation of selected parts of the Alaska coastline using numerical tsunami modeling.

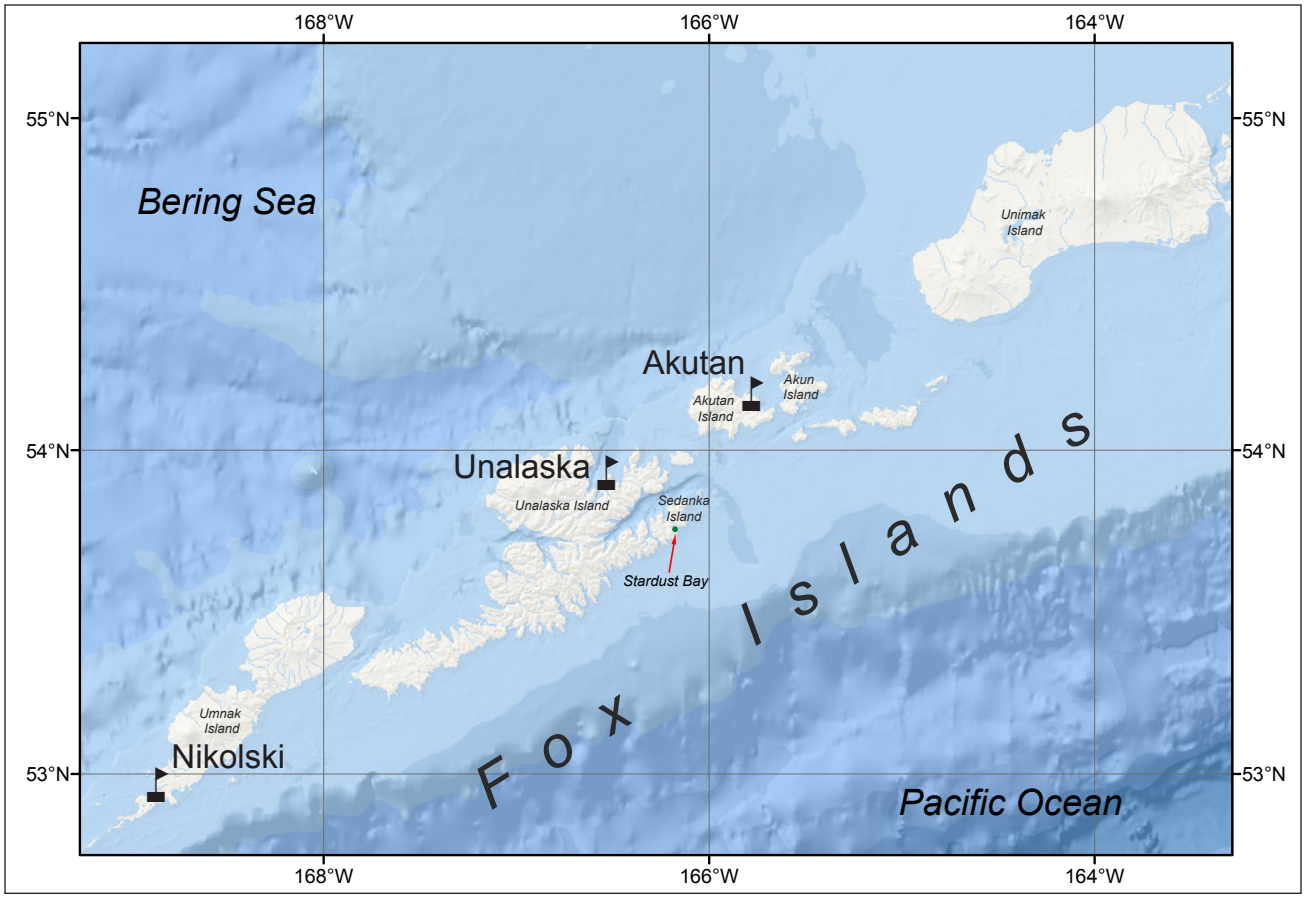

Figure 3. Map of Umnak, Unalaska, Akutan, and Unimak islands, showing the locations of the city of Unalaska and communities of Akutan and Nikolski.

and covers a 1,200-km-long (745-mi-long) region from Amchitka Pass to Unimak Island (Sykes, 1971; Kanamori, 1977) (fig. 4). Later in the 20th century the western part of the 1957 aftershock zone ruptured again in two major events, the 1986 M_W 8.0 Andreanof Island (Engdahl and others, 1989) and 1996 M_W 7.9 Adak Island earthquakes (Tanioka and González, 1998). The epicenters of these two earthquakes are close to the epicenter of the 1957 event, demonstrating that "recently" ruptured regions of the megathrust can still produce damaging earthquakes.

The lack of good quality instrument records for the 1957 earthquake, which occurred before the deployment of the World Wide Standardized Seismograph Network, resulted in the eastern part of the 1957 aftershock area being poorly defined. House and others (1981) hypothesize that the eastern part of the aftershock zone near Unalaska Island is anomalous and the 1957 event did not rupture this part of the plate interface. Thus the Unalaska Seismic Gap, a segment of the active fault that has not slipped in a long time compared to nearby areas, is thought to exist near Unalaska Island (fig. 4) (House and others, 1981; Boyd and Jacob, 1986). Numerical modeling results by Johnson and others (1994) seem to confirm the hypothesis that even if the eastern part of the 1957 aftershock zone ruptured, the tectonic plates did not slip significantly near Unalaska Island. Therefore future earthquakes similar to the 1986 and 1996 events could occur in the Unalaska seismic gap (Boyd and Jacob, 1986) potentially at any time. On Sedanka Island (fig. 3) in the hypothesized gap, Witter and others (2013) identified debris from the 1957 tsunami at an elevation of 18 m (60 ft). This observation appears to contradict the above-mentioned hypothesis of low moment release in the eastern part of the 1957 rupture. Witter and others (2013) report that, in addition to the 1957 tsunami debris, they encountered multiple layers of sand interpreted to be related to prehistoric tsunamis in Stardust Bay. In a related study at Driftwood Bay on Umnak Island, Witter and others (2014) documented nine sand sheets with characteristics similar to deposits at Stardust Bay, lending further support to the possibility of great megathrust earthquakes in the Unalaska seismic gap.

Several research groups (for example, La Selle and Gelfenbaum, 2013) have attempted to model the 1957 tsunami in light of the Sedanka Island observations; however, such an effort is not within the scope of this report. We note that potential sources of great tsunamis are in close proximity to Unalaska/Dutch Harbor and Akutan and that a significant tsunami could be generated at or near the so-called Unalaska Seismic Gap. In the remainder of this section we summarize historic events that have resulted in observed wave action in Unalaska.

Numerous earthquakes have been felt in Unalaska since the 1800s. Figure 4 shows seismic activity along the Alaska–

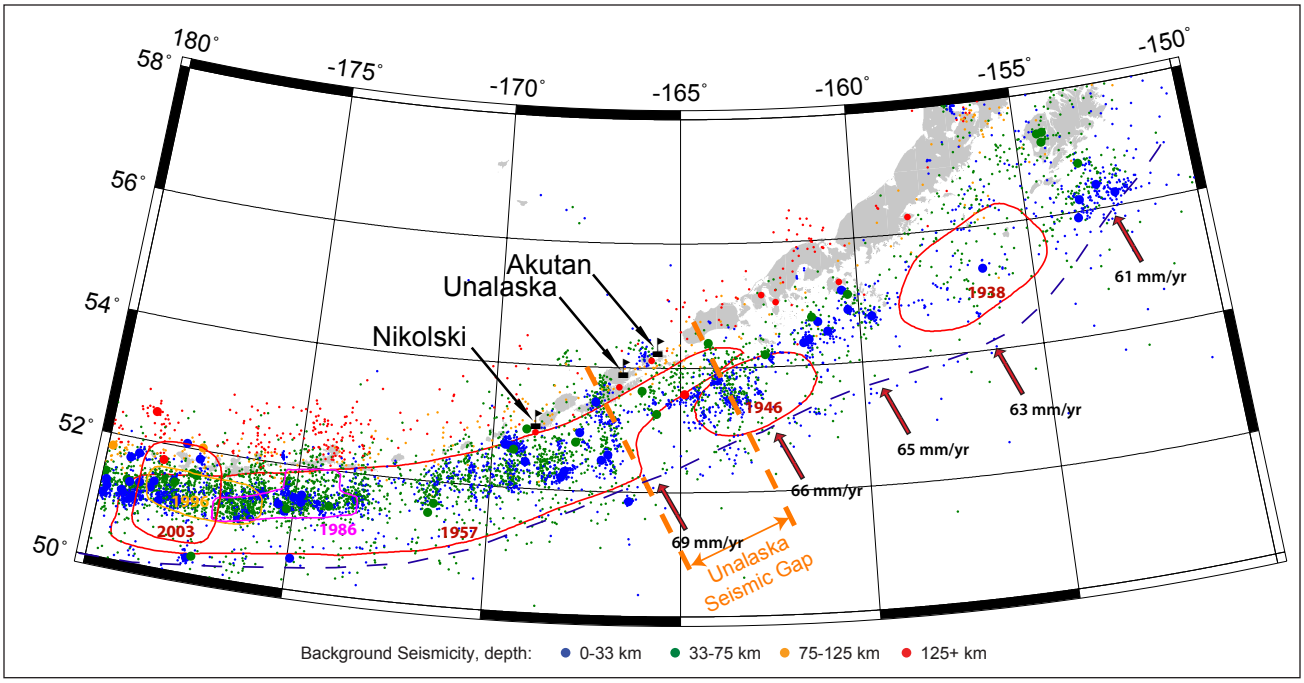

Figure 4. Earthquakes along the Alaska Peninsula and Aleutian Islands, from the Alaska Earthquake Center catalog (http://www.aeic.alaska.edu/html_docs/db2catalog.html), as of October 2015 from 1980 to 2013. Small dots correspond to earthquakes with magnitude less than 6; larger circles correspond to earthquakes with magnitude of 6 or greater. Red contours mark locations of previous rupture zones, according to aftershocks recorded in the catalog. Red arrows indicate the rate of convergence of the Pacific and North American plates. The Aleutian trench is marked by a dashed line.

Aleutian Subduction Zone with locations determined by the Alaska Earthquake Center (AEC) at the University of Alaska Fairbanks. The epicenters and dates of the most significant events are shown on figure 5. Following are descriptions of these events in Dutch Harbor according to the National Geophysical Data Center Global Historical Tsunami Database (and references therein).

- **March 1–2, 1820 Event**
  A powerful volcanic eruption, accompanied by a strong earthquake, caused "highly disturbed seas." Volcanic ash from Pogromni Volcano on Umnak Island spread across the area from Unalaska Island to Unimak Island (Lander, 1996). There is no specific mention of a tsunami in Dutch Harbor.

- **July 15, 1865 Event**
  The earthquake continued for about five minutes. Some cliffs collapsed and the earthquake caused considerable ground subsidence in Unalaska. It was reported that immediately after the earthquake the water began to rise and low-lying areas were flooded. However, no significant wave action occurred (Lander, 1996).

- **August 23 1872 Event**
  An earthquake in the area of the Fox Islands triggered a major tsunami that propagated through the Pacific Ocean and affected Oregon, California, and Hawai'i. The earthquake epicenter was estimated to be at approximately 52°12′ N, 168°30′ W, south of Umnak Island. The wave height (trough to crest) at St. Paul Island was about 0.45 m (1.5 ft) with an apparent period of oscillation of about 33 minutes (Cox and Lander, 1995). The magnitude of this earthquake is thought to be close to 7.5. This event was the first instrumentally located earthquake and tsunami.

- **August 29, 1878 Event**
  A major volcanic eruption and earthquake occurred simultaneously. It was reported that the village Makushin on Unalaska Island was destroyed by the earthquake and tsunami (Soloviev and Go, 1974; Lander, 1996).

- **March 7, 1929 Event**
  A strong M 7.5–8.6 earthquake occurred near the Fox Islands. A severe tremor and seaquake was noticed in Dutch Harbor as well as by several vessels in the ocean (Cox and Pararas-Carayannis, 1976; Lander, 1996).

- **April 1, 1946 Event**
  A strong M_W 8.6 earthquake (Lopez and Okal, 2006) near Unimak Island triggered a major destructive tsunami in the Pacific Ocean. The local waves reached up to 35 m (115 ft) on Unimak Island, 6.1 m (20 ft) in Cold Bay, 3 m (10 ft) in King Cove, and about 1.5 m (5 ft) in Chignik. Dutch Harbor reported a "minor" tidal wave, which damaged boat landings and pilings (Lander, 1996).

- **November 4, 1952 Event**
  A devastating M_W 9.0 earthquake (Kanamori, 1977) offshore of the Kuril Islands and Kamchatka Peninsula produced a tsunami that struck numerous locations along

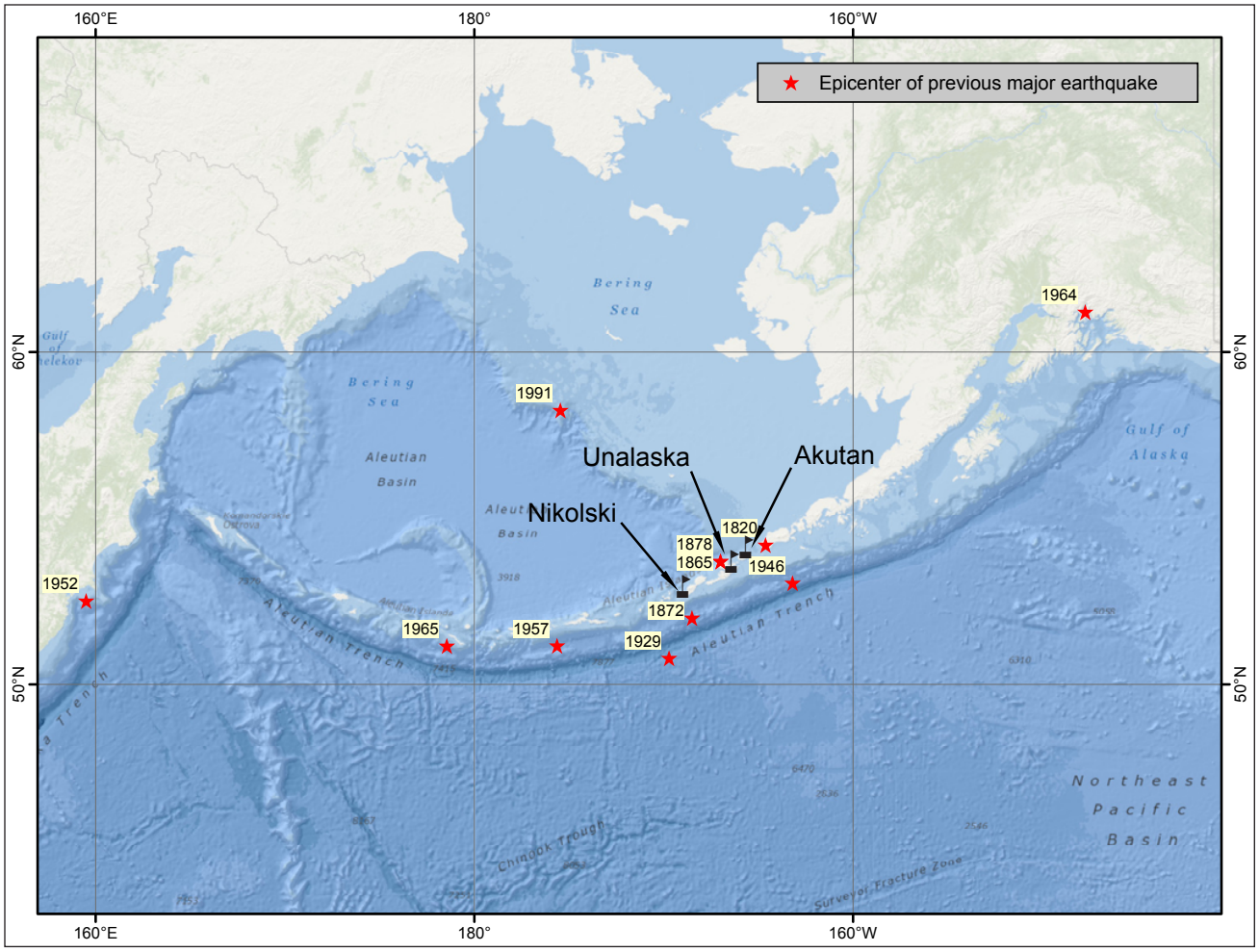

Figure 5. Map of the northern Pacific Ocean, showing epicenters of historical earthquakes associated with water disturbances in Unalaska and Dutch Harbor.

the coast of the Pacific Ocean (Kaistrenko and others, 2013). In Dutch Harbor an evacuation order was in place; however, the tsunami wave was only 0.9 m (3 ft) high (Lander, 1996).

- **March 9, 1957 Event**
  A strong M_W 8.6 earthquake (National Earthquake Information Center [NEIC], 2013) occurred offshore of Andreanof Island. The aftershock area is thought to be approximately 1,200 km (745 mi) and extended from Amchitka Pass to Unimak Pass (Sykes, 1971; Kanamori, 1977). There is still considerable uncertainty about the length of the rupture, especially about the easternmost limit of the rupture (Johnson and others, 1994). Despite the fact that a major tsunami was generated in the Pacific Ocean, the maximum wave height at Dutch Harbor was only 0.68 m (2.23 ft) (Lander, 1996).

- **May 22, 1960 Event**
  The great Chilean M_W 9.5 earthquake (Kanamori, 1977) generated a significant tsunami that traveled across the ocean. A wave more than 1.7 m (5.6 ft) high was recorded at Massacre Bay, Attu Island, 0.7 m (2.3 ft) in Seward, 0.8 m (2.6 ft) in Yakutat, and 0.7 m (2.3 ft) in Dutch Harbor. Cox and Pararas-Carayannis (1976) report "some cracking of the ice was noted in the afternoon," but do not provide a location. At Cape Pole, Prince of Wales Island, a log boom was broken by a strong current associated with this tsunami. The runup there was about 1 m (3.3 ft) and a buoy was moved by the tsunami in Craig (Lander and Lockridge, 1989).

- **March 28, 1964 Event**
  The M_W 9.2 Alaska earthquake of 5:36 p.m. March 27, 1964, shook south-central Alaska and generated the most devastating tsunami in Alaska history. Simultaneously with the major tectonic tsunami generated by an ocean-floor displacement, multiple local tsunamis were generated by submarine landslides; in some glacial fjords the local runup reached up to 52 m (170 ft) (Plafker and others, 1969). Local tsunamis arrived within minutes after the onset of the earthquake, causing most of the damage and accounting for 76 percent of tsunami fatalities in Alaska (Lander, 1996). Because the Fox Islands are outside of the rupture area and away from the primary direction of the tsunami propagation, the recorded am-

plitude of the 1964 tsunami in Dutch Harbor was about 0.4 m (1.3 ft) (Lander, 1996).

- **February 4, 1965 Event**
  A M_W 8.7 earthquake (Kanamori, 1977) in the Rat Island region generated a tsunami that was recorded to be 0.24 m (0.79 ft) in Dutch Harbor (Lander, 1996). In addition to the tsunami, local settlements suffered from the ground subsidence and the development of ground fissures caused by the shaking.

- **February 21, 1991 Event**
  A M_W 6.7 earthquake (NEIC catalog, 2013) occurred along the Bering Shelf edge (a particularly unusual location) and generated a 0.3 m (1 ft) tsunami in Dutch Harbor (Lander, 1996). The earthquake was rather shallow and located near the elongated Zhemchug basin. This event indicates that one of the near-surface faults in Zhemchug basin is active.

LANDSLIDE-GENERATED TSUNAMI HAZARDS IN UNALASKA AND AKUTAN

Alaska has a long recorded history of tsunamis generated by submarine and subaerial landslides, avalanches, and rockfalls (Kulikov and others, 1998). A primary cause of submarine slumps or landslides is the accumulation of sediments on underwater slopes and the consequent oversteepening of unconsolidated deposits. These conditions typically occur at the mouths of glacier-fed rivers, creeks, and streams. The absence of substantial glacial creeks near Unalaska and Akutan suggests that the potential is not high for significant local submarine landslide-generated tsunamis near either community.

We speculate that the closest possible submarine landslide sources to Dutch Harbor are at the heads of Captains Bay, Nateekin Bay, or Broad Bay; however, little is known about potential slide volumes and geometries. In figure 6a we show the location of these hypothetical submarine slides and their possible direction(s) of propagation. Dutch Harbor is relatively protected so we speculate that most of the wave energy would dissipate before the waves reach the Dutch Harbor waterfront.

Other potential locations for submarine slump failures (fig. 6b) include the continental shelf in Bering Canyon, Zhemchug Canyon, and Umnak Plateau (Carlson and others, 1991; David Scholl, USGS, oral commun., 2012). Unfortunately, little is known about the extent, volume, and locations of these potential landslides and even less about the slope stability in these areas. However, it is known that massive landslides along continental slopes can cause large tsunamis. The Storegga Slide (Bryn and others, 2005) and the Grand Banks Slide (Fine and others, 2005) generated catastrophic tsunamis along the Norway and Canada coastlines, respectively. Similarly, Grilli and others (2013) propose that the 2011 Tohoku-Oki tsunami was generated by a combination of tectonic processes and submarine mass failures. In Alaska the location of the submarine landslide that might have caused the 35 m (115 ft) wave runup at Unimak Island during the 1946 tsunami was recently located using high-resolution seismic profiles (Miller and others, 2014). Therefore the 1946 tsunami was probably generated by both tectonic deformation and a submarine mass failure triggered by the earthquake, as earlier hypothesized by Fryer and Watts (2001). Refer to Schwab and others (1993) for a valuable discussion of submarine mass wasting in Alaska.

Some numerical simulations of these landslide-generated tsunamis along the Aleutian Arc are possible (Waythomas and others, 2009). Our preliminary modeling of a potential 200 km^3 (48 mi^3) mass failure at Umnak Plateau in the Bering Sea (the slide volume is estimated from the GLORIA images in Carlson and others [1991], p 44) shows that a simulated wave in Unalaska/Dutch Harbor is similar in height to a tsunami generated by a M_W 9.1 earthquake along the Fox Islands. However, these simulations require more scientific research to further constrain potential slide locations and their volumes before accurate wave inundations can be estimated.

The destructive effects of tsunamis generated by subaerial and underwater slope failures have been identified previously in south-central and southeastern Alaska. During the 1865 event some cliffs near Unalaska collapsed into the ocean (Lander, 1996). In light of recent field observations in western Passage Canal, a steep-walled glacial fjord in south-central Alaska, we appended the tsunami modeling and mapping report for the city of Whittier and western Passage Canal with an additional hypothetical rockfall-generated tsunami scenario (Nicolsky and others, 2011a). Similar steep mountain slopes are present near Unalaska/Dutch Harbor and Akutan. Thus the threat of avalanches, debris flows, and rock falls plunging into the ocean and consequently generating a tsunami exists in both communities. Our ability to accurately model effects of a potential rapid subaerial mass failure and the subsequent impact of the rockfall/landslide/avalanche-generated tsunami on these communities is dependent on our knowledge of the type and geometry of the mass movement, local bedrock geology, and location (Nicolsky and others, 2011c). Unfortunately, landslide assessments on Unalaska and Akutan are limited and the location and geometry of these potential mass failures are currently unknown. Although numerical simulations of the rockfall/landslide/avalanche-generated tsunamis are possible, more field data and scientific research are necessary to constrain the landslide sources before meaningful results can be generated.

In this report we do not model tsunamis generated by any mass failures, due to insufficient data on the locations and volumes of these potential hazards[4].

Figure 6 (right). Locations of potential submarine landslides in (A) the vicinity of Unalaska and (B) the Bering Sea. Directions of landslide-generated wave propagation are marked by red arrows.

[4]Guidelines and best practices for tsunami inundation modeling for evacuation planning state that the modeling should add value to mapping products (National Tsunami Hazard Mapping Program [NTHMP], 2010).

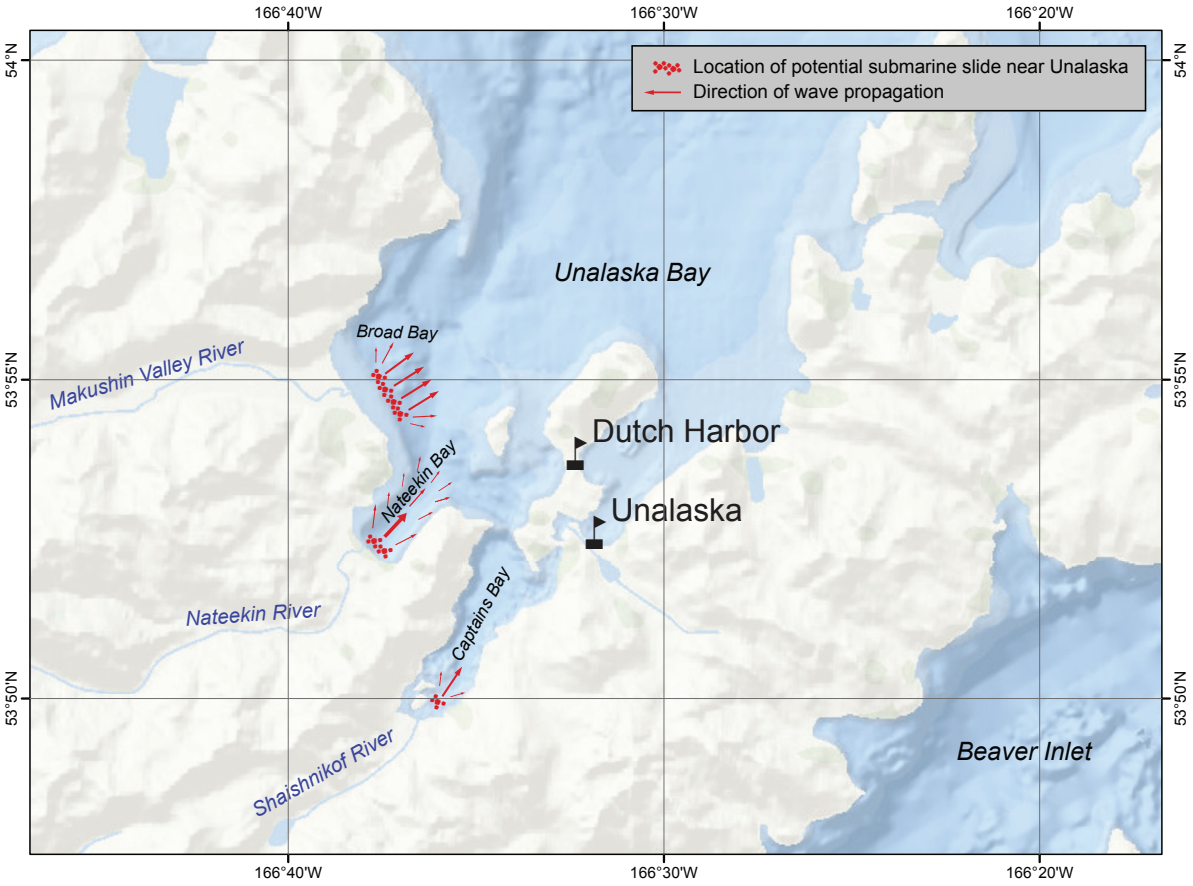
166°40'W
166°30'W
166°20'W
54°N
53°55'N
53°50'N
Location of potential submarine slide near Unalaska
Direction of wave propagation
Unalaska Bay
Broad Bay
Makushin Valley River
Dutch Harbor
Unalaska
Nateekin Bay
Nateekin River
Captains Bay
Shaishnikof River
Beaver Inlet

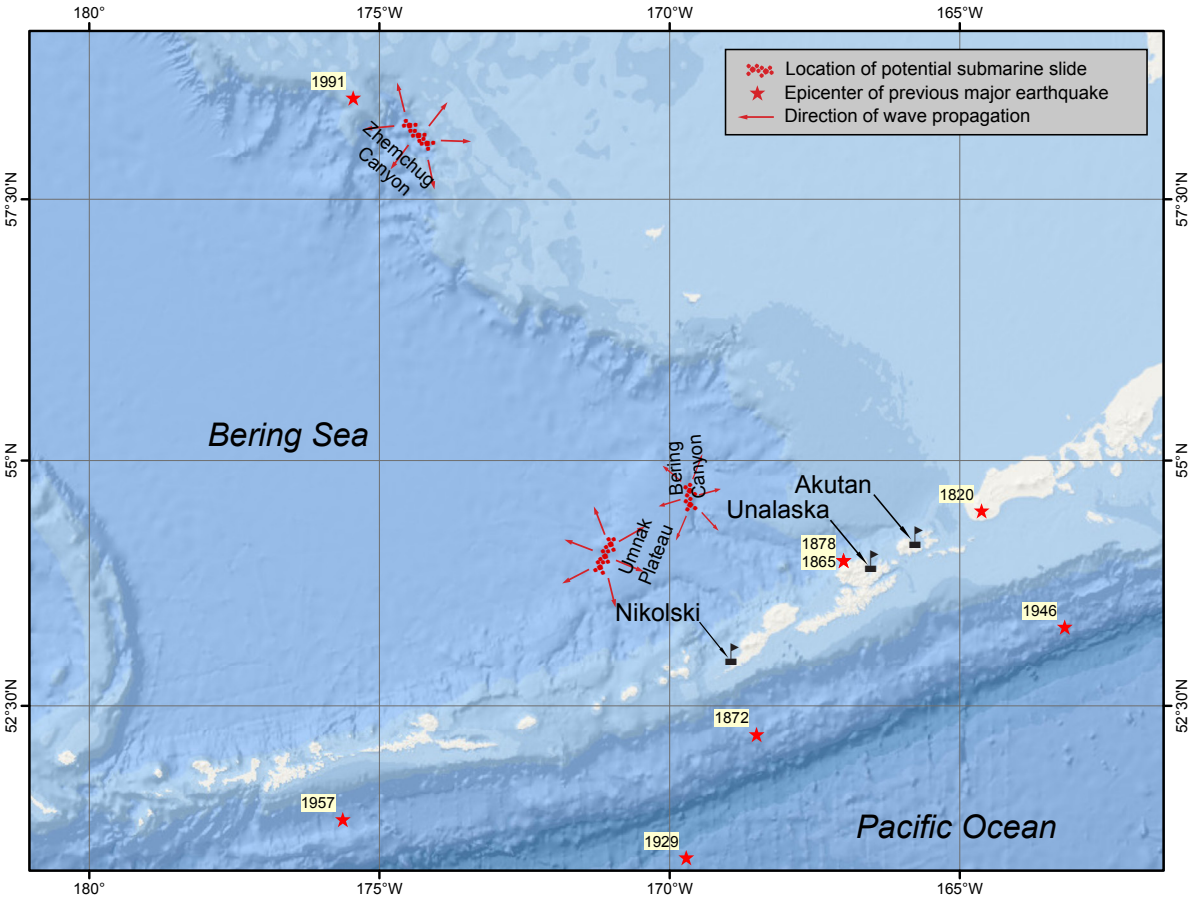
180°
175°W
170°W
165°W
57°30'N
55°N
52°30'N
Location of potential submarine slide
Epicenter of previous major earthquake
Direction of wave propagation
1991
Zhemchug Canyon
Bering Sea
Bering Canyon
Umnak Plateau
Akutan
Unalaska
1820
1878
1865
1946
Nikolski
1872
1957
1929
Pacific Ocean

METHODOLOGY AND DATA

GRID DEVELOPMENT AND DATA SOURCES

Numerical modeling of the governing equations for water dynamics requires a discrete approximation of the motion of a continuous medium—the water. In this work we discretize the shallow-water equations in spherical coordinates using a finite difference method. To resolve a wave the grid must be fine enough, with at least four points per wavelength (Titov and Synolakis, 1995); however, more points are often necessary to achieve satisfactory accuracy (for example, Titov and Synolakis, 1997). To compute a detailed map of potential tsunami inundation triggered by local and distant earthquakes we employ a series of nested computational grids. A nested grid allows for higher resolution in areas where it is needed without expending computer resources in areas where it is not. The bathymetric and topographic relief in each nested grid is based on digital elevation models (DEMs) developed at the National Geophysical Data Center (NGDC) of the National Oceanic & Atmospheric Administration (NOAA) in Boulder, Colorado. The extent of each grid used for the Unalaska/Dutch Harbor and Akutan mapping is shown in figure 7 and listed in table 1. The coarsest grid, with 2-arc-minute (approximately 2 km) resolution, spans the central and northern Pacific Ocean. The highest-resolution grid for Unalaska/Dutch Harbor covers Amaknak Island, Broad Bay, Nateekin Bay, Captains Bay, Iliuliuk Bay, Summer Bay, Morris Cove, and a part of Unalaska Bay. The highest-resolution grid for Akutan covers the village of Akutan, the Trident Seafood processing plant, and the new boat harbor at the head of Akutan Harbor. The spatial resolution of the high-resolution grid cells, about 16 × 16 m (53 × 53 ft), satisfies NOAA minimum recommended requirements for computation of tsunami inundation (National Tsunami Hazard Mapping Program [NTHMP], 2010). We use three intermediate grids between the coarsest- and highest-resolution grids (table 1).

The bathymetric data for the 2-arc-minute-resolution grid is extracted from the ETOPO2 dataset (NGDC/NOAA). To develop 8/3-, 8-, and 24-arc-second-resolution grids, we obtained shoreline, bathymetric, and topographic digital datasets from the following U.S. federal agencies: NOAA's National Ocean Service (NOS), Office of Coast Survey, and National Geophysical Data Center (NGDC); and the U.S. Army Corps of Engineers (USACE). All data were shifted to World Geodetic System 1984 (WGS 84) horizontal and Mean Higher High Water (MHHW) vertical datums. Bathymetric datasets used in the compilation of the Fox Islands DEMs included NOS hydrographic surveys, a recent USACE harbor survey, NOAA electronic navigational charts and multi-beam swath sonar surveys, and NGDC trackline surveys. The topographic dataset was obtained from the 1-arc-second NASA Space Shuttle Radar Topography Mission (SRTM). The data sources and methodology used to develop high-resolution 8/3-, 8-, and 24-arc-second DEMs are described in detail by Carignan and others (2012) and Taylor and others (2008).

Accuracy of the high-resolution DEM is dependent on the SRTM dataset, which has a vertical accuracy of 10–15 m (33–ft) (Caldwell and others, 2009). Because the

Table 1. Nested grids used to compute propagation of tsunami waves generated in the Pacific Ocean to the communities of Unalaska/Dutch Harbor and Akutan. The high-resolution grids are used to compute the inundation. Note that the grid resolution in meters is not uniform and is used to illustrate grid fineness in the Fox Islands region. The first dimension is the longitudinal grid resolution, while the second is the latitudinal resolution.

Grid name	Resolution		West–East boundaries	South–North boundaries
	arc-seconds	meters (near Fox Islands)		
Level 0, Northern Pacific	120 × 120	≈ 1,850 × 3,700	120°00' E–100°00' W	10°00' N–65°00' N
Level 1, Eastern Aleutians	24 × 24	≈ 430 × 740	171°58' W–157°02' W	52°00' N–57°28' N
Level 2, Coarse resolution Fox Islands	8 × 8	≈ 150 × 250	165°03' W–169°25' W	52°37' N–54°23' N
Level 3, Fine resolution Fox Islands	8/3 × 8/3	≈ 48 × 82	165°10' W–166°45' W	53°40' N–54°21' N
Level 4, High resolution Unalaska	8/9 × 8/15	≈ 16 × 16	166°25' W–166°39' W	53°48' N–53°56' N
Level 4, High resolution Akutan	8/9 × 8/15	≈ 16 × 16	165°42' W–165°50' W	54°06' N – 54°09' N

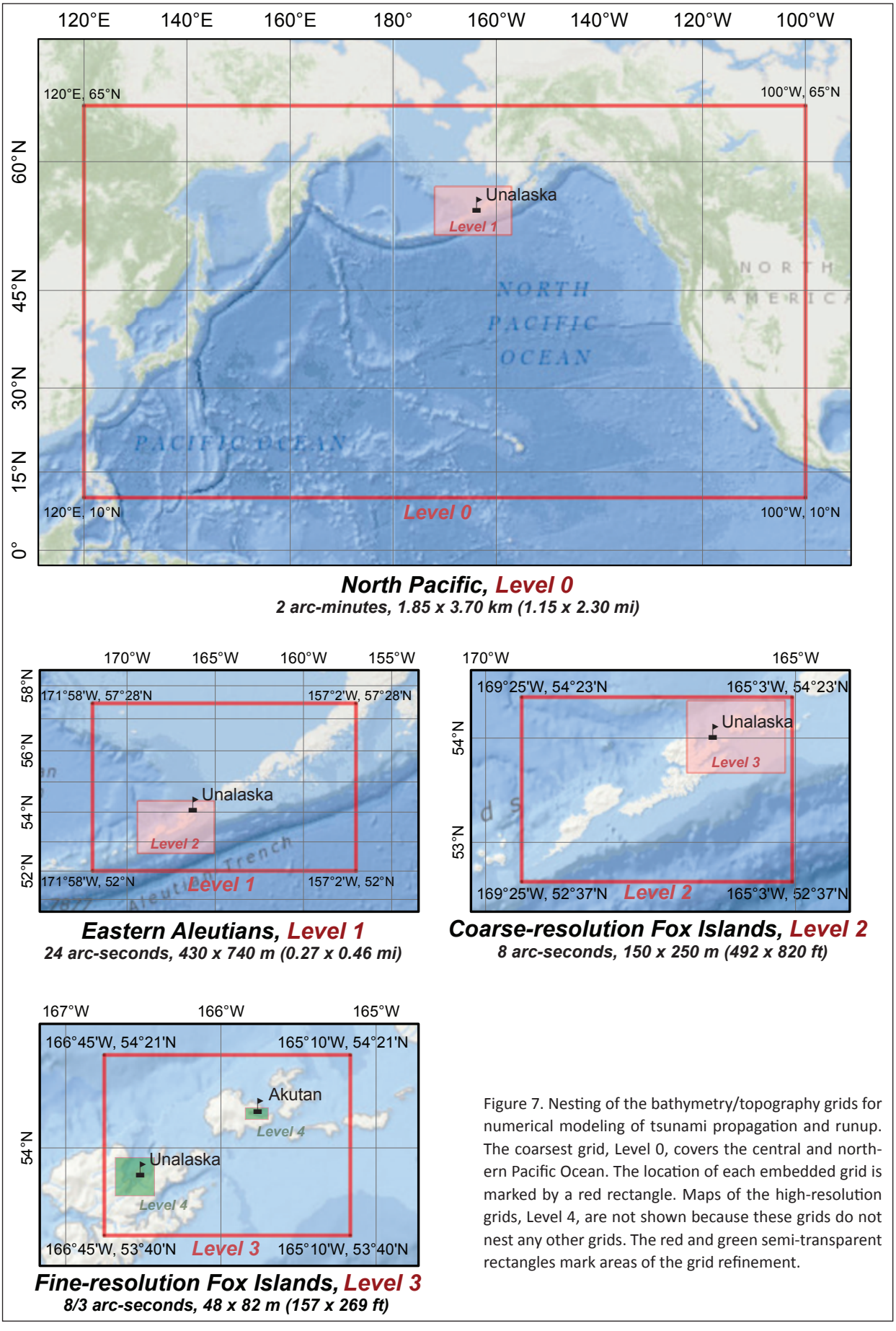

Figure 7. Nesting of the bathymetry/topography grids for numerical modeling of tsunami propagation and runup. The coarsest grid, Level 0, covers the central and northern Pacific Ocean. The location of each embedded grid is marked by a red rectangle. Maps of the high-resolution grids, Level 4, are not shown because these grids do not nest any other grids. The red and green semi-transparent rectangles mark areas of the grid refinement.

SRTM data can possess large vertical errors near the shoreline, prediction of the potential tsunami inundation using those data can be invalid. Hence this topographic dataset is augmented with contour data from the City of Unalaska and some high-accuracy data such as a real-time kinematic (RTK) GPS survey in the harbor areas and along nearshore areas in Unalaska/Dutch Harbor and Akutan. The survey in Akutan was conducted September 1–2, 2011, and the survey in Unalaska/Dutch Harbor September 3–6, 2011. Locations of the GPS measurements in Unalaska/Dutch Harbor are shown in figure 8. The collected GPS measurements had 3–5 cm (1.2–2 in) lateral and vertical accuracy relative to the base station (Leica Geosystems AG, 2002). Therefore to achieve sub-meter accuracy for all GPS measurements related to the MHHW datum, the base station datum must relate to the MHHW datum with sub-meter accuracy. Such base station accuracy can be achieved if the base station is set up at a well-known benchmark or monument. We could not find a conveniently located benchmark in either Unalaska/Dutch Harbor or Akutan to securely set up the surveying equipment so we used the technique described below to convert the collected GPS measurements into the MHHW datum.

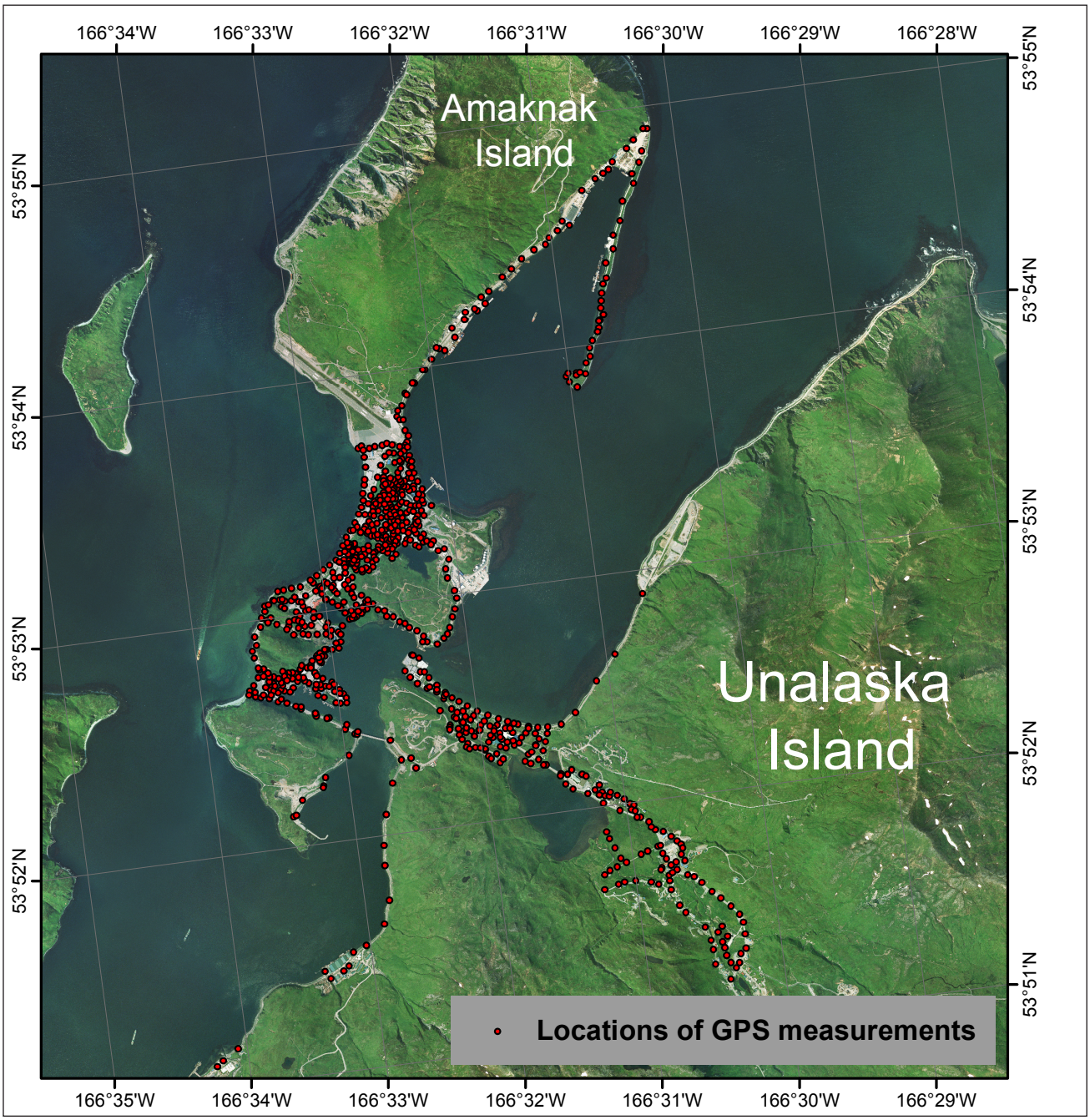

Figure 8. Locations of RTK GPS measurements at Unalaska and Dutch Harbor.

During the survey we took GPS measurements of the sea surface height at some partially enclosed locations where the water was relatively still (for example, in the harbor), as shown by the red arrow in figure 9a. The sea level was measured at low and high tides as well as at some intermediate tide stages. Recall that all RTK GPS measurements have an accuracy of several centimeters relative to the base station datum. Therefore the measured tide level, denoted by H_2, is known relative to the base station datum at some instance of time, t_k, with an accuracy of several centimeters. Here k stands for the index number of the sea level measurement.

The tide level, $H_1(t)$, with respect to the MHHW datum is observed every 6 minutes at the NOAA tide stations in Unalaska (predictions by NOAA, http://tides and currents.noaa.gov/). Because Unalaska and Akutan are close to each other and are connected by deep water, we assume that the MHHW datums in both locations coincide and that observations in Unalaska provide a good approximation to the tide level dynamics in Akutan. Therefore we calculate the vertical shift between the MHHW datum and the base station datum by finding a difference (in the least-squares sense) between the GPS-measured sea level, H_2, and the NOAA-observed sea level, H_1, at the instances t_k. The results of the least-square fitting for Unalaska are shown in figure 9b. Once the vertical shift is calculated we apply the same shift to all collected GPS measurements and convert the entire survey to the MHHW datum.

We check the accuracy of our conversion of the GPS data to the MHHW level by measuring the height of the tidal benchmark "2694 A 2009" in Akutan. According to the NOAA website (http://tidesandcurrents.noaa.gov) the disk is 2.311 m (7.58 ft) above the MHW, or 2.217 m (7.27 ft) above the MHHW. After measuring the height of this disk during the GPS survey and converting to the MHHW datum we estimate that the disk is 2.218 m (7.28 ft) above the MHHW. In Dutch Harbor we measured and estimated tidal station disk "2620 O 1990." According to NOAA the tidal disk is set at 2.532 m (8.307 ft) above the MHHW. After converting the survey to the MHHW we find that the same disk is 2.537 m (8.323 ft) above the MHHW. The difference of 0.01 m (0.033 ft) between the NOAA stamping and our estimates demonstrates that the conversion of the GPS measurements to the MHHW level provides sub-meter accuracy in Dutch Harbor and Akutan. We emphasize that sub-meter differences between the measured and estimated elevations of tidal disks show a general consistency of the method used. Therefore the approach described can be applied to adjust raw RTK GPS surveys at locations without tidal disks. Finally we note that GPS measurements were collected using the WGS84 horizontal datum, with a horizontal accuracy of approximately 3–5 m (10–16 ft) (Leica Geosystems AG, 2002). The converted GPS survey has been provided to the NGDC, where the high-resolution DEM of Unalaska/Dutch Harbor and adjacent areas has been developed. Incorporation

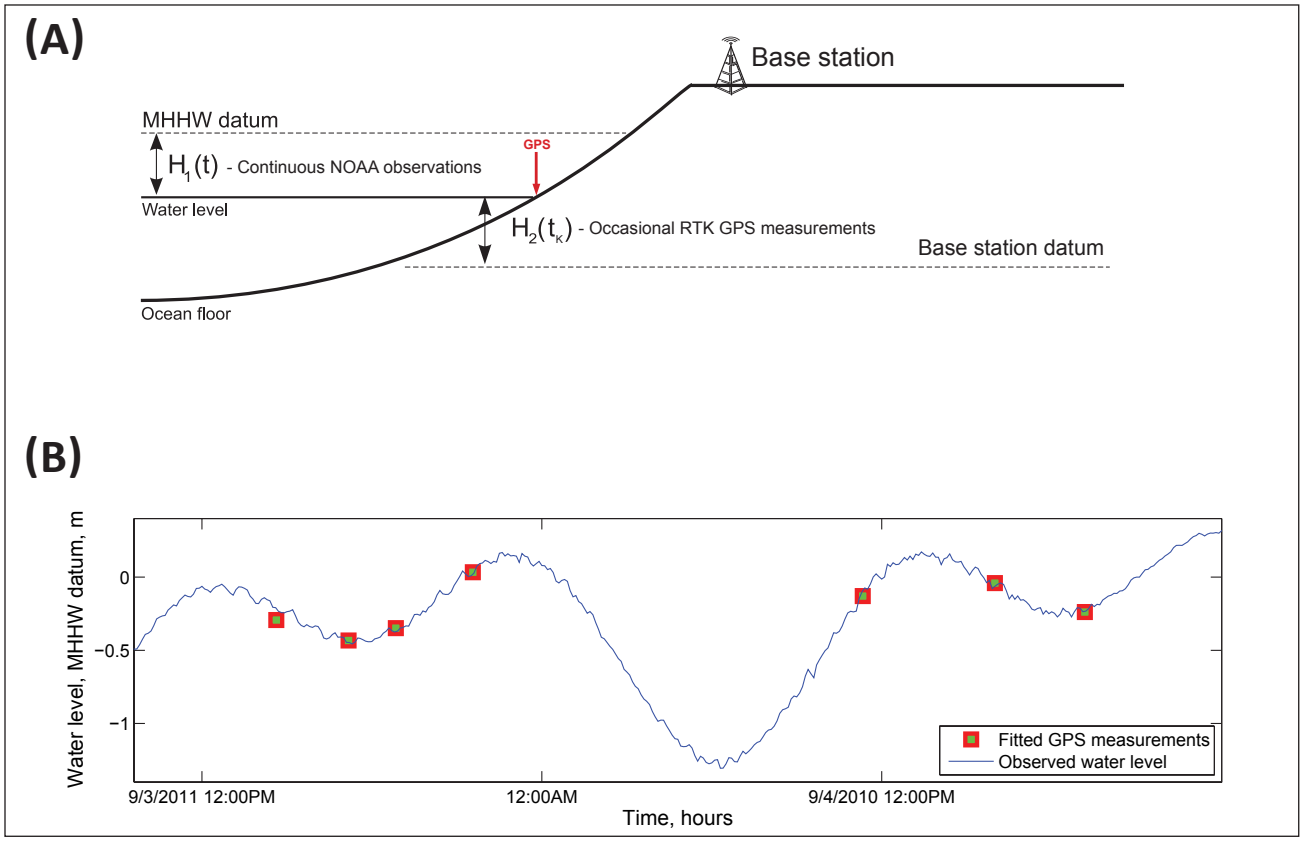

Figure 9. (A) Measurement of sea level in the MHHW datum and the relation of the base station datum to the MHHW datum. (B) Predicted water-level dynamics in Unalaska and the fitted GPS measurements of the water level in the MHHW datum.

of the GPS measurements in the DEM covering Akutan was completed locally at the Geophysical Institute, University of Alaska Fairbanks.

NUMERICAL MODEL OF TSUNAMI PROPAGATION AND RUNUP

The numerical model currently used by the Alaska Earthquake Center (AEC) for tsunami inundation mapping has been validated through a set of analytical benchmarks and tested against laboratory and field data (Nicolsky and others, 2011b; Nicolsky, 2012). The model solves the nonlinear shallow-water equations using a finite-difference method on a staggered grid. For any coarse–fine pair of computational grids we apply a time-explicit numerical scheme as follows. First we compute the water flux in a coarse-resolution grid. These calculated flux values are used to define the water flux on a boundary of the fine-resolution grid. Next the water level and then the water flux are calculated over the fine-resolution grid. Finally the water level computed in the fine-resolution grid is used to define the water level in the area of the coarse-resolution grid that coincides with the fine grid. Subsequently we compute the water elevation for all other points in the coarse grid and proceed to the next time step. More details about the numerical scheme, grid nesting, and time stepping can be found in Goto and others (1997) and in Nicolsky and others (2011b). Even though the nested grids decrease the total number of grid cells needed to preserve computational accuracy in certain regions of interest, actual simulations are still unrealistic if parallel computing is not implemented. Here we use the Portable Extensible Toolkit for Scientific computation (PETSc), which provides sets of tools for the parallel numerical solution of shallow-water equations (Balay and others, 2012). In particular, each computational grid listed in table 1 can be subdivided among an arbitrary number of processors. The above-mentioned passing of information between the water flux and level is implemented efficiently using PETSc subroutines.

We assess hazards related to tectonic tsunamis in Dutch Harbor/Unalaska and Akutan by performing model simulations for each hypothetical earthquake source scenario. To simulate tsunami dynamics caused by seafloor deformation from an earthquake we assume some simplifications. First, the initial displacement of the ocean surface is equal to the vertical displacement of the ocean floor induced by the earthquake rupture process. The contribution of horizontal displacements is not considered[5]. Second, the finite speed of rupture propagation along the fault is not taken into account. We consider ocean bottom displacement to be instantaneous. Third, the initial topography is modified to account for coseismic deformation of land due to the earthquake, which can be either uplift or subsidence depending on the location of a point relative to the earthquake's slip patch. In the case of Unalaska and Akutan all scenarios result in subsidence of the towns.

At the end of a tsunami simulation each of the on-land grid points has a value of either 0 if no inundation occurs or 1 if seawater reaches the grid point at any time. The inundation line lies halfway between grid points with values of 0 and 1 but is adjusted visually to accommodate obstacles or local variations in topography not represented by the DEM. Although the developed algorithm has passed through rigorous benchmarking procedures (Nicolsky and others, 2011b; Nicolsky, 2012) there is still uncertainty in locating an inundation line. The accuracy is affected by many factors on which the model depends, including suitability of the earthquake source model, accuracy of the bathymetric and topographic data, and the adequacy of the numerical model in representing the generation, propagation, and runup of tsunamis. In this report we do not attempt to adjust the modeled inundation limits to account for these uncertainties. Another important limitation of the model is that it does not account for the periodic change of sea level due to tides. We conducted all model runs using bathymetric data that correspond to the MHHW tide level in Unalaska and Akutan.

MODELING OF THE MARCH 11, 2011, TOHOKU TSUNAMI

As part of this project we completed a model verification study of the Tohoku tsunami of March 11, 2011. We emphasize that among many reasons for model verification listed in Synolakis and others (2007), the one that has special importance for distant tsunami events is checking the consistency of the DEM nesting.

Several deformation models representing the slip distribution of the 2011 Tohoku earthquake were published after the event. Here we employ a finite fault model III by Shao and others (2011). For each fault we calculate the corresponding vertical coseismic deformation using Okada's formula (1985). The resulting vertical deformation is illustrated in figure 10. Figure 11 shows a comparison between the observed wave dynamics at several DART (Deep-ocean Assessment and Reporting of Tsunamis) buoys along the central and eastern Aleutian Islands (https://www.ngdc.noaa.gov/hazard/dart/2011honshu_dart.html). Note that the comparison between the computed and measured water level dynamics is relatively good for the first 2 to 3 hours after the wave arrived at the buoy. After the initial 2–3 hour interval, waves reflected from the shore started to arrive at buoys and the computed wave is no longer in phase with the observed tsunami dynamics. Similarly to Tang and others (2012) we observe a time delay between the computed and observed waves. The computed wave arrives at the DART buoys δT = 7–8 minutes sooner than the observed one.

Additionally we compare the computed and measured and de-tided water level dynamics at the Unalaska tidal station (fig. 11-D; https://tidesandcurrents.noaa.gov/). The catastrophic Tohoku tsunami of March 11, 2011, produced a 0.5 m (1.6 ft) wave in Unalaska (NCEI/WDS Global His-

[5]Numerical modeling of the tsunami generated by a M_W 9.1 earthquake (scenario 1) shows that contribution of horizontal displacements into the model increases the maximum wave height in Captains Bay by 0.1 m (0.3 ft). This effect is small compared to the corresponding uncertainties related to the slip distribution.

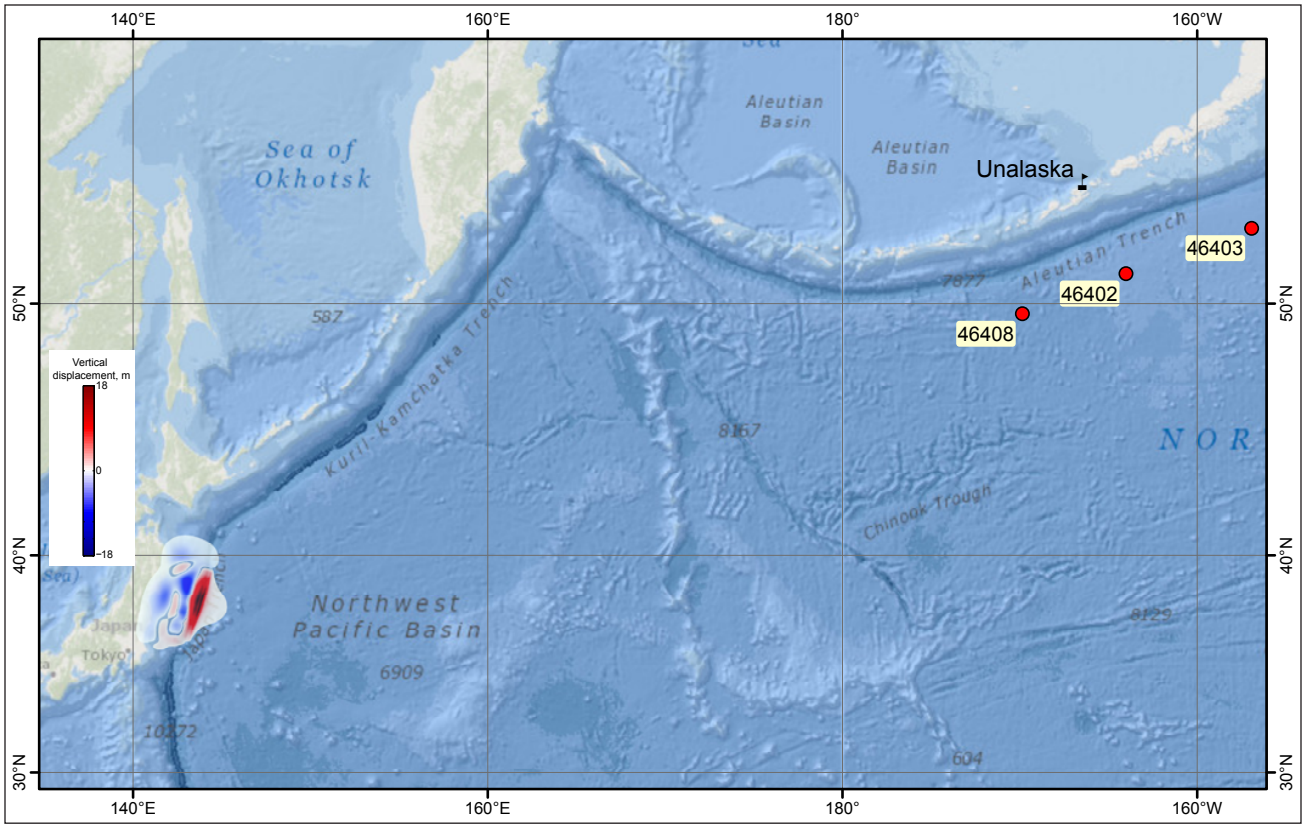

Figure 10. Vertical deformations of the ocean floor and adjacent coastal region in meters corresponding to the March 11, 2011, Tohoku earthquake, based on a finite fault model III by Shao and others (2011). Red indicates uplift; blue indicates subsidence. DART buoys near Unalaska are identified by red circles.

torical Tsunami Database), whereas the simulation predicts a 0.6 m (2 ft) wave. Note that the time delay between the computed and measured water level dynamics increased to $\delta T = 15$ minutes. A similar time lag is observed by Tang and others (2012). The probable causes of this increase are errors in the bathymetry and some dispersion effects.

The far-field Tohoku tsunami did not result in a significant wave at Unalaska because of its distance from the Fox Islands and directivity patterns of the energy propagation. However, other distant events could produce greater wave heights in Unalaska and should not be dismissed without a proper evaluation. Refer to the NOAA report by Wei (in review) for more information.

The numerical modeling of this historic tsunami demonstrates that the employed numerical model of tsunami propagation and runup generates tsunami waveforms that mesh with the observed arrival times and wave phases. The model also provides a good approximation to the recorded tsunami amplitudes in Unalaska Bay, which indicates that the proposed coseismic deformation model adequately describes the coseismic slip distribution and that the DEM nesting is selected appropriately.

TSUNAMI SOURCES

It is believed that all of the devastating great events along the Alaska–Aleutian arc occurred on the megathrust—the contact surface between the subducting Pacific plate and the North American plate. Along the Aleutian Islands the Pacific plate subducts underneath the North American plate at a relative convergence rate of about 65–70 mm/yr (2.56–2.76 in/yr) (DeMets and others, 1990; Page and others, 1991; Argus and others, 2010). Because of friction on the megathrust, the two converging tectonic plates generally cohere to each other at depths shallower than 25–40 km (16–25 mi) and thus shear stress builds up between the plates. The shear stress is typically released instantaneously during an earthquake and the seismic energy propagates through the ground, causing strong shaking. It is theorized that the shear stress is primarily acquired in the locked or coupled regions of the megathrust where friction is the greatest. In creeping regions where the converging plates manage to slip relative to each other, a lesser amount of shear stress builds up and hence the release of seismic energy during earthquakes can be small. Therefore before discussing hypothetical tsunamigenic earthquakes near Unalaska and Akutan, we review some aspects of the region's plate tectonics and locations of the locked and creeping zones along the Aleutian megathrust. We aim to exploit the limits of the GPS-observed coupled regions near Unalaska and Akutan to parameterize the spatial extents of hypothetical ruptures. A sensitivity study then helps us to analyze the waves arriving at each community by varying the location of the idealized rupture in the locked region. Results of the sensitivity study are then applied to construct the maximum credible scenarios.

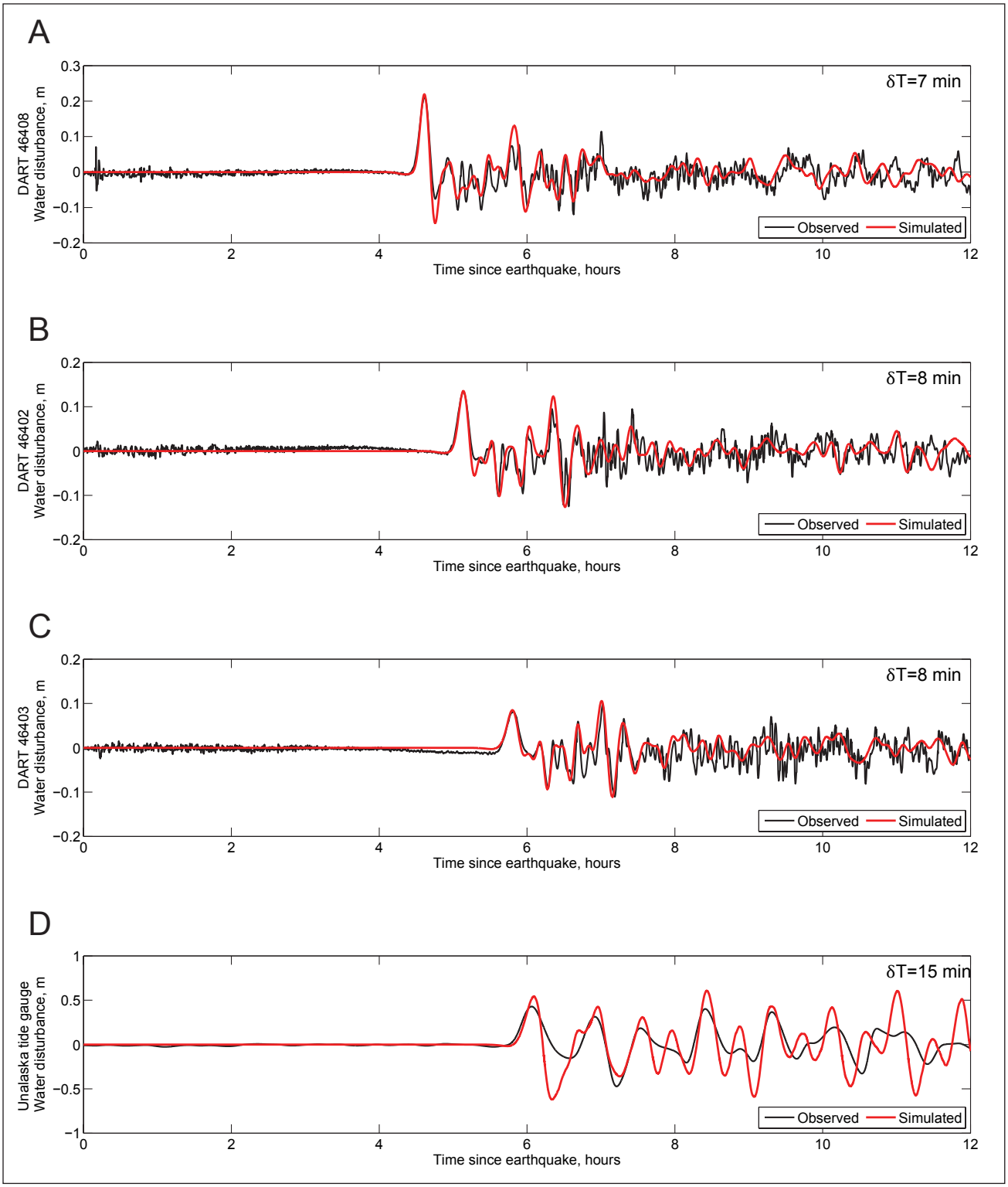

Figure 11. Modeled water-level dynamics at DART buoys (A) 46408, (B) 46402, and (C) 46403; and (D) at the tide station in Unalaska during the March 11, 2011, tsunami. The de-tided observations of the tsunami at DART buoys are provided by NCEI (https://www.ngdc.noaa.gov/hazard/dart/2011honshu_dart.html); the observed water level at the tide station is provided by NOAA (https://tidesandcurrents.noaa.gov/).

Delineating earthquake rupture zones in the Fox Islands

Delineating the locked or coupled regions in various subduction zones has been the subject of extensive research (Uyeda, 1982; Pacheco and others, 1993; Tichelaar and Ruff, 1993; Uchida and others, 2009; Scholz and Campos, 2012). Most of this research has focused on determining the spatial extent of the locked zone and its updip and downdip limits (fig. 12). It is thought that the locked regions can be determined by locating rupture zones of previous great earthquakes (Kelleher and others, 1973; Kato and Seno, 2003). The rupture zone of any significant earthquake is typically delineated by numerous aftershocks that follow the event. The region in which aftershocks occur is thought to extend down to the boundary of coupled and uncoupled regions of the megathrust (Tichelaar and Ruff, 1993).

Near Unalaska Island the 1957 Great Andreanof Islands earthquake occurred before the deployment of the World Wide Standardized Seismograph Network and, unfortunately, this event is poorly understood. According to studies of this event (Sykes, 1971; Kanamori, 1977) it is assumed that the aftershock area is 1,200 km (745 mi) long. The aftershocks in the easternmost part of the rupture area, near Unalaska Island, are less constrained and the extent of the 1957 rupture zone to the deeper part of the megathrust is debatable (House and others, 1981), so the actual length of rupture in 1957 is currently unknown. Numerical inversion of all available seismic and tsunami data related to the 1957 earthquake indicate that either Unalaska Island is not within the eastern part of the 1957 rupture zone or the slip on the interface near Unalaska was relatively small (Johnson and others, 1994). This appears to support the hypothesized 200-km-wide (125-mi-wide) Unalaska Seismic Gap (House and others, 1981; Boyd and Jacob, 1986); however, this conclusion is apparently contradicted by the large runup recently observed on Sedanka Island (Witter and others, 2013, 2014).

The location of the locked region derived from analysis of the previous rupture could be biased because the rupture might propagate outside of the locked region to the weakly coupled areas of the plate interface. Therefore the previous rupture can provide some preliminary assessment of the spatial location as well as updip and downdip limits of hypothetical events. However, the moment distribution from a single great earthquake might tell us little about what the distribution of moment release will look like during the next earthquake (Boyd and others, 1995). Therefore in order to accomplish a tsunami hazard analysis it is necessary to develop various hypothetical earthquake scenarios.

Finally we note that historical events help to divide the subduction zone into seismic segments. Each segment is determined by aftershocks of great historical events. Currently the Alaska–Aleutian plate interface is split into ten segments from the western Aleutians to Prince William Sound in south-central Alaska (Nishenko and Jacob, 1990). We hypothesize that during future events different segments might rupture separately or together (Sykes and others, 1981) and hence a thorough study of worst-case scenarios is necessary for development of tsunami inundation maps for Unalaska and Akutan.

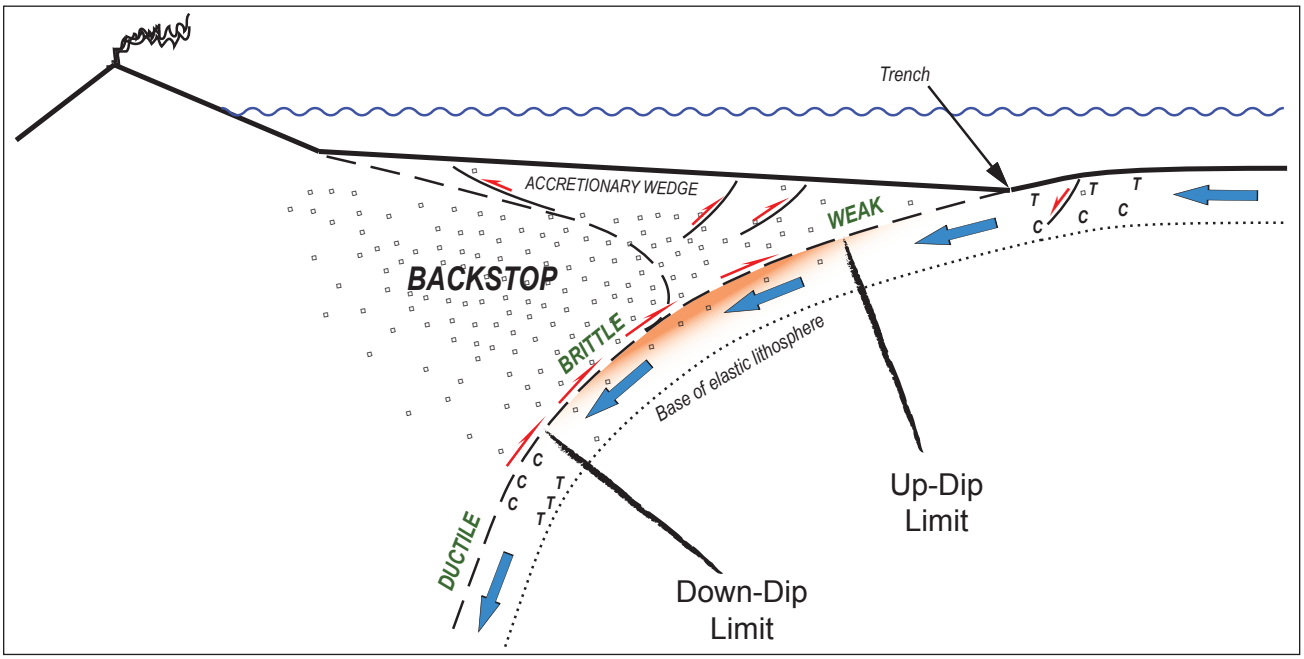

Figure 12. A conceptual model illustrating forearc morphological elements and locations of active faults. The upper-plate seismicity is shown by small squares, extending down to the limit of the brittle region. Approximate locations of the updip and downdip limits of the locked zones are shown by thick black lines. Locations of the intraplate bending-related normal (tensional) and thrust (compressional) events are shown by the letters T and C, respectively. The locked region is marked by orange shading. Ocean surface shown by wavy blue line. Modified after Byrne and others (1988).

Defining the updip and downdip limits of the hypothetical rupture

From the seismological point of view earthquakes tend to occur in the brittle part of the Earth's lithosphere (Byrne and others, 1988). Thus, in addition to analyzing previous great earthquakes, Tichelaar and Ruff (1993) mapped all thrust earthquakes with a magnitude greater than 5.5 along the subduction thrust interface. The coupled region is thought to be capable of generating thrust earthquakes, and mapping their locations could help define the downdip limit of the coupled zone. Locations of events with a magnitude greater than about 6.0 along the Aleutian Island chain and particularly near the Fox Islands, according to Tichelaar and Ruff (1993), are shown in figure 13. It is consequently inferred that seismic coupling along the Aleutians extends down to a depth of 35–41 km (22–26 mi). Refer to Tichelaar and Ruff (1993) for further details.

With the availability of new data and techniques, assessment of the downdip limit of the seismogenic zone can be accomplished by analyzing upper plate seismicity (Ruff and Kanamori, 1983; Tichelaar and Ruff, 1993), modeling the thermal regime of the plates (Chen and Molnar, 1983; Hyndman and others, 1995), analyzing the electrical resistivity (Heise and others, 2013), gravity (Song and Simons, 2003), and magnetic anomalies (Blakely and others, 2005). Refer to Tichelaar and Ruff (1993) and Kaye (2003) for further details.

Temperature and pressure are thought to be the main factors controlling the downdip limit of the coupled region. For example, as temperature and pressure increase with depth, the mechanical properties of the fault zone and surrounding rocks change, and rocks constituting the Earth's lithosphere become more plastic. It is thus theorized that great earthquakes can only occur in regions where certain temperature, pressure, and structural conditions prevail (Oleskevich and others, 1999). Unfortunately, no single physical process alone can explain the observed downdip extent of thrust earthquakes. Modeling techniques typically incorporate many assumptions and uncertainties regarding the mechanical and thermal properties of earth materials and can only provide first-order approximations of locked zones.

A more accurate method of determining locations of locked regions is the analysis of crustal deformation using the techniques of Savage (1983). Over the last decade Fletcher and others (2001), Zweck and others (2002), Cross and Freymueller (2008), and Freymueller and others (2008) have used geodetic observations of strain accumulation to assess

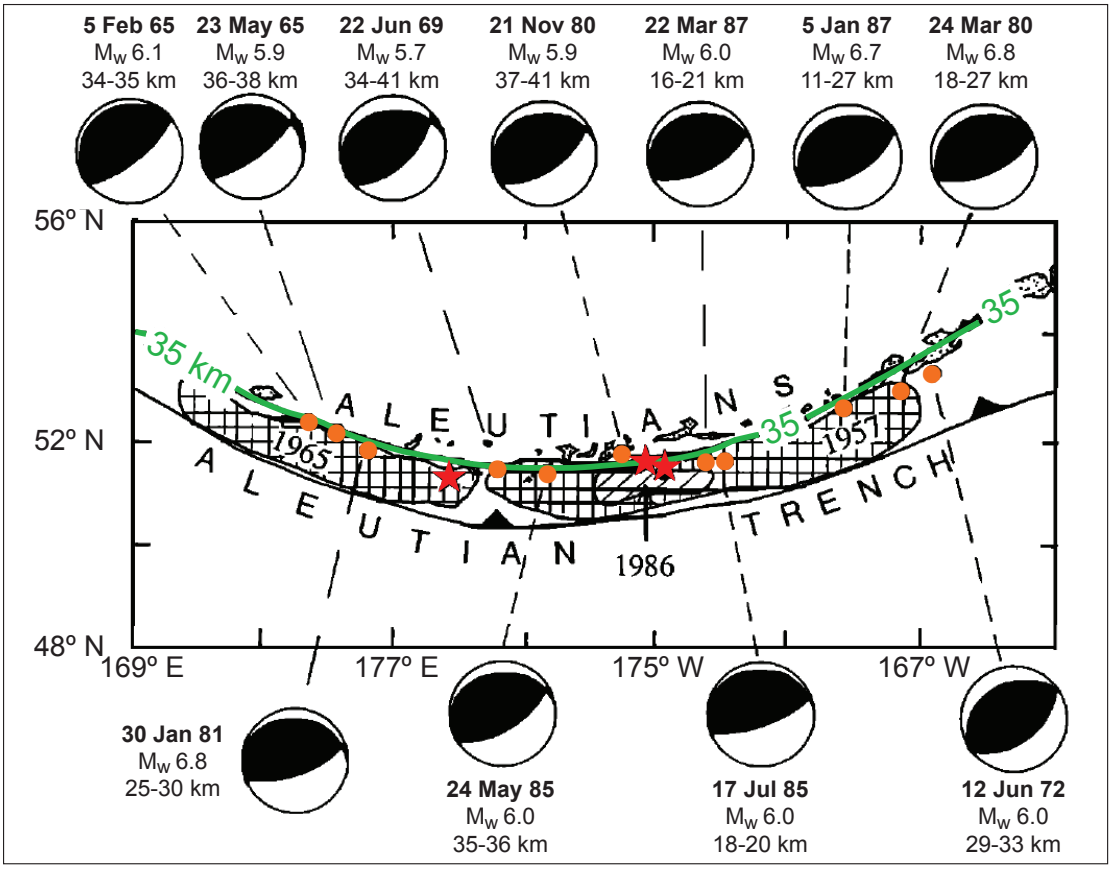

Figure 13. Epicenters of underthrusting earthquakes (solid orange dots) north of the Aleutian trench, with corresponding depths and focal mechanisms (figure 8 by Tichelaar and Ruff, 1993). Epicenters (red stars) and aftershock regions (cross-hatched) of the large earthquakes are also labeled. The 35 km (22 mi) depth contour of the plate interface, as inferred by Tichelaar and Ruff (1993), is shown by a solid green line. Seismic coupling extends down to 35–41 km (22–25 mi).

active deformation processes along the Aleutian subduction zone. The locations of strongly coupled segments derived from geodetic data are in agreement with gravity modeling studies by Song and Simons (2003) for this region.

Modeling results for the Fox Islands region are presented in Cross and Freymueller (2008). The interface between the Pacific and North American plates near the Fox Islands is parameterized by five regions or planes (fig. 14). The coupling ratio is determined for each plane. By definition the zero value is prescribed to planes where there is no coupling between the tectonic plates, while a 100 percent value is associated with planes that are fully locked. The modeling results by Cross and Freymueller (2008) reveal that the tectonic plates near Plane 4 are neither fully locked nor creeping, and hence some shear stress might be accumulating from 30 to 47 km (19–29 mi) depth. The plate coupling coefficient for each plane is marked by percentage values shown in red in figure 14. Note that most magnitude 6+ earthquakes recorded by the AEC from 1980 to 2013 are above 47 km (29 mi) depth. The downdip extent of the estimated plate coupling quantitatively agrees with both the location of the 1957 rupture zone (Boyd and Jacob, 1986) and with the analysis of the upper plate seismicity (Tichelaar and Ruff, 1993). The latter study predicts the downdip limit of the locked region to be at 35–41 km (22–26 mi) depth.

The location of the updip limit of the locked zone is poorly known because of the lack of geodetic data close to the Aleutian trench. For example, the indicated zero coupling at Plane 1 from 7 to 14 km (4.3–8.7 mi) has large modeling uncertainties. Recent studies comparing the Alaska and

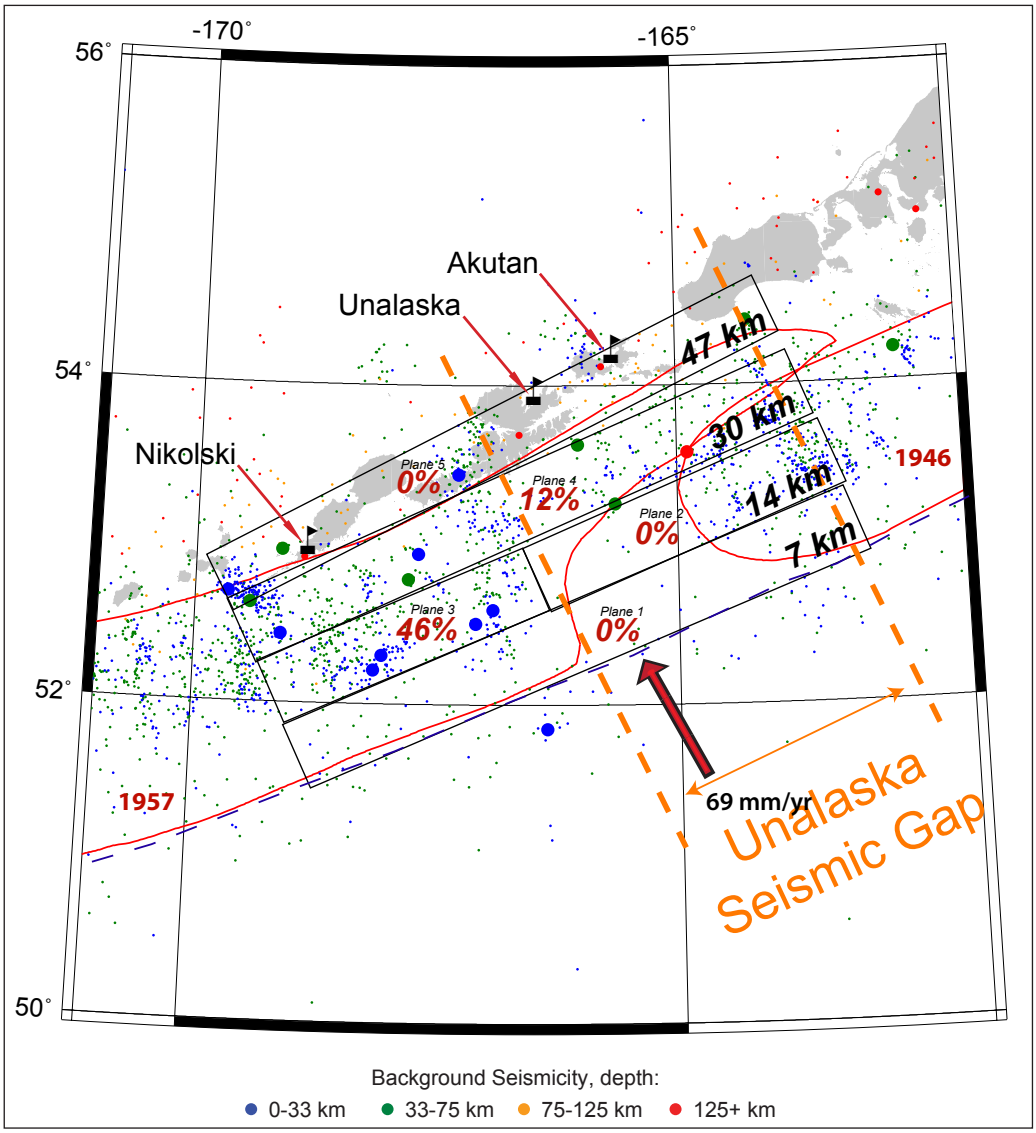

Figure 14. Earthquakes near the Fox Islands (data from the Alaska Earthquake Center catalog, http://www.aeic.alaska.edu/html_docs/db2catalog.html, as of October 2015). Small and large dots correspond to earthquakes with magnitudes less than 6.0 and 6.0 or greater, respectively; the color of the dots indicates the depth of the earthquake. The trench is marked by the dashed blue line. Black rectangles mark locations of fault planes, for which the percent of unit coupling is estimated by Cross and Freymueller (2008). The depth (in kilometers) to the top of each set of fault planes is shown at the eastern end of each plane. Location of the Unalaska Seismic Gap is marked by dashed orange lines.

Tohoku margins (Ryan and others, 2012; Kirby and others, 2013) imply that a hypothetical rupture might propagate to shallow depth, similar to the M_W 9.0 Tohoku earthquake. The occurrence of a Tohoku-type earthquake in the Fox Islands region is partially supported by gravity data (Song and Simons, 2003). These authors show that a predominantly negative trench-parallel gravity anomaly (TPGA) persists in the Unalaska seismic gap and that the negative TPGA coincides with regions where previous great earthquakes (such as the 1960, 1964, 1957, and 1965 events) occurred. Therefore the tectonic plates near the trench might be coupled and capable of rupturing with large slip and hence large seafloor deformation.

In the remainder of this section we develop several hypothetical tsunamigenic earthquake models based on the assessment of locked regions near the Fox Islands. We conduct a sensitivity study to determine a location along the plate interface where an earthquake could trigger a devastating tsunami in Unalaska and Akutan. We focus on the Unalaska Seismic Gap as one of the locations for a potential earthquake (for example, Boyd and Jacob, 1986). For each modeled hypothetical slip distribution on the plate interface we simulate the impact of the potential tsunami in Unalaska and Akutan. Finally we consider a rupture of the Cascadia subduction zone involving the Juan de Fuca plate from mid-Vancouver Island (British Columbia) to northern California, and a Tohoku-type event in the Fox Islands region.

Sensitivity Study

To simulate various earthquakes on the Aleutian megathrust we start with a model of the Alaska–Aleutian plate interface between the subducting and overriding plates. We discretize the plate interface model by Hayes and others (2012) into a number of rectangles ranging from 3 to 6 km (2–4 mi) in the along-strike direction of the plate interface. The upper and lower edges of each rectangle coincide with 1 km (0.6 mi) depth contours of the reconstructed plate interface (fig. 15). Next, coseismic ground deformation is computed for all rectangles, called subfaults, using formulas developed by Okada (1985). Each hypothetical earthquake scenario is developed by first prescribing a general pattern of slip distribution along the interface, then computing the slip at the center of each subfault using seismic moment as a constraint. Similar to Geist and Dmowska (1999) and Sobolev and others (2007), we used theoretical slip distribution formulas by Freund and Barnett (1976) to model coseismic slip on the fault. The most important parameters in the Freund and Barnett formulas are the upper and lower boundaries of the hypothetical rupture in the local downdip direction. These boundaries prescribe a range of depths at which the

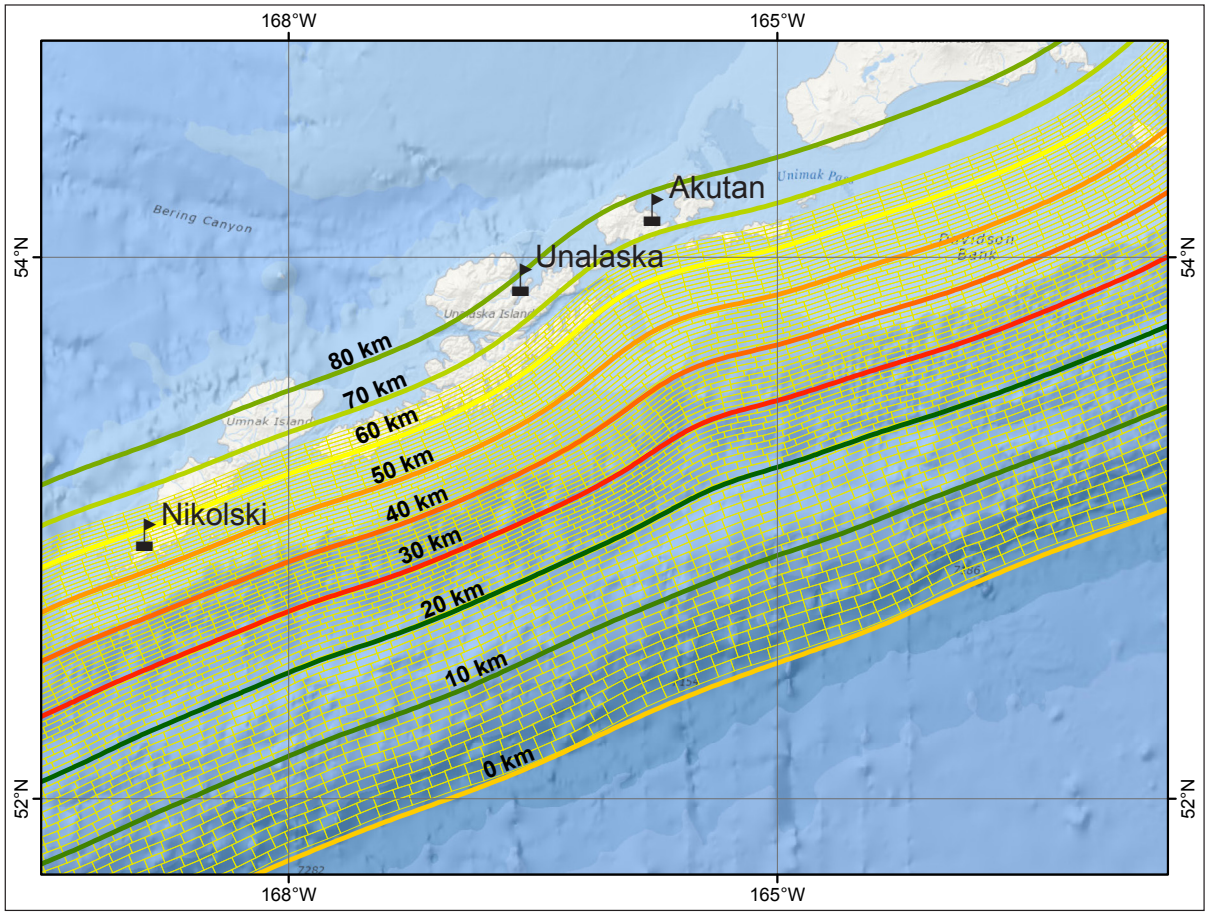

Figure 15. Discretization of the plate interface model into a set of rectangles used to compute the coseismic vertical displacement by formulas developed by Okada (1985). The colored lines mark depth contours (in kilometers) of the reconstructed plate interface.

hypothetical earthquake would occur. Note that to consider geophysically plausible scenarios the assumed downdip and updip boundaries must conform with the above-mentioned estimates for the locked zones near the Fox Islands.

For example, we develop six hypothetical cases of the slip distribution (cases A–F) for M_W 8.2 earthquakes near the Fox Islands (fig. 16). Slip at the center of each subfault is in meters and is color coded. Depth contours of the plate interface models are in kilometers and shown by red lines; Unalaska and Akutan are marked by red dots. The relative slip distribution for all six cases is identical: uniform in the along-strike direction with tapering at the ends of the rupture, and a bell-type slip curve in the downdip direction with the maximum slip at about 40 km (25 mi) depth. The only difference between the considered cases is in the along-strike location of the hypothetical slip with respect to the plate interface. In case A the maximum slip is across from the western tip of Unalaska Island, while in case F the maximum slip is at the western tip of Unimak Island. The vertical deformation for each case is displayed in figure 17. Blue shading indicates ground subsidence while red shading marks areas of uplift.

There are no geologic or paleoseismological constraints on the modeled ground subsidence or uplift near the Fox Islands. In previous tsunami modeling studies for Valdez (Nicolsky and others, 2013) and Cordova (Nicolsky and others, 2014) some preliminary scenarios of the ground deformation could be eliminated by comparison with estimates of previous great earthquake ground deformation obtained from paleoseismic studies. In this report we assume that all cases considered are geologically plausible. For each case we simulate the water dynamics near the waterfront in Unalaska and Akutan; simulated water levels in Unalaska and Akutan are shown in figure 18. Hypothetical earthquakes based on cases C and D are associated with producing the highest waves in Unalaska, while cases C, D, and E generate the highest waves in Akutan. Scenarios with slip along the eastern end of Unalaska Island are the most sensitive for Unalaska, while scenarios with slip in the Krenitzin Island region are the most sensitive for Akutan. We emphasize that maximum amplitudes for the simulated waves occur almost simultaneously (such as in cases C and D for Unalaska) and thus a simultaneous rupture of the most sensitive segments probably will not result in a mutual cancellation of the waves arriving from the neighboring segments.

In an additional sensitivity study we conduct a series of numerical experiments relative to the downdip location of slip. In each experiment we use a slip distribution similar to that modeled in hypothetical rupture cases C and D described above while varying the location of the slip distribution in the downdip direction. Figure 19 illustrates five different slip distributions used in this sensitivity study. Between any two consecutive cases the hypothetical rupture is offset by about 10 km (6.2 mi) in the downdip direction and is located across from the eastern part of Unalaska Island, which is the area most sensitive to slip for Unalaska/Dutch Harbor. To distinguish the current cases from the ones considered in the previous sensitivity study we label the cases resulting from the second study with Roman numerals. Case I corresponds to a rupture at 50 km (31 mi) depth, case II corresponds to a rupture at 40 km (25 mi) depth, case III corresponds to a rupture at 30 km (18.6 mi) depth, and case IV corresponds to a rupture at 20 km (12.5 mi) depth. Finally, case V simulates a scaled-down SAFRR-type rupture between 3 and 40 km (2–25 mi) depth with maximum slip at the shallowest depths, similar to the hypothetical rupture considered by Kirby and others (2013). The vertical deformation associated with each case is shown in figure 20.

After computing the water dynamics near Unalaska and Akutan for the five cases (fig. 21), we find that the modeling results indicate that cases I and II result in the most significant subsidence (fig. 20) and maximum simulated wave height in Unalaska (fig. 21). On the basis of the results of both the hypothetical slip distribution (cases A–F) and the downdip sensitivity studies (cases I–V), we find that the most sensitive areas are cases C, D, I, and II for Unalaska, and cases C, D, E, I, and II for Akutan. Therefore we construct a maximum credible scenario[6] for Unalaska and Akutan by assuming a maximum slip near the most sensitive areas, that is, around cases C, D, E, I, and II. The maximum slip is based on the magnitude of the hypothetical earthquake.

Scenario 1. M_W 9.1 earthquake in the Fox Islands region based on hypothetical cases C, D, E, I, and II

This event is a hypothetical M_W 9.1 earthquake rupturing the Aleutian megathrust with maximum slip at the eastern part of the 1957 aftershock area. The slip is uniformly distributed in the along-strike direction of the plate interface from Akutan Island to Unalaska Island and is tapered on both ends of the rupture. The maximum slip of 37 m (121 ft) is at a depth of 40–45 km (25–28 mi). The proposed slip distribution is shown in figure 22a; vertical coseismic deformations for this scenario are shown in figure 23a.

Although the above sensitivity study implies that scenario 1 might result in the maximum wave height in Unalaska and Akutan, we assume some important simplifications that could reduce the accuracy of the sensitivity study. In particular we assume that non-linear effects in the water dynamics could be omitted. Therefore to ensure that we do not accidentally omit other relevant scenarios, we supplement scenario 1 with two similar scenarios, scenarios 2 and 3. In the latter scenarios the maximum slip is less than in scenario 1 but it is also located in the most sensitive area for generating large waves for both for Unalaska and Akutan. Other scenarios are based on the SAFRR scenario or other proposed great earthquake scenarios. Table 2 lists different variations of the maximum credible scenarios in this study. Finally, note that the considered scenarios show the sensitivity of runup in Unalaska and Akutan with respect to the slip distribution and are valuable in determining the tsunami hazard zone.

[6]A realistic, very complex slip distribution is not available from this modeling study. The presented scenarios try to capture the maximum credible scenarios and provide a starting point for development of more complex models.

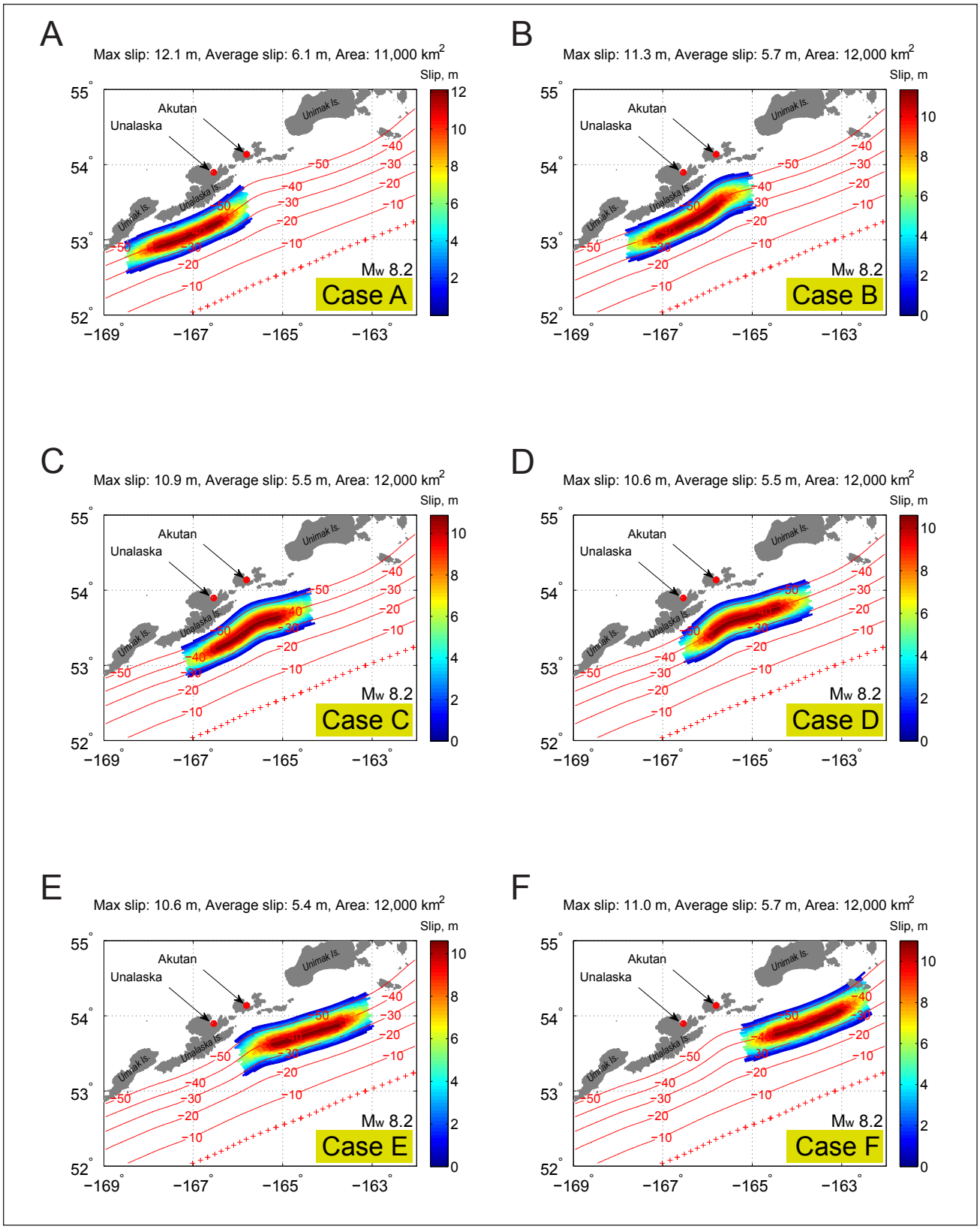

Figure 16. Assumed slip distribution along the plate interface for cases A through F, modeling a M_w 8.2 rupture along the Fox Islands. The slip location varies in the along-strike direction of the plate interface, but the slip distribution patch is the same for all six cases—uniform in the along-strike direction and slightly tapered at both ends of the potential rupture. The slip is localized at 40 km (25 mi) depth. The parameterization of slip in the along-dip direction is based on the analytical approximation by Freund and Barnett (1976). Red lines indicate depth contours in kilometers; the Alaska–Aleutian trench is marked with red crosses.

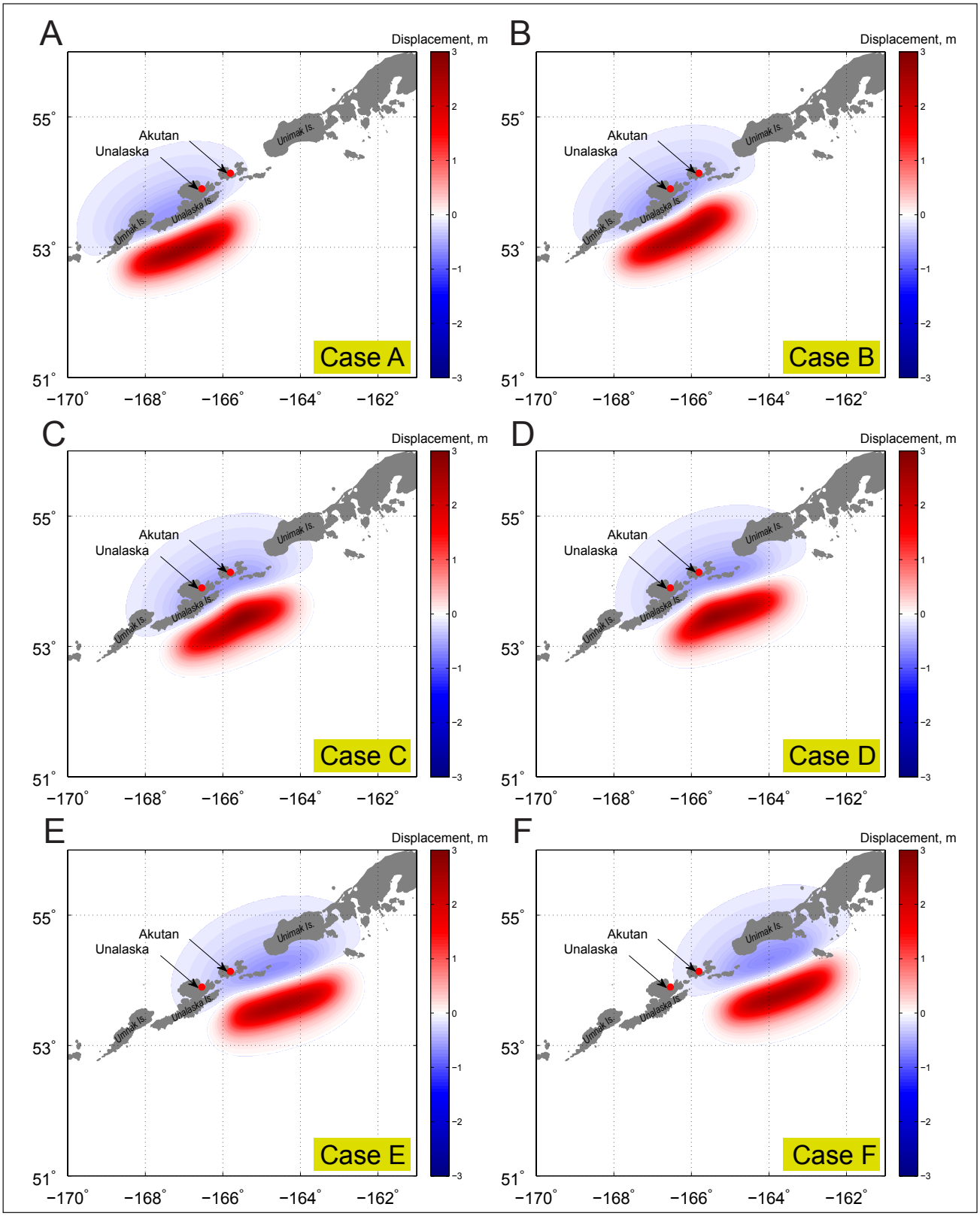

Figure 17. Computed vertical ground-surface deformation related to cases A through F shown in figure 16. Blue areas are associated with coseismic ground subsidence; areas of uplift are shown in red.

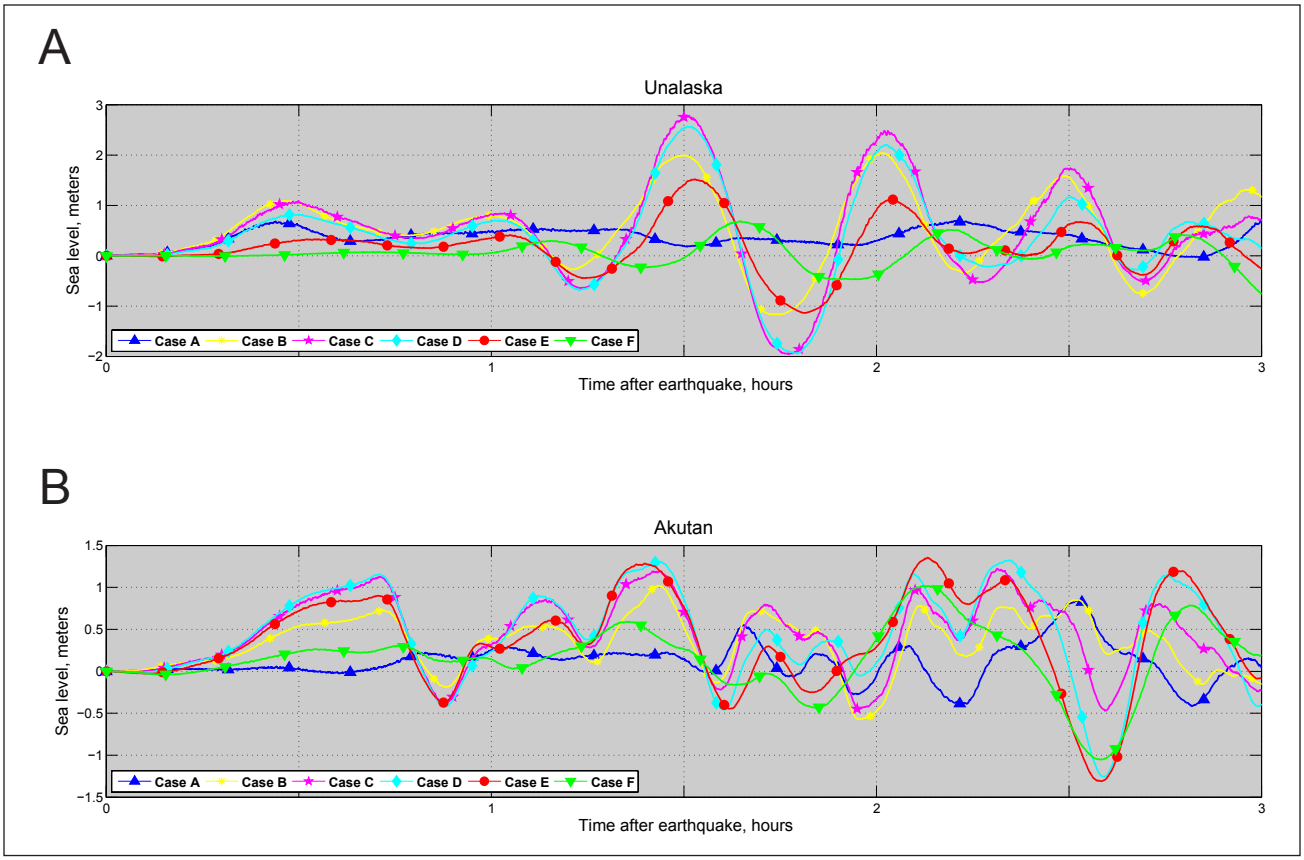

Figure 18. Modeled water-level dynamics in (A) Unalaska and (B) Akutan for the ground-surface deformations shown in figure 17.

In the downdip direction the slip is parameterized using the specifications of Freund and Barnett (1976). The average and maximum slip as well as the rupture area for scenarios 1–3 are set according to the scaling relations of Papazachos and others (2005) and Moss and Travasarou (2006). Although there are other alternative scaling relations (Blaser and others, 2010; Murotani and others, 2013; Strasser and others, 2010) the slip for the considered scenarios in the most sensitive location of the plate interface for Unalaska and Akutan is assumed to be the maximum credible slip of 35–40 m (115–131 ft), which is consistent with other modeling studies for this region (for example, Butler, 2014). We emphasize that the scaling relationships primarily define the western lateral extent of the hypothetical rupture, which plays a minor role in generating tsunamis in Unalaska and Akutan, and thus the considered scenarios are thought to produce the maximum credible wave height at both locations.

Scenario 2. M_W 9.0 earthquake in the Fox Islands region based on hypothetical cases C, D, E, I, and II

This event is a hypothetical M_W 9.0 earthquake rupturing the Aleutian megathrust. The maximum slip of 30 m (98 ft) is in the eastern part of the 1957 aftershock area at a depth of 40–45 km (25–28 mi). The proposed slip distribution is shown in figure 22b; vertical coseismic deformations for this scenario are shown in figure 23b.

Scenario 3. M_W 8.8 earthquake in the Fox Islands region based on hypothetical cases C, D, I, and II

This event is a hypothetical M_W 8.8 earthquake rupturing the Aleutian megathrust. The maximum slip of 30 m (98 ft) is at the eastern part of the 1957 aftershock area at a depth of 40–50 km (24.9–31.1 mi). The proposed slip distribution is shown in figure 22c; vertical coseismic deformations for this scenario are shown in figure 23c.

In view of the recent M_W 9.0 earthquake off the Pacific coast of Tohoku in 2011, we consider similar events along the Aleutian megathrust (David Scholl, USGS, oral commun., 2013). During the Tohoku earthquake a large amount of slip occurred between the subducting and overriding plates near the Japan trench (Fujii and others, 2011; Shao and others, 2011).

Scenario 4. M_W 9.0 earthquake according to the SAFRR project

The USGS Science Application for Risk Reduction (SAFRR) project, in collaboration with NOAA and State of California agencies, has developed a plausible hypothetical tsunami scenario (Kirby and others, 2013) to describe the impacts of a tsunami generated by an earthquake in the Alaska Peninsula region (Ross and others, 2013). The USGS Tsunami Source Working Group defined the

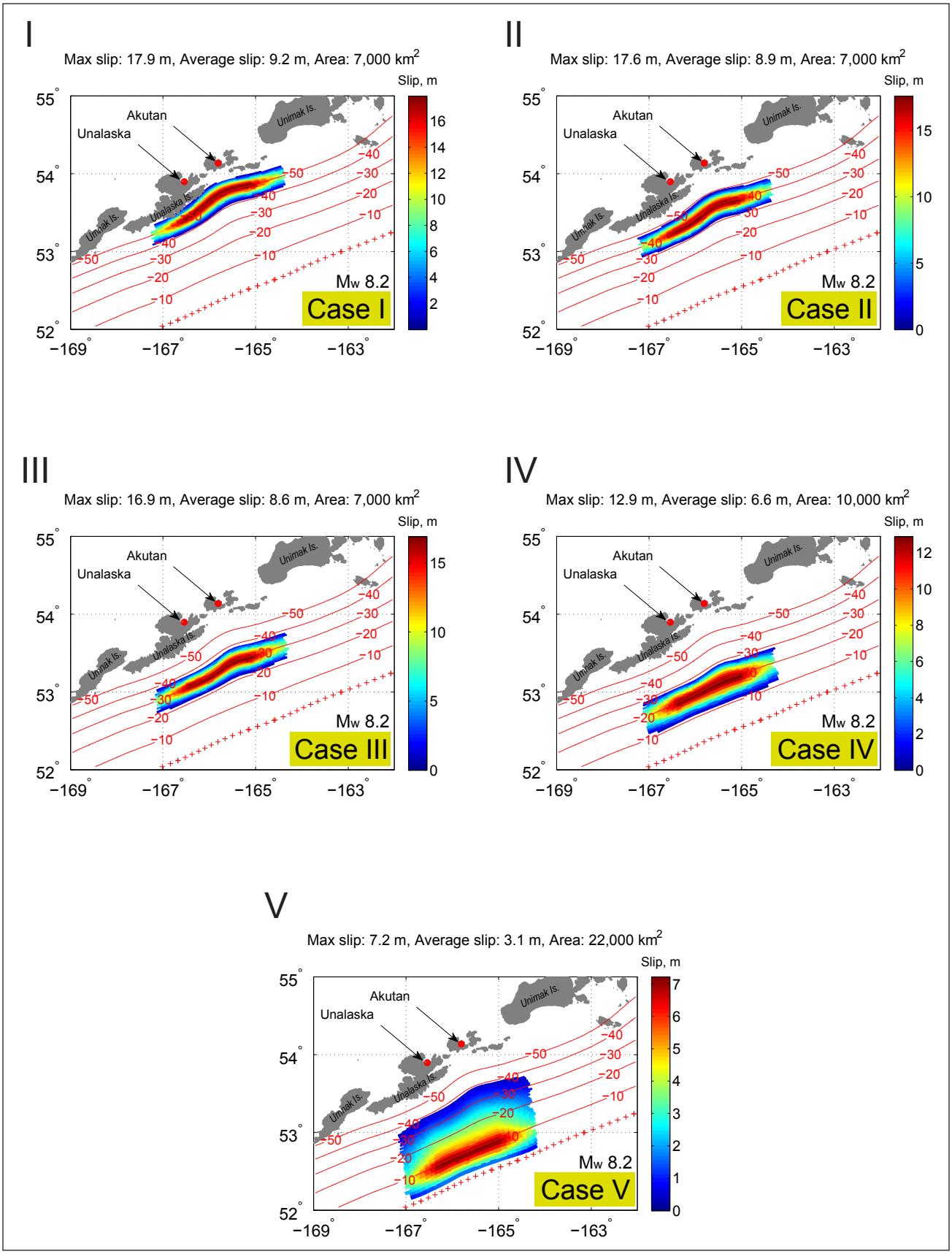

Figure 19. Assumed slip distribution along the plate interface for cases I through V, modeling a M_W 8.2 rupture near cases C and D, shown in figure 16. The slip location varies in the downdip direction of the plate interface while preserving the same patch configuration. Red lines are associated with the depth contours in kilometers; the Alaska–Aleutian trench is marked with red crosses.

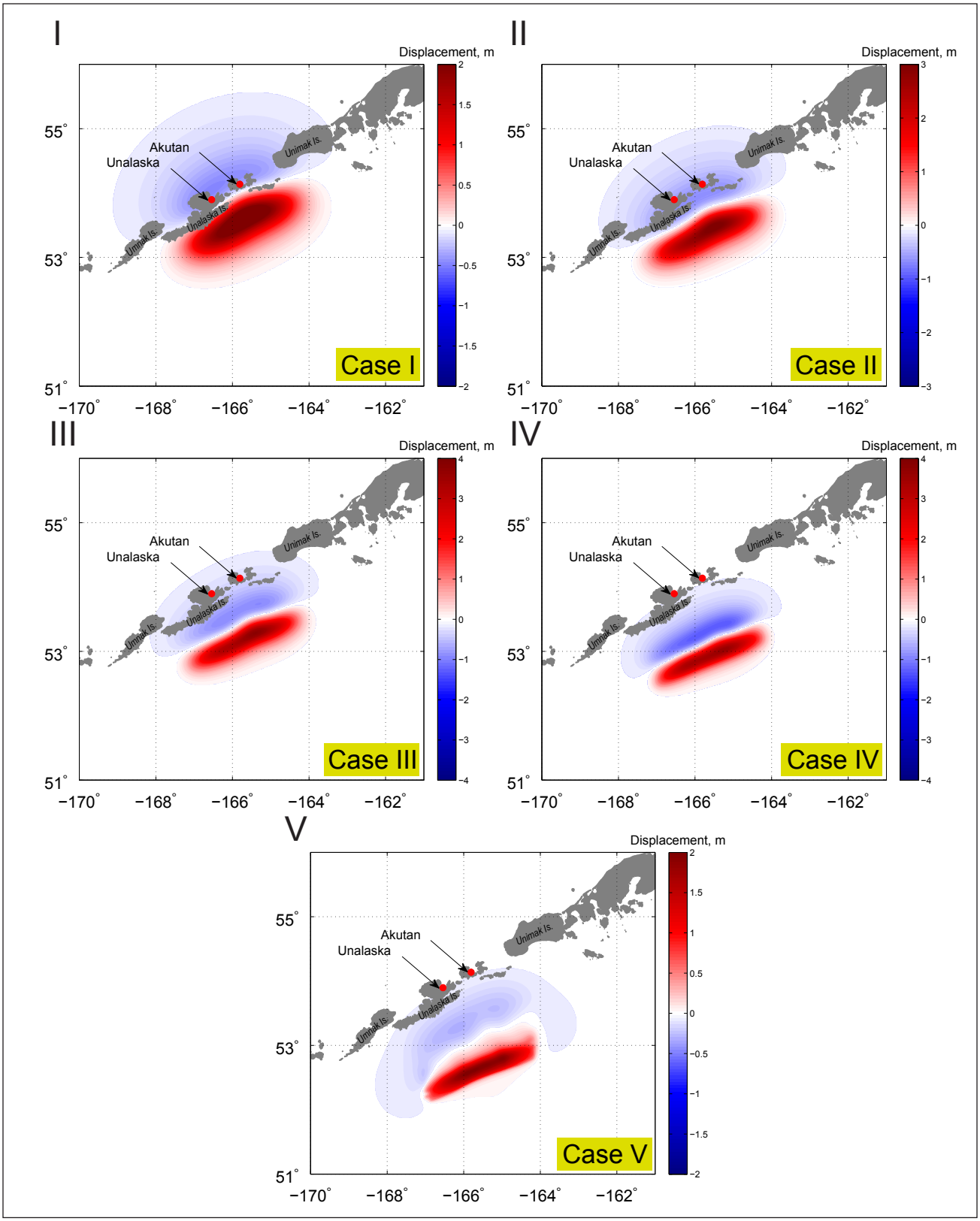

Figure 20. Computed vertical ground-surface deformation related to cases I through V shown in figure 19. Blue areas are associated with coseismic ground subsidence; areas of uplift are shown in red.

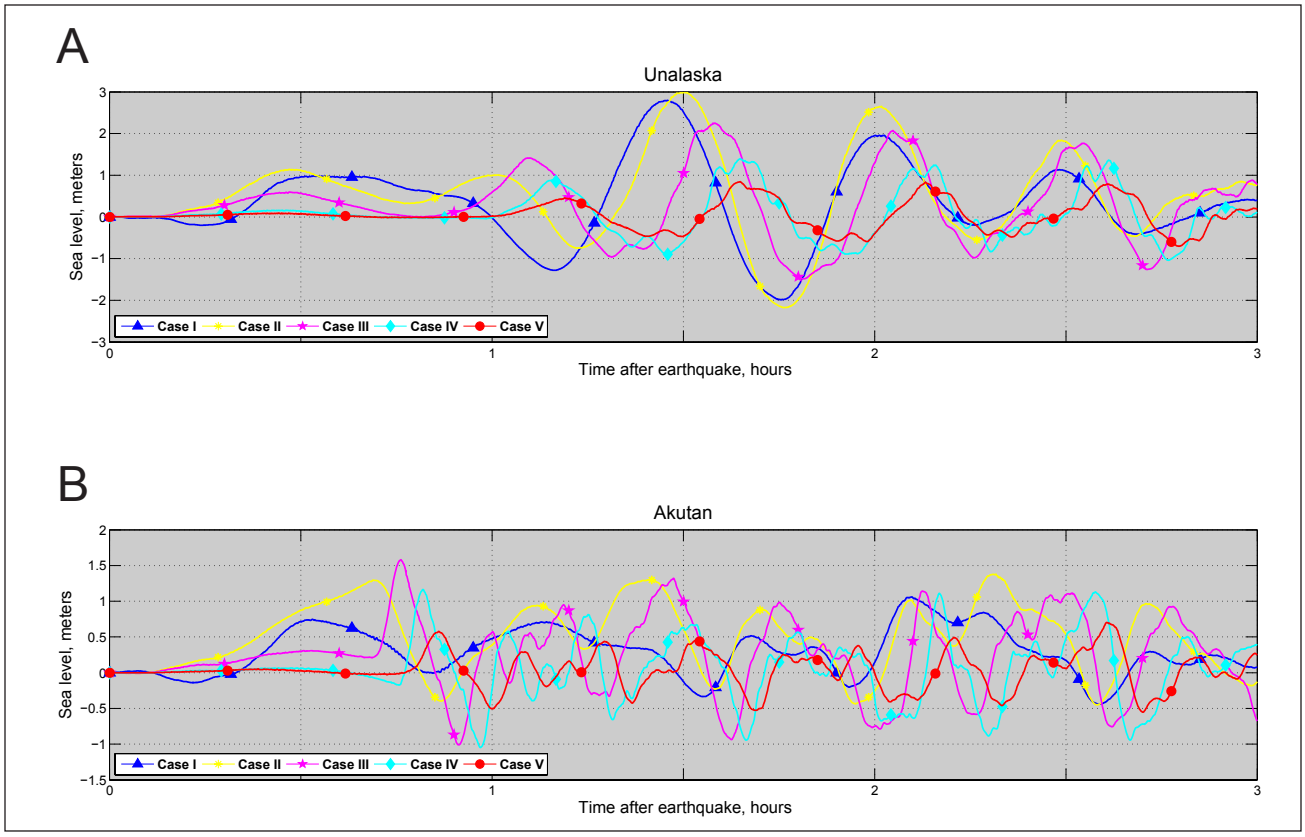

Figure 21. Modeled water-level dynamics in (A) Unalaska and (B) Akutan for the ground-surface deformations shown in figure 20.

scenario source as a M_W 9.0 earthquake similar to the Tohoku 2011 event but located between the Shumagin Islands and Kodiak Island. The rupture area, represented by 56 subfaults, is about 350 × 200 km (217 × 124 mi) with an average slip of 15.7 m (51.5 ft) and a maximum slip of 75 m (246 ft). Larger values of slip are near the trench, as for the Tohoku earthquake. The slip distribution is shown in figure 22d; the coseismic deformations for this scenario are shown in figure 23d.

Scenario 5. M_W 9.0 SAFRR-type earthquake in the Fox Islands region

In this scenario we assume that the slip distribution in the downdip direction is the same as that in scenario 4, where greater slip occurs closer to the trench but is shifted westward along the trench. The slip is distributed almost uniformly along the strike except for the edges of the rupture where it tapers. The rupture is centered across from the Fox Islands and its lateral extent is chosen to be about the same as that in scenario 4. The proposed slip distribution is shown in figure 22e; vertical coseismic deformations for this scenario are shown in figure 23e.

Scenario 6. M_W 9.0 SAFRR-type earthquake in the Krenitzin Island region

In this scenario we assume that the slip distribution in the downdip direction is the same as that in scenario 4, where the greater slip occurs closer to the trench but is shifted westward along the trench (farther west than scenario 5). The slip is distributed almost uniformly along strike except for the edges of the rupture, where it tapers. The rupture is centered across from the Krenitzin Islands and its lateral extent is chosen to be about the same as that in scenario 4. The proposed slip distribution is shown in figure 22f; vertical coseismic deformations for this scenario are shown in figure 23f.

A recent study by Butler and others (2014) describes a layer of sand that was discovered in the Makauwahi sinkhole on the Island of Kaua'i, Hawai'i. The origin of this layer is attributed to inundation of the sinkhole by a giant paleotsunami following a M_W 9+ earthquake in the eastern Aleutian Islands. It is hypothesized that the great earthquake was located between the source regions of 1946 and 1957 earthquakes and had a magnitude larger than 9.25. Refer to Butler (2012) for an in-depth examination of previous great Aleutian earthquakes and tsunamis impacting Hawai'i. In subsequent research Butler (2014) considered several hypothetical events with a 35 m (115 ft) displacement on the megathrust and up to a 50 m (164 ft) displacement near the trench. Thus, in addition to the above-mentioned scenarios, we consider two scenarios as follows.

Scenario 7. M_W 9.2 East Aleutian earthquake

In this scenario we assume 35 m (115 ft) slip on the plate interface and up to a 46 m (151 ft) slip near the trench. The slip is distributed almost uniformly along the strike except

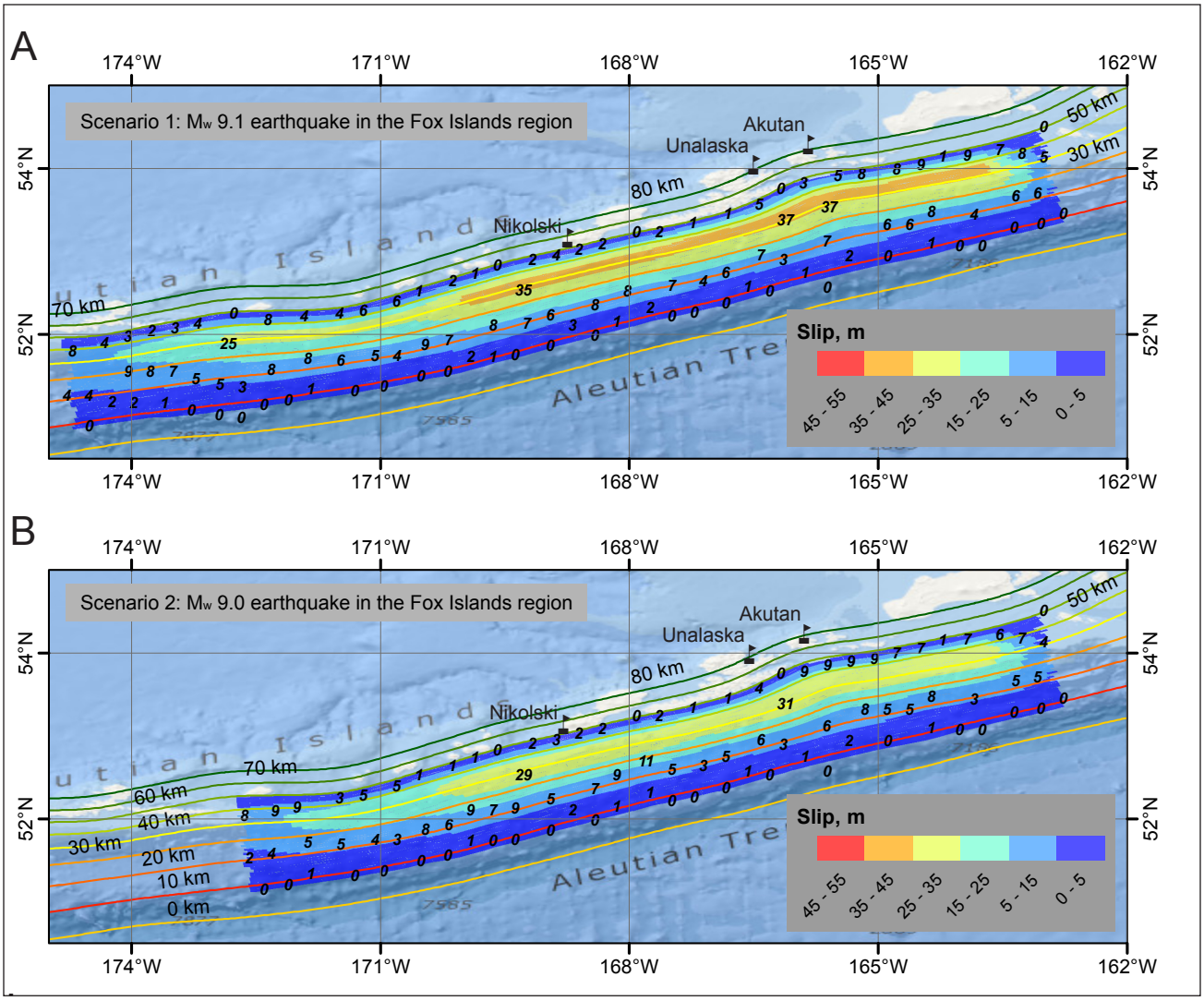

Figure 22. Proposed slip distribution along the plate interface for scenarios 1–8; note that slip distributions are not provided for scenarios 9 and 10. **A.** Scenario 1, hypothetical M_W 9.1 earthquake in the Fox Islands region. **B.** Scenario 2, hypothetical M_W 9.0 earthquake in the Fox Islands region. The proposed slip distribution along the plate interface is uniform in the along-strike direction and is slightly tapered at both ends of the potential rupture. Slip values in meters are marked by small black labels. The depth contours of the Aleutian interface are shown by colored lines.

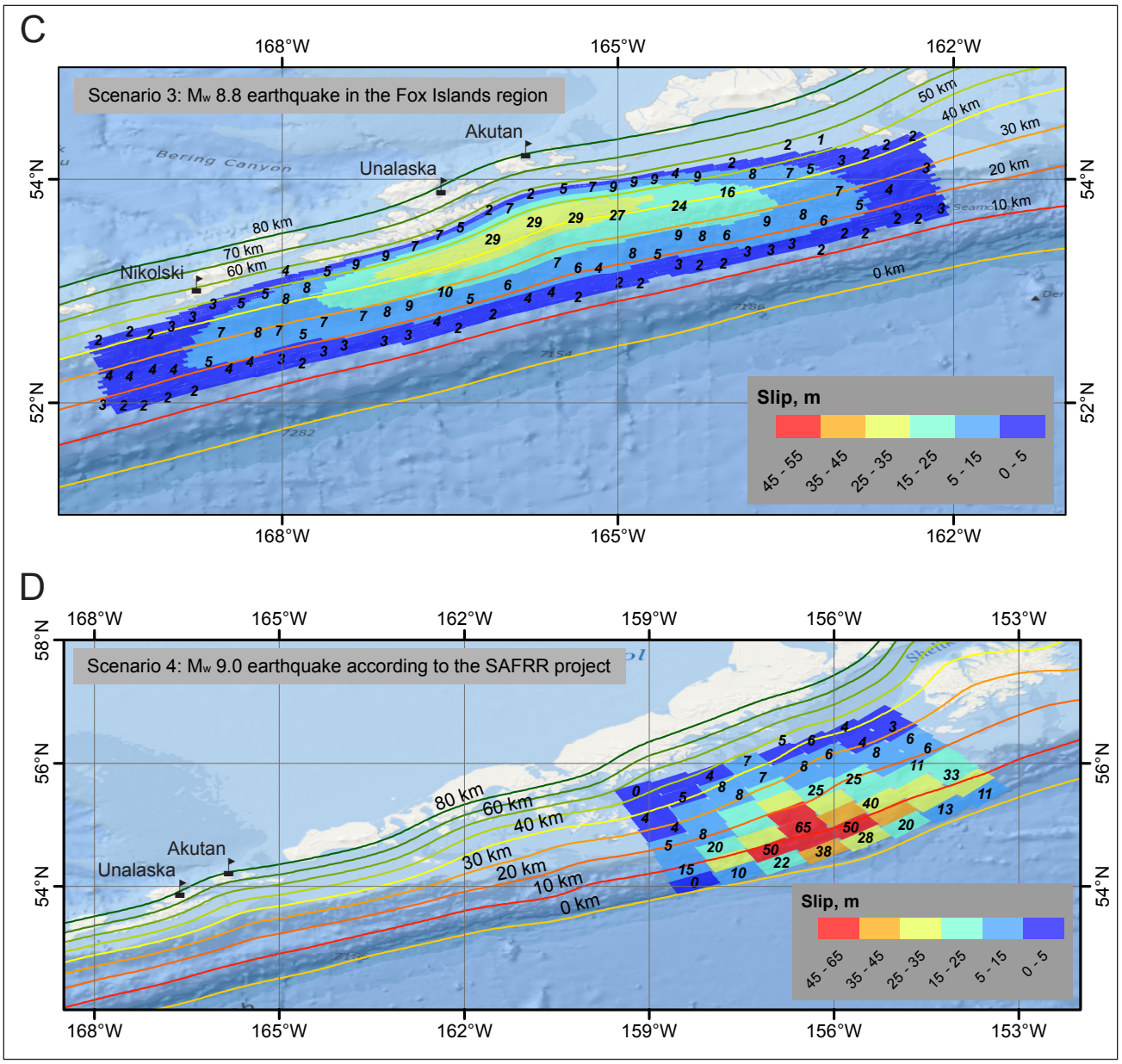

Figure 22 (cont.). Proposed slip distribution along the plate interface for scenarios 1–8; note that slip distributions are not provided for scenarios 9 and 10. **C.** Scenario 3, hypothetical M_W 8.8 earthquake in the Fox Islands region. **D.** Scenario 4, hypothetical M_W 9.0 earthquake according to the SAFRR project. The proposed slip distribution along the plate interface is uniform in the along-strike direction and is slightly tapered at both ends of the potential rupture. Slip values in meters are marked by small black labels. The depth contours of the Aleutian interface are shown by colored lines.

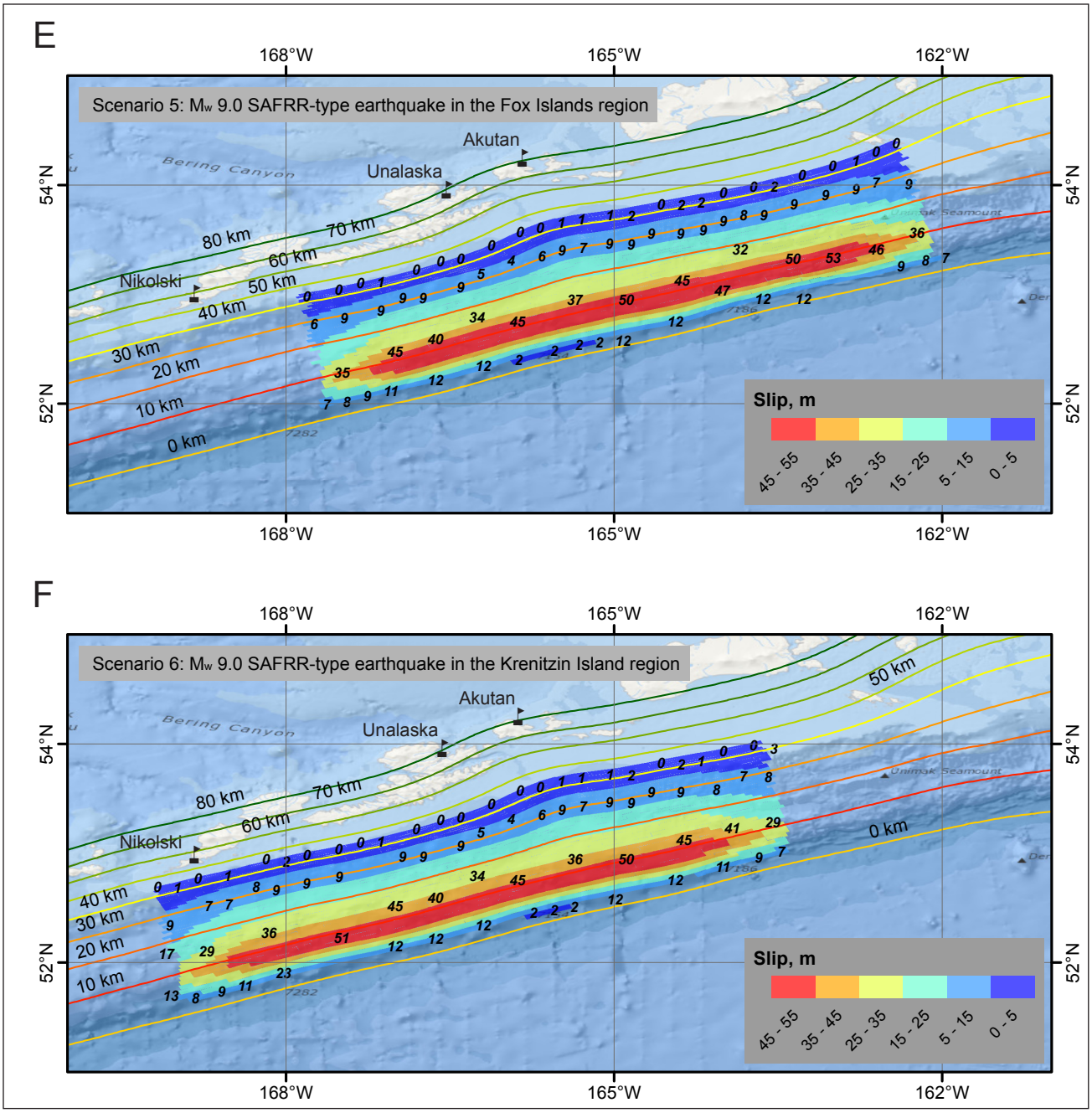

Figure 22 (cont.). Proposed slip distribution along the plate interface for scenarios 1–8; note that slip distributions are not provided for scenarios 9 and 10. **E.** Scenario 5, hypothetical M_W 9.0 SAFRR-type earthquake in the Fox Islands region. **F.** Scenario 6, hypothetical M_W 9.0 SAFRR-type earthquake in the Krenitzin Island region. The proposed slip distribution along the plate interface is uniform in the along-strike direction and is slightly tapered at both ends of the potential rupture. Slip values in meters are marked by small black labels. The depth contours of the Aleutian interface are shown by colored lines.

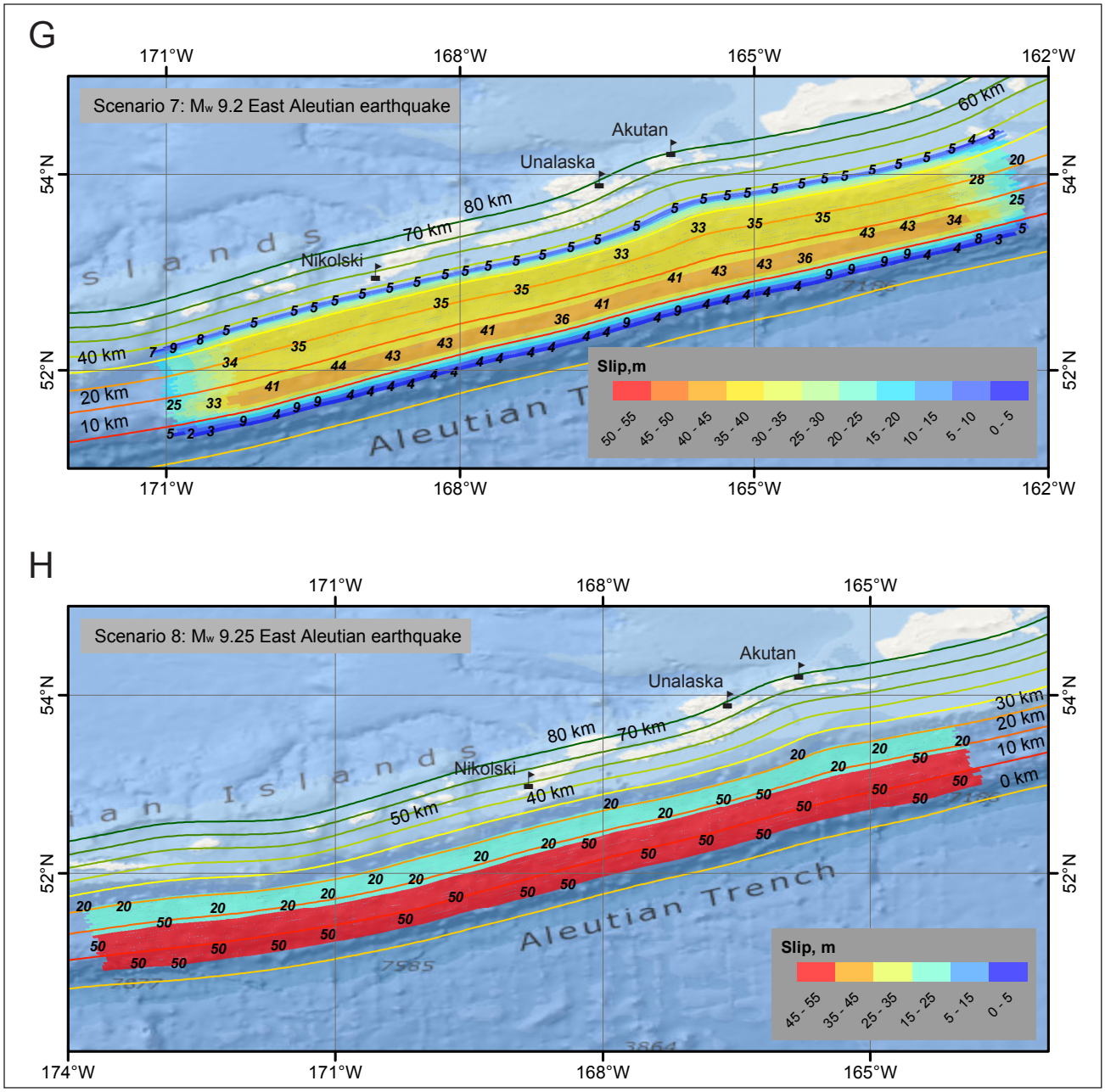

Figure 22 (cont.). Proposed slip distribution along the plate interface for scenarios 1–8; note that slip distributions are not provided for scenarios 9 and 10. **G.** Scenario 7, hypothetical M_W 9.2 East Aleutian earthquake. **H.** Scenario 8, hypothetical M_W 9.25 East Aleutian earthquake. The proposed slip distribution along the plate interface is uniform in the along-strike direction and is slightly tapered at both ends of the potential rupture. Slip values in meters are marked by small black labels. The depth contours of the Aleutian interface are shown by colored lines.

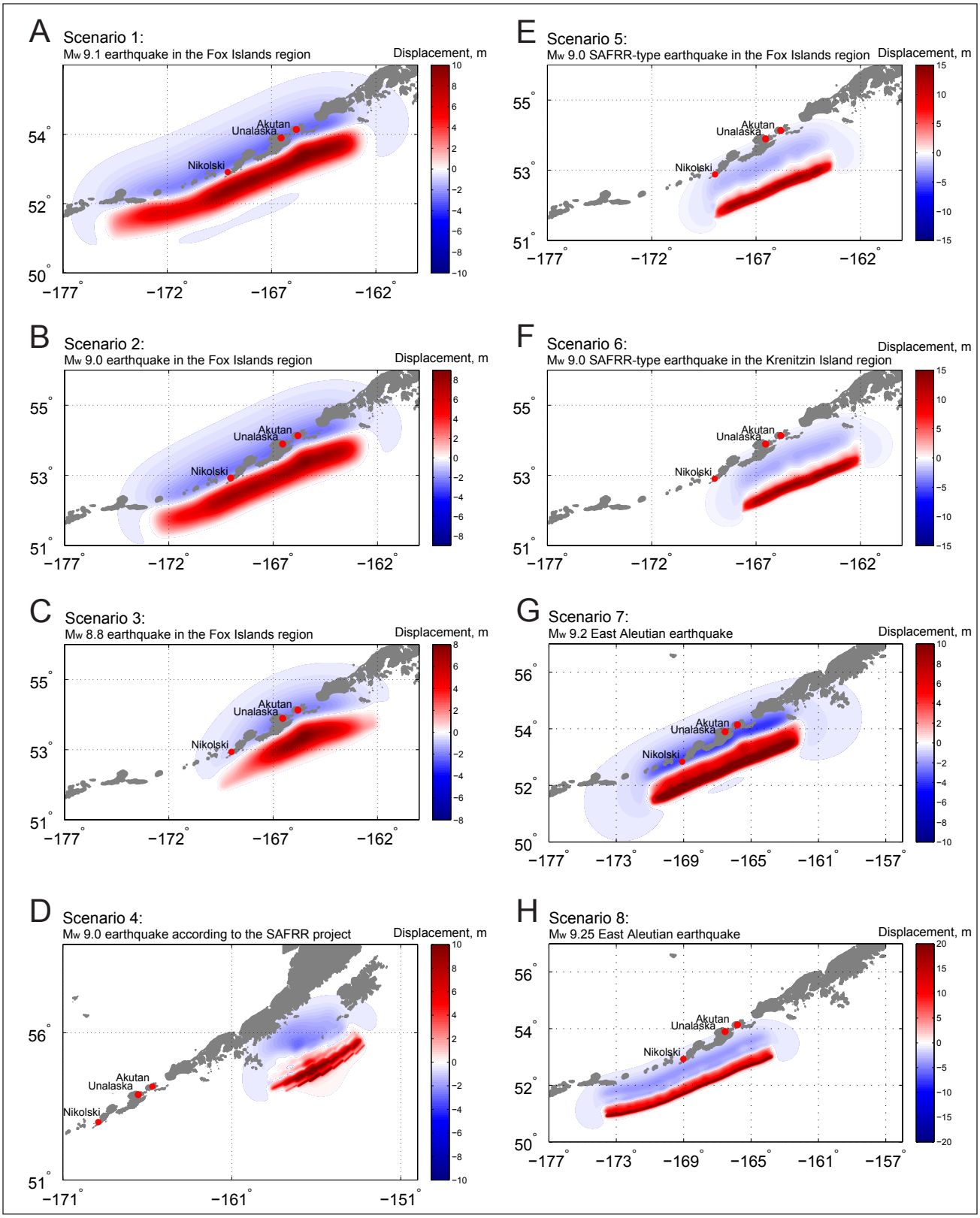

Figure 23. Computed vertical ground-surface deformation related to the proposed slip distributions for scenarios 1–8. Blue shaded areas are associated with coseismic ground subsidence; areas of uplift are shown in red.

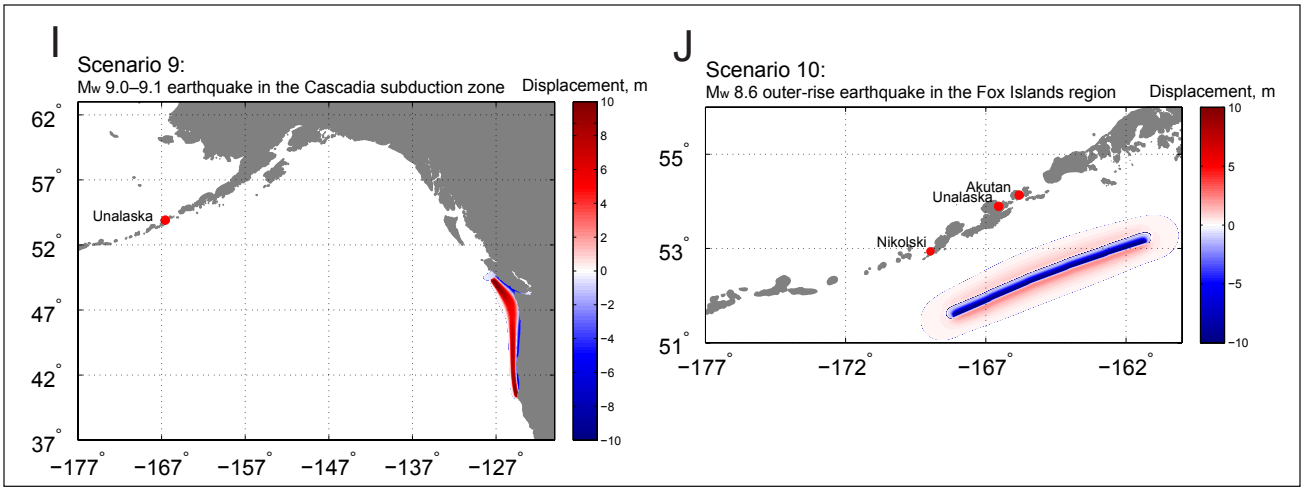

Figure 23 (cont). Computed vertical ground-surface deformation related to scenarios 9 and 10. Blue shaded areas are associated with coseismic ground subsidence; areas of uplift are shown in red. Note that graphical representation of slip distributions is not provided for scenarios 9 and 10.

Table 2. All hypothetical scenarios used to model tsunami runup in Unalaska and Akutan.

Tectonic Scenarios		Depth range (km)	Maximum slip depth range (km)	Maximum slip (m)	Maximum Subsidence (m)	Maximum Uplift (m)	Vertical displacement (m)	
							Unalaska	Akutan
1	Mw 9.1 earthquake, Fox Islands region	8–50	40–45	37	2.9	10.8	-2.8	-2.6
2	Mw 9.0 earthquake, Fox Islands region	8–50	40–45	30	2.4	8.8	-2.3	-2.1
3	Mw 8.8 earthquake, Fox Islands region	14–56	40–50	30	2.0	8.4	-2.0	-1.8
4	Mw 9.0 earthquake according to the SAFRR project	8–54	11–14	55–65	2.8	14.8	-0.1	-0.1
5	Mw 9.0 SAFRR-type earthquake, Fox Islands region	8–54	10–12	53	2.4	14.3	-0.4	-0.4
6	Mw 9.0 SAFRR-type earthquake, Krenitzin Island region	8–54	10–12	53	2.4	14.9	-0.4	-0.4
7	Mw 9.2 East Aleutian earthquake	7–50	12–18	44	4.0	14.4	-2.5	-2.4
8	Mw 9.25 East Aleutian earthquake	5–31	5–18	50	4.1	21.8	-0.5	-0.4
9	Mw 9.0–9.1 earthquake, Cascadia subduction zone	Wang & others (2003)	Wang & others (2003)	35–45	7.5	10.9	0.0	0.0
10	Mw 8.6 outer-rise earthquake, Fox Islands region	2–23	2–23	25	14.3	2.5	-0.1	-0.1

for the edges of the rupture, where it tapers. The proposed slip distribution is shown in figure 22g; vertical coseismic deformations for this scenario are shown in figure 23g.

Scenario 8. M_W 9.25 East Aleutian earthquake

In this scenario similar to Butler (2014) we assume a 20 m (65 ft) slip on the plate interface between the 17.9 km (11.1 mi) and 30.8 km (19.1 mi) depth, and up to a 50 m (164 ft) slip near the trench, that is, between 5 km (3.1 mi) and 17.9 km (11.1 mi) depth. The slip is distributed uniformly along strike. According to the USGS letter (Butler, 2014, Appendix 2), this so-called 50/20 slip model "is starting to approach that more realistic model" that could occur in the Aleutian Islands. The proposed slip distribution is shown in figure 22h; vertical coseismic deformations for this scenario are shown in figure 23h.

Paleoseismic records for the Pacific Northwest region of the western U.S. reveal that great tsunamigenic earthquakes repeatedly occur in the Cascadia subduction zone, with irregular intervals averaging about 500 years (Atwater, 1987). The latest trans-Pacific tsunami generated by an earthquake at Cascadia occurred in January 1700 (Satake and others, 1996; Atwater and others, 2005). The impact of this tsunami on Alaska coastal communities was not documented, likely due to low population density along the Alaska coast at that time. Multiple models of Cascadia subduction zone ruptures are suggested by Satake and others (2003), Priest and others (2009), and in references therein. These models describe hypothetical coseismic displacement fields with various levels of detail. Because a Cascadia subduction zone earthquake is considered an intermediate-field tsunami source to the southeastern Alaska coast, a relatively simple "worst case, but credible" rupture of the Cascadia subduction zone is used in this report.

Scenario 9. Rupture of the Cascadia zone including the entire megathrust between British Columbia and northern California

Wang and others (2003) conclude that the downdip limit of the rupture in the 1700 Cascadia earthquake couldn't be constrained using the tsunami heights in Japanese historical records. The authors suggest a conservative approach for Cascadia coseismic deformations, assuming that full coseismic rupture takes place over the entire locked zone and the slip decreases linearly downdip halfway into the present effective transition zone. The most recently updated, and probably more reasonable, model assumes that the slip distribution in the downdip direction is bell-shaped (Witter and others, 2011), which is different from what was used to model the coseismic deformation shown in figure 14 of Wang and others (2003). In this report the assumed M_W 9 rupture recovers 1,200 years' worth of plate convergence with about 36 m (118 ft) of maximum slip (Witter and others, 2011). The vertical coseismic deformations for this scenario are shown in figure 23i.

Great outer-rise earthquakes such as the March 2, 1933, Sanriku M_W 8.4 event (Kanamori, 1971) and the March 30, 1965, Rat Islands M_S 7.5 event (Abe, 1972) are thought to be capable of rupturing through the entire oceanic lithosphere in response to the pull of the down-dipping slab. As a result, the Sanriku-Oki and Sumba earthquakes generated a significant tsunami that resulted in at least 3,000 deaths in Japan (USGS, 2015) and 180 deaths in Indonesia (Soloviev and others, 1992). The recent comparable 2009 M_W 8.0 Samoa event also generated significant tsunamis that propagated throughout the Pacific Ocean. Thus an outer-rise event is entirely plausible along the Aleutian–Alaska subduction zone.

Scenario 10. Rupture of the tensional outer-rise part of the subduction plate south of the trench in the Fox Islands area

Outer-rise earthquakes are known to have occurred in the subducting plate in the vicinity of the oceanic trench and can be subdivided into two groups: tensional (normal) and compressional (thrust) events (Stauder, 1968b; Byrne and others, 1988). Great tensional outer-rise events occurred near Japan on March 2, 1933 (the Mw 8.4 Sanriku-oki earthquake [Kanamori, 1971]) and near Indonesia on August 19, 1977 (the Mw 8.3 Sumba earthquake [Gusman and others, 2009]). At least 24 significant outer-rise events have occurred along the Alaska–Aleutian Arc (Christensen and Ruff, 1988).

In this report we consider a hypothetical M_W 8.6 outer-rise event parallel to Umnak and Unimak islands and parameterize it by five subfaults, listed in table 3. The fault parameters required to compute seafloor deformation are the epicenter location, area, dip, rake, strike, and amount of slip on the fault. We use the equations of Okada (1985)

Table 3. Fault parameters for the hypothetical tensional M_W 8.6 outer-rise earthquake.

Latitude (deg. N)	Longitude (deg. W)	Depth (km)	Length (km)	Width (km)	Strike (deg.)	Dip (deg.)	Rake (deg.)	Slip (m)
53°7'44.4''	-161°5'03.6''	2	100	15	252.32	45	-90	25
52°0'45.6''	-162°0'12.0''	2	100	15	251.71	45	-90	25
52°3'14.4''	-164°4'33.6''	2	100	15	250.15	45	-90	25
52°4'24.0''	-165°7'36.0''	2	100	15	247.56	45	-90	25
51°3'09.6''	-166°8'36.0''	2	100	15	247.42	45	-90	25

to calculate distribution of coseismic uplift and subsidence resulting from this slip distribution. The dip of each subfault is in a range reported by Stauder (1968a) and we assume that the hypothetical earthquake ruptures through the entire slab. Vertical coseismic deformations for this scenario are shown in figure 23j.

MODELING RESULTS

We performed numerical calculations for all ten scenarios. The water dynamics are modeled in each grid (listed in table 1) and we compute the extent of inundation only in the high-resolution grids. The simulated extents of inundation in Unalaska for all considered scenarios are shown in figure 24.

We begin discussion of the modeling results by noting that scenario 1 (a hypothetical M_W 9.1 earthquake) predicts a 9 m (30 ft) wave in Iliuliuk Bay. The computational station location in the bay is marked by the red triangle in figure 24. Scenarios 2 and 3 generate waves of about 7 m (23 ft) and 6 m (20 ft) at the same station in Iliuliuk Bay, respectively. The modeled water level dynamics for scenarios 1–3 are plotted in figure 25a. Recall that scenarios 2 and 3 simulate hypothetical earthquakes that are somewhat smaller than the earthquake assumed in scenario 1; however, the computed wave heights in Iliuliuk Bay are nevertheless significant and could cause widespread damage. The numerical simulations reveal that the first wave could arrive as quickly as 30 minutes after the earthquake, whereas the highest wave might arrive 80–90 minutes after the earthquake. Significant wave activity could continue for at least 18 hours after the earthquake, and the predicted average time interval between successive waves is about 40 minutes.

Scenario 4, a hypothetical Tohoku-type earthquake (considered in the SAFRR project) between Shumagin and Kodiak islands, produces a 1 m (3 ft) wave in Iliuliuk Bay. The modeled water level is shown by the cyan line in figure 25b. The hypothetical tsunami might flood only low-lying areas along the shoreline. However, scenarios 5 and 6, which simulate the SAFRR-type earthquake offshore of Unalaska Island, result in 4–5 m (13–16 ft) waves in Iliuliuk Bay and produce significant inundation of the city and harbor. The estimated extents of inundation as well as the water level dynamics are shown in figures 24 and 25b, respectively. A key reason for lesser extents of flooding by the SAFRR-type scenarios 5 and 6 is that the modeled sea floor deformation predominantly occurs on the Pacific side of Fox Islands and the generated tsunami is mostly reflected by the islands into the Pacific Ocean. Some of the waves, which penetrate through passages between the islands, refract on the complex bathymetry and therefore indirectly impact Unalaska.

The modeled inundation due to scenario 7 resembles the inundation simulated by scenario 2. In the computational experiment the waves flood the city, penetrate deep beyond Unalaska Lake, and then surge above the bridge on Steward Road. It is important to mention that the bathymetry of Unalaska Lake is rather uncertain. In this report the lake was assumed to have a constant depth of 3 m (10 ft). The uncertainty in the lake bathymetry, coupled with the rather flat topography in the valley, lead us to speculate that the Ounalashka Community Park area potentially could be inundated. Scenario 8 resembles a Tohoku-type rupture and results in some flooding along the coast. Scenarios 9 and 10 might produce flooding in low-lying areas, similar to the inundation simulated according to scenario 4. For the sake of clarity the limits of inundation for scenarios 9 and 10 are not shown on figure 24 but are included in the data distribution package for this report. The modeled water level dynamics for scenarios 7–10 are shown in figures 25c and 25d.

Similar results are obtained for Akutan. Scenarios 1, 2, and 7 produce the highest waves, ranging from 5 to 15 m (16–50 ft) along the shoreline of the community. The simulated extent of inundation in Akutan for scenarios 1–8 is shown in figure 26. Scenarios 9 and 10 might produce flooding in low-lying areas similar to the inundation predicted according to scenario 4, and their limits of inundation are included in the data distribution package. The modeled water level dynamics near the village for all scenarios is shown in figure 27. The simulations reveal that a series of waves could inundate the village. The simulated water level starts to steadily rise immediately after the earthquake and the highest waves follow shortly. Significant wave action could continue afterward for at least eight hours. Uncertainties in the digital elevation model (DEM) at the head of Akutan Bay impede the development of accurate inundation estimates near the newly constructed boat harbor.

TIME SERIES AND OTHER NUMERICAL RESULTS

To help emergency managers assess the tsunami hazard in Unalaska and Akutan we supplement the inundation maps with the time series of the modeled water level and velocity dynamics at certain locations around the communities (appendices A and B). For each labeled location in figures A-1 and B-1 we plot the sea level and water velocity in figures A-2 and A-3, and B-2 and B-3, respectively. Zero time corresponds to the time when the earthquake occurs. The pre-earthquake elevation/depth with respect to the MHHW is stated for each location. The post-earthquake elevations/depth corresponding to the MHHW datum are also listed for each scenario. To show the height of arriving tsunamis for offshore locations we use a vertical datum with a zero mark corresponding to the pre-earthquake sea level. The dashed lines show water levels after the tsunami. The velocity magnitude is calculated as water flux divided by water depth, thus the velocity value can have large uncertainties when the water depth is small. In the plots provided, the velocity is computed only where the water depth is greater than 0.3 m (1 ft).

Analysis of the time series plot shows that a hypothetical earthquake with a magnitude greater than 8.8 (for example, scenarios 1, 2, 3, and 7) can create a devastating wave that penetrates deep inside the city of Unalaska and floods beyond Steward Road. The maximum water level and velocity for all considered scenarios is listed in table A-1. Numerical modeling also predicts that tsunami currents in narrow channels separating Amaknak from Unalaska Islands might

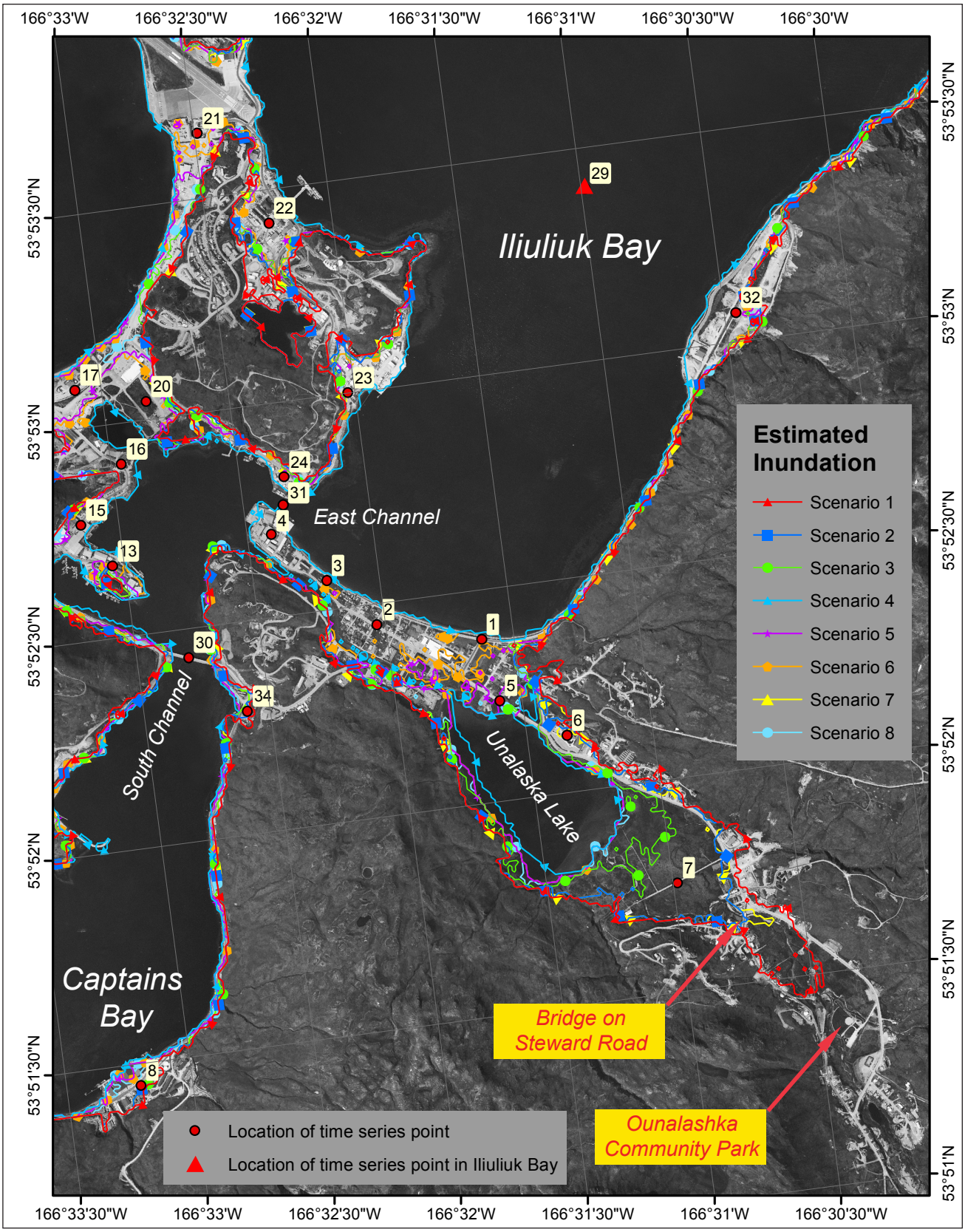

Figure 24. Modeled potential inundation in Unalaska by tectonic waves for all scenarios that result in a significant inundation. The shoreline corresponds to the present-day MHHW datum. Due to the steep topography, inundation areas for several tsunami scenarios have a common boundary, and the plotted extents of the inundation areas may overlie one another. The location with the recorded water level dynamics in Iliuliuk Bay is marked by a red triangle.

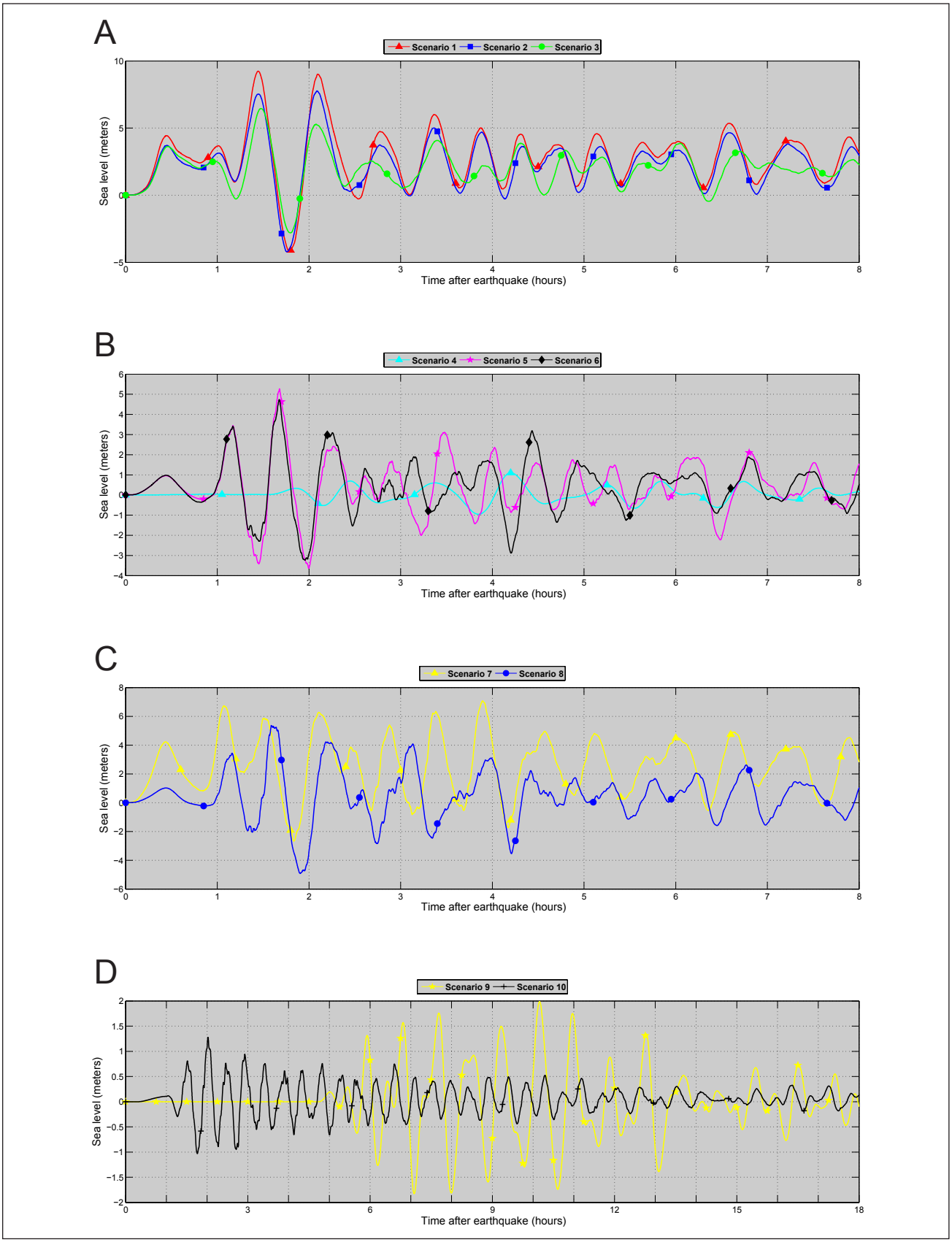

Figure 25. Modeled time series of water level for station 29 in Iliuliuk Bay: (A) for scenarios 1–3; (B) for scenarios 4–6; (C) for scenarios 7 and 8; and (D) for scenarios 9 and 10. The station location is marked by the red triangle in figure 24. The vertical datum is such that zero corresponds to the pre-earthquake sea level.

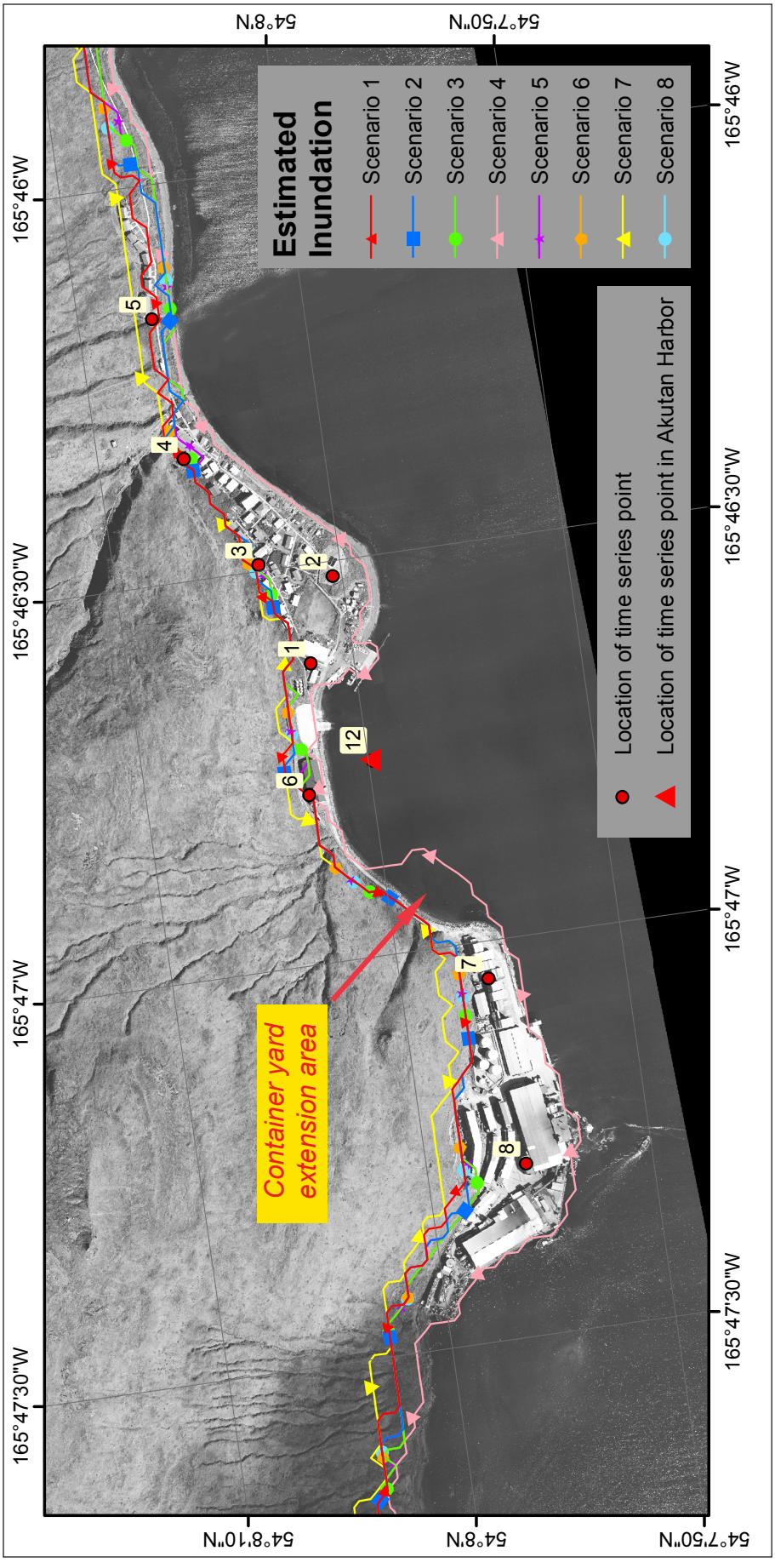

Figure 26. Modeled potential inundation in Akutan by tectonic waves for all scenarios that result in a significant inundation. The shoreline corresponds to the present-day MHHW datum. Due to the steep topography, inundation areas for several tsunami scenarios have a common boundary, and plotted extents of inundation areas may overlie one another. Point 12, the location with the recorded water level dynamics in Akutan Harbor, is marked by a red triangle. This aerial image of Akutan was taken before the extension of the container yard, east of the Trident Seafoods Plant.

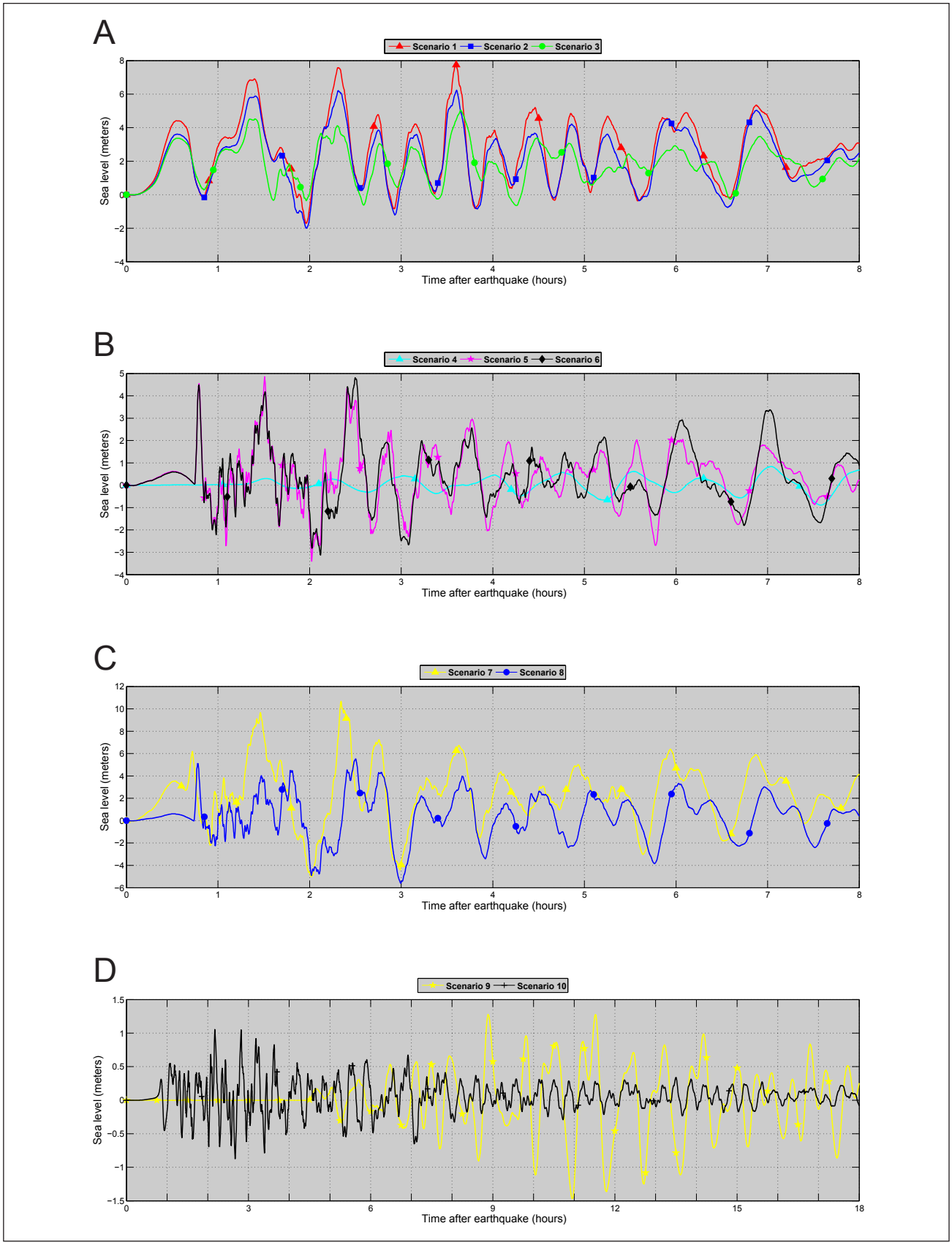

Figure 27. Modeled time series of water level for station 12 in Akutan Harbor: (A) for scenarios 1–3; (B) for scenarios 4–6; (C) for scenarios 7 and 8; (D) for scenarios 9 and 10. The station location is marked by the red triangle in figure 26. The vertical datum is such that zero corresponds to the pre-earthquake sea level.

reach dangerous velocities. For example, tsunami currents in the strait between Captains Bay and Unalaska Bay (point 12) could reach a velocity of 10.5 m/s (20.5 knots or 34.4 ft/s); the tsunami currents near the bridge (see point 30), could reach a velocity of 7.5 m/s (14.5 knots or 24.6 ft/s). It could be possible for eddies to form near the straits and travel across the bays. In scenario 9 (the Cascadia event), a large-scale sustained eddy might form in the northern part of Captains Bay; however, further analysis of its dynamics is beyond the scope of this report.

All local scenarios predict inundation in the city of Akutan. Locations near Post Office (point 1) and the Salmonberry Inn (point 3) might be flooded by waves reaching 8 m (26 ft). The water level near the Trident Seafood cannery (point 8) could reach 9.5 m (31 ft). Unsecured shipping containers could be floated by the tsunami waves and could hit other buildings. The maximum water level and velocity for all considered scenarios are listed in table B-1.

SOURCES OF ERRORS AND UNCERTAINTIES

The hydrodynamic model used to calculate propagation and runup of tsunami waves is a nonlinear, flux-formulated, shallow-water model (Nicolsky and others, 2011b) that has passed the validation and verification tests required for models used in production of tsunami inundation maps (Synolakis and others, 2007; NTHMP, 2012). The modeling process does not take into account tsunami–tide interactions. The scientific research community has not yet reached a full understanding of possible interactions between tsunamis and tides in shallow inlets. Although the current model is validated to simulate the hypothetical inundation, it does not take into account wave dispersion and cannot explicitly model the origination and development of bore-like waves. Moreover, a hypothetical rupture of normal faults in concert with a subduction earthquake might produce some additional short-period waves that could also contribute to formation of bore-like waves. Therefore the numerical modeling results can be used only as a guideline for predicting an actual inundation event.

Because the initial condition for the modeling is determined by the displacement of the ocean bottom, the largest source of error is the earthquake model. When a tsunami is generated in the vicinity of the coast the direction of the incoming waves, their amplitudes, and times of arrival are determined by the initial displacements of the ocean floor in the source area because the distance to the shore is too small for the waves to dissipate. Therefore the near-field inundation modeling results are especially sensitive to the fine structure of the tsunami source. The modeling process is highly sensitive to errors when the complexity of the source function is combined with its proximity to the coastal zone.

During development of tsunami inundation maps a spatially-averaged ground subsidence/uplift model is assumed for Unalaska/Dutch Harbor and Akutan. However, during a potential earthquake, soil compaction in areas of unconsolidated deposits in the coastal zone might occur, and tsunami inundation could extend farther landward. Finally, we mention that the horizontal resolution of the grid used for inundation modeling is about 16 m (52 ft). This resolution is high enough to describe major relief features, but small topographic features, buildings, and other facilities cannot be resolved accurately by the existing model.

In addition to the time series of the modeled water level and velocity dynamics, we added a supplemental appendix to this report that includes maps of the potential maximum subsidence for each community (appendix C). According to scenario 1, the maximum subsidence in Unalaska and Akutan could be about 2.8 m (9.2 ft) and 2.6 m (8.5 ft), respectively. Most low-lying areas could be permanently flooded as a result of the hypothetical earthquake.

SUMMARY

We present the results of numerical modeling of earthquake-generated tsunamis for Unalaska/Dutch Harbor and Akutan, Alaska. Hypothetical scenarios 1, 2, 3, and 7 (M_W >8.8 earthquakes along the Fox Islands region of the subduction zone) result in the "worst case" tsunami-inundation hazards for Unalaska and Akutan. The earthquake scenarios considered in this report are in the range of magnitudes 8 to 9.2 for the western Aleutian segment in the USGS Probabilistic Seismic Hazard Assessment for Alaska (Wesson and others, 2007, 2008).

We emphasize that each of the scenarios considered are geologically reasonable and present potential hazards to each community. Sheets 1 and 2, which show the results of our modeling for Unalaska and Akutan, have been completed using the best information available and are believed to be accurate; however, their preparation required many assumptions. We considered several tectonic scenarios and provided an estimate of maximum credible tsunami inundation for each scenario. Actual conditions during a tsunami event may vary from those considered, so the accuracy cannot be guaranteed. The limits of inundation shown should be used only as a guideline for emergency planning and response action. The tsunami hazard maps by the DDCG and URS seem to overestimate the potential inundation. However, the decision to choose an appropriate map for evacuation purposes will depend on the local emergency management agencies. Actual areas inundated will depend on specifics of earth deformation, land construction, and tide level, and may differ from areas shown on the map. The information on this map is intended to assist state and local agencies in planning emergency evacuation and tsunami response actions in the event of a major tsunamigenic earthquake. These results are not intended for land-use regulation or building-code development.

ACKNOWLEDGMENTS

This project received support from the National Oceanic and Atmospheric Administration (NOAA) under Reimbursable Services Agreement ADN 0931000 with the State of Alaska's Division of Homeland Security & Emergency Management (a division of the Department of Military and Veterans Affairs). Some of the research in this publication is sponsored by the Cooperative Institute for Alaska Research

with funds from NOAA under cooperative agreement NA08OAR4320751 with the University of Alaska Fairbanks. Numerical calculations for this work were supported by a grant of High Performance Computing (HPC) resources from the Arctic Region Supercomputing Center (ARSC) at the University of Alaska Fairbanks. We thank Zebulon Maharrey for his help with the RTK GPS survey in Unalaska/Dutch Harbor and Akutan and Amy Macpherson for her help with the cartography. We are grateful to Douglas Christensen and Natasha Ruppert for their help in assessing potential earthquakes in the Fox Islands and for sharing the data with us. Thoughtful reviews by Rob Witter (USGS, Alaska Science Center) and Hong Kie Thio (AECOM) improved the report.

REFERENCES

Abe, Katsuyuki, 1972, Lithospheric normal faulting beneath the Aleutian Trench: Physics of the Earth and Planetary Interiors, v. 5, no. 3, p. 190–198.

Alaska Division of Community and Regional Affairs (DCRA), 2015, Community Database Online: Alaska Department of Commerce, Community, and Economic Development, Division of Community and Regional Affairs. https://www.commerce.alaska.gov/web/dcra/, last accessed November 25, 2015.

Alaska Earthquake Center, 2015, Alaska Earthquake Center online catalog: University of Alaska Geophysical Institute. http://www.aeic.alaska.edu/html_docs/db2catalog.html, last accessed 11-25-15.

Argus, D.F., Gordon, R.G., Heflin, M.B., Ma, Chopo, Eanes, R.J., Willis, Pascal, Peltier, W.R., and Owen, S.E, 2010, The angular velocities of the plates and the velocity of the Earth's centre from space geodesy: Geophysics Journal International, v. 180, no. 3, p. 913–960. doi:10.1111/j.1365-246X.2009.04463.x Don Argus kindly provided us with the GEODVEL NNR angular velocities.

Atwater, B.F., 1987, Evidence for great Holocene earthquakes along the outer coast of Washington state: Science, v. 236, p. 942–944.

Atwater, B.F., Musumi-Rokkaku, Satoku, Satake, Kenji, Tsuji, Yoshinobu, Ueda, Kazue, and Yamaguchi, D.K., 2005, The orphan tsunami of 1700—Japanese clues to a parent earthquake in North America: U.S. Geological Survey Professional Paper 1707 [prepared in cooperation with the Geological Survey of Japan, the University of Tokyo, and the University of Washington, and published in association with University of Washington Press], 133 p.

Balay, S., Brown, J., Buschelman, K., Eijkhout, V., Gropp, W., Kaushik, D., Knepley, M., Curfman McInnes, L., Smith, B., and Zhang, H., 2012, PETSc Users Manual ANL-95/11, Revision 3.3: Argonne, IL, Argonne National Laboratory, Mathematics and Computer Science Division, 211 p. www.mcs.anl.gov/petsc/petsc-3.3/docs/manual.pdf

Blakely, R.J., Brocher, T.M., and Wells, R.E., 2005, Subduction-zone magnetic anomalies and implications for hydrated forearc mantle: Geology, v. 33, no. 6, p. 445–448.

Blaser, Lilian, Kruger, Frank, Ohrnberger, Matthias, and Scherbaum, Frank, 2010, Scaling relations of earthquake source parameter estimates with special focus on subduction environment: Bulletin of the Seismological Society of America, v. 100, no. 6, p. 2,914–2,926. doi:10.1785/0120100111

Boyd, T.M., and Jacob, Klaus, 1986, Seismicity of the Unalaska region, Alaska: Bulletin of the Seismological Society of America, v. 76, no. 2, p. 463–481.

Boyd, T.M., Engdahl, E.R., and Spence, W., 1995, Seismic cycles along the Aleutian arc—Analysis of seismicity from 1957 through 1991: Journal of Geophysical Research, v. 100, no. B1, p. 621–644. doi:10.1029/94JB02641

Bryn, Petter, Berg, Kjell, Forsberg, C.F., Solheim, Anders, and Kvalstad, T.J., 2005, Explaining the Storegga slide: Marine and Petroleum Geology, v. 22, no. 1-2, p. 11–19. doi:10.1016/j.marpetgeo.2004.12.003

Butler, Rhett, 2012, Re-examination of the potential for great earthquakes along the Aleutian island arc with implication for tsunamis in Hawai'i: Seismological Research Letters, v. 83, no. 1, p. 30–39. doi:10.1785/gssrl.83.1.29

Butler, Rhett, 2014, Great Aleutian tsunamis: Honolulu, HI, University of Hawai'i at Manoa, Hawai'i Institute of Geophysics & Planetology, Peer-Reviewed Report HIGP-2014-1, 170 p., www.higp.hawaii.edu/reports/2014

Butler, Rhett, Burney, David, and Walsh, David, 2014, Paleotsunami evidence on Kaua'i and numerical modeling of a great Aleutian tsunami: Geophysical Research Letters, v. 41, no. 19, p. 6,795–6,802. doi:10.1002/2014GL061232

Byrne, D.E., Davis, D.M., and Sykes, L.R., 1988, Loci and maximum size of thrust earthquakes and the mechanics of the shallow region of subduction zones: Tectonics, v. 7, no. 4, p. 833–857.

Caldwell, R.J., Eakins, B.W., and Lim, E., 2009, Digital elevation models of Prince William Sound, Alaska—Procedures, data sources, and analysis: Boulder, CO, National Geophysical Data Center, NOAA, 43 p. www.ngdc.noaa.gov/dem/report/download/1305

Carignan, K.S., Taylor, L.A., Eakins, B.W., and Love, M., 2012, Digital elevation model of Unalaska, Alaska—Procedures, data sources, and analysis: Boulder, CO, National Geophysical Data Center, NOAA, 5 p.

Carlson, P.R., Karl, H.A., and Edwards, B.D., 1991, Mass sediment failure and transport features revealed by acoustic techniques, Beringian margin, Bering Sea, Alaska: Marine Geotechnology, v. 10, no. 1-2, p. 33–51. doi:10.1080/10641199109379881

Chen, W.-P., and Molnar, Peter, 1983, Focal depths of intracontinental and intraplate earthquakes and their implications for the thermal and mechanical properties of the lithosphere: Journal of Geophysical Research, v. 88, no. B5, p. 4,183–4,214.

Christensen, D.H., and Ruff, L.J., 1988, Seismic coupling and outer rise earthquakes: Journal of Geophysical Research, v. 93, no. B11, p. 13,421–13,444. doi:10.1029/JB093iB11p13421

Cox, D.C., and Lander, J.F., 1995, Revised source of the tsunami of August 23, 1872: Honolulu, HI, Science of Tsunami Hazards, the International Journal of the Tsunami Society, v. 12, no. 2, p. 117–126.

Cox, D.C., and Pararas-Carayannis, G., 1976, Catalog of tsunamis in Alaska, revised 1976: Boulder, CO, World Data Center A, NOAA, Report SE-1, 43 p.

Cross, R.S., and Freymueller, J.T., 2008, Evidence for and implications of a Bering plate based on geodetic measurements from the Aleutians and western Alaska [abs.]: Journal of Geophysical Research, v. 113, no. B7, p. 405. doi:10.1029/2007JB005136

Davies, J.N., Sykes, L.R., House, L.S., and Jacob, K.H., 1981, Shumagin seismic gap, Alaska Peninsula—History of great earthquakes, tectonic setting, and evidence for high seismic potential: Journal of Geophysical Research, v. 86, no. B5 p. 3,821–3,855. doi:10.1029/JB086iB05p03821

DeMets, Charles, Gordon, R.C., Argus, D.F., and Stein, Seth, 1990, Current plate motions: Geophysical Journal International, v. 101, no. 2, p. 425–478.

Department of Public Safety, Unalaska, Tsunami Inundation Zones and Evacuation Routes, http://www.ci.unalaska.ak.us/publicsafety/page/emergency-preparedness, last accessed October, 2015.

Dunbar, P.K., and Weaver, C.S., 2008, U.S. states and territories national tsunami hazard assessment—Historical record and sources for waves: Technical Report, National Oceanic and Atmospheric Administration and U.S. Geological Survey, 59 p. http://nthmp.tsunami.gov/documents/Tsunami_Assessment_Final.pdf

Engdahl, E.R., Billington, Selena, and Kisslinger, C., 1989, Teleseismically recorded seismicity before and after the May 7, 1986, Andreanof Islands, Alaska, earthquake: Journal of Geophysical Research, v. 94, no. B11, p. 15,481–15,498. doi:10.1029/JB094iB11p15481

Estabrook, C.H., Jacob, K.H., and Sykes, L.R., 1994, Body wave and surface wave analysis of large and great earthquakes along the eastern Aleutian arc, 1923–1993—Implications for future events: Journal of Geophysical Research, v. 99, no. B6, p. 11,643–11,662.

Fine, I.V., Rabinovich, A.B., Bornhold, B.D., Thompson, R.E., and Kulikov, E.A., 2005, The Grand Banks landslide-generated tsunami of November 18, 1929—Preliminary analysis and numerical modeling: Marine Geology, v. 215, no. 1-2, p. 45–57.

Fletcher, H.J., Beavan, John, Freymueller, J.T., and Gilbert, Lewis, 2001, High interseismic coupling of the Alaska subduction zone SW of Kodiak Island inferred from GPS data: Geophysical Research Letters, v. 28, no. 3, p. 443–446. doi:10.1029/2000GL012258

Freund, L.B., and Barnett, D.M., 1976, A two-dimensional analysis of surface deformation due to dip-slip faulting: Bulletin of the Seismological Society of America, v. 66, p. 667–675.

Freymueller, J.T., Woodard, H., Cohen, S., Cross, R., Elliott, J., Larsen, C., Hreinsdottir, S., and Zweck, C., 2008, Active deformation processes in Alaska, based on 15 years of GPS measurements, *in* Freymueller, J.T., Haeussler, P.J., Wesson, R., and Ekström, G., eds., Active Tectonics and Seismic Potential of Alaska: Washington, D.C., American Geophysical Union Geophysical Monograph, v. 179, p. 1–42. doi:10.1029/179GM02

Fryer, G.J., and Watts, P., 2001, Motion of the Ugamak slide, probable source of the tsunami of 1 April 1946: Proceedings of the International Tsunami Symposium 2001, NOAA PMEL, p. 683–694.

Fujii, Yushiro, Satake, Kenji, Sakai, Shin'ichi, Shinohara, Masanao, and Kanazawa, Toshihiko, 2011, Tsunami source of the 2011 off the Pacific coast of Tohoku earthquake: Earth Planets Space, v. 63, p. 815–820. www.terrapub.co.jp/journals/EPS/pdf/2011/6307/63070815.pdf

Geist, E.L., and Dmowska, Renata, 1999, Local tsunamis and distributed slip at the source: Pure and Applied Geophysics, v. 154, no. 3-4, p. 485–512. http://link.springer.de/link/service/journals/00024/index.htm

Goto, C., Ogawa, Y., Shuto, N., and Imamura, Fumihiko, 1997, Numerical method of tsunami simulation with the leap-frog scheme: UNESCO, IUGG/IOC TIME Project, Manuals and Guides, no. 35.

Grilli, S.T., Harris, J.C., Kirby, J.T., Shi, F., Ma, G., Masterlark, T., Tappin, D.R., and Tajali-Bakhsh, T.S., 2013, Modeling of the Tohoku-Oki 2011 tsunami generation, far-field and coastal impact—A mixed co-seismic and SMF source, *in* Bonneton, P., ed., Proceedings of the 7th International Conference on Coastal Dynamics: Arcachon, France, June 2013, paper 68, p. 749–758.

Gusman, A.R., Tanioka, Y., Matsumoto, H., and Iwasaki, S.I., 2009, Analysis of the tsunami generated by the great 1977 Sumba earthquake that occurred in Indonesia: Bulletin of the Seismological Society of America, v. 99, no. 4, p. 2,169–2,179. doi:10.1785/0120080324

Hayes, G.P., Wald, D.J., and Johnson, R.L., 2012, Slab1.0—A three-dimensional model of global subduction zone geometries: Journal of Geophysical Research, v. 117, no. B1, 1 p. doi:10.1029/2011JB008524

Heise, Wiebke, Caldwell, T.G., Bertrand, E.A., Hill, G.J., Bennie, S.L., and Ogawa, Yasuo, 2013, Changes in electrical resistivity track changes in tectonic plate coupling: Geophysical Research Letters, v. 40, no. 19, p. 5,029–5,033. doi:10.1002/grl.50959

House, L.S., Sykes, L.R., Davies, J.N., and Jacob, K.H., 1981, Identification of a possible seismic gap near Unalaska Island, eastern Aleutians, Alaska, *in* Simpson, D.W., and Richards, P.G.,eds., Earthquake Prediction—An International Review: American Geophysical Union, Maurice Ewing Series, no. 4, p. 81–92.

Hyndman, R.D., Wang, K., and Yamano, M., 1995, Thermal constraints on the seismogenic portion of the southwestern Japan subduction thrust: Journal of Geophysical Research, v. 100, no. B8, p. 15,373–15,392.

Johnson, J.M., and Satake, Kenji, 1993, Source parameters of the 1957 Aleutian earthquake from tsunami waveforms: Geophysical Research Letters, v. 20, no. 14, p. 1,487–1,490.

Johnson, J.M., Tanioka, Yuichiro, Ruff, L.J., Satake, Kenji, Kanamori, Hiroo, and Sykes, L.R., 1994, The 1957 Great

Aleutian Earthquake: Pure and Applied Geophysics, v. 142, no. 1, p. 3–28.

Kaistrenko, V.M., Razjigaeva, Nadezhda, Kharlamov, Andrey, and Shishkin, Alexander, 2013, Manifestation of the 2011 Great Tohoku tsunami on the coast of the Kuril Islands—A tsunami with ice: Pure and Applied Geophysics, v. 170, no. 6-8, p. 1,103–1,114.

Kanamori, Hiroo, 1970, The Alaska earthquake of 1964—Radiation of long-period surface waves and source mechanism: Journal of Geophysical Research, v. 75, no. 26, p. 5,029–5,040.

Kanamori, Hiroo, 1971, Seismological evidence for a lithospheric normal faulting—The Sanriku earthquake of 1933: Physics of the Earth and Planetary Interiors, v. 4, no. 4, p. 289–300.

Kanamori, Hiroo, 1977, The energy release in great earthquakes: Journal of Geophysical Research, v. 82, no. 20, p. 2,981–2,987.

Kato, Naoyuki, and Seno, Tetsuzo, 2003, Hypocenter depths of large interplate earthquakes and their relation to seismic coupling: Earth and Planetary Science Letters, v. 210, no. 1-2, p. 53–63. doi:10.1016/S0012-821X(03)00141-9

Kaye, G. David, 2003, Spatial correlation of subduction interplate coupling and forearc morpho-tectonics: Corvallis, OR, Oregon State University, M.S. Thesis, 118 p. http://hdl.handle.net/1957/9011

Kelleher, John, Sykes, Lynn, and Oliver, Jack, 1973, Possible criteria for predicting earthquake locations and their application to major plate boundaries of the Pacific and the Caribbean: Journal of Geophysical Research, v. 78, no. 14, p. 2,547–2,585.

Kirby, Stephen, Scholl, David, von Huene, Roland, and Wells, Ray, 2013, Alaska earthquake source for the SAFRR tsunami scenario, chapter B, *in* Ross, S.L., and Jones, L.M., eds., The SAFRR (Science Application for Risk Reduction) Tsunami Scenario: U.S. Geological Survey Open-File Report 2013–1170, 40 p. http://pubs.usgs.gov/of/2013/1170/b/

Knecht, R.A., and Davis, R.S., 2005, South channel bridge, project no. MGS-STP-BR-0310(S)/52930: Amaknak bridge site data recovery project final report: Anchorage, Alaska Department of Transportation & Public Facilities. Available at http://www.aleutians.org/Amaknak_Bridge_report__UNL-50_.pdf

Kulikov, E.A., Rabinovich, A.B., Fine, I.V., Bornhold, B.D., and Thomson, R.E., 1998, Tsunami generation by landslides at the Pacific coast of North America and the role of tides: Oceanology, v. 38, no. 3, p. 323–328.

Lander, J.F., 1996, Tsunamis affecting Alaska, 1737–1996: Boulder, CO, National Oceanic and Atmospheric Administration, National Geophysical Data Center (NGDC), Key to Geophysical Research Documentation, v. 31, 155 p.

Lander, J.F., and Lockridge, P.A., 1989, Tsunami in Alaska, chapter 3, *in* United States Tsunamis (including United States possessions), 1690–1988: U.S. Department of Commerce, National Oceanic and Atmospheric Administration, National Geophysical Data Center (NGDC). Publication 41-2, 265 p. www.ngdc.noaa.gov/hazard/data/publications/pub41-2.pdf

LaSelle, SeanPaul, and Gelfenbaum, G.R., 2013, Modeling potential tsunami sources for deposits near Unalaska Island, Aleutian Islands [poster]: AGU Fall Meeting 2013, Poster NH41A-1700.

Leica Geosystems AG, 2002, GPS User Manual, Version 4, Leica Geosystems AG, Heerbrugg, Switzerland, 62 p.

Lopez, A.M., and Okal, E.A., 2006, A seismological reassessment of the source of the 1946 Aleutian 'tsunami' earthquake: Geophysical Journal International, v. 165, no. 3, p. 835–849. doi:10.1111/j.1365-246X.2006.02899.x

McCartney, A.P., 1984, Prehistory of the Aleutian region, *in* Damas, D., ed., Handbook of North American Indians, v. 5, Arctic: Washington, DC, Smithsonian Institution Press, p. 119–135.

Miller, J.J., von Huene, Roland, and Ryan, H.F., 2014, The 1946 Unimak tsunami earthquake area—Revised tectonic structure in reprocessed seismic images and a suspect near field tsunami source: U.S. Geological Survey Open-File Report 2014-1024, 19 p. doi:10.3133/ofr20141024

Moss, Robb E.S., and Travasarou, Thaleia, 2006, Tsunamigenic probabilistic fault displacement hazard analysis for subduction zones—Proceedings of the 8th U.S. National Conference on Earthquake Engineering: Earthquake Engineering Research Institute, Paper 238, 9 p.

Murotani, Satoko, Satake, Kenji, and Fujii, Yushiro, 2013, Scaling relations of seismic moment, rupture area, average slip, and asperity size for M~9 subduction-zone earthquakes: Geophysical Research Letters, v. 40, no. 19, p. 5,070–5,074. doi:10.1002/grl.50976

National Centers for Environmental Information/World Data Service (NCEI/WDS), in progress, Global historical tsunami database at NGDC, 2100 BC to present (interactive map): National Geophysical Data Center, NOAA. doi:10.7289/V5PN93H7

National Earthquake Information Center (NEIC), 2013. http://earthquake.usgs.gov/earthquakes/search/

National Tsunami Hazard Mapping Program (NTHMP), 2010, Guidelines and best practices for tsunami inundation modeling for evacuation planning: National Oceanic and Atmospheric Administration (NOAA), NTHMP Mapping & Modeling Subcommittee.

National Tsunami Hazard Mapping Program (NTHMP), 2012, Proceedings and results of the 2011 NTHMP Model Benchmarking Workshop: Boulder, CO, U.S. Department of Commerce/NOAA/NTHMP, NOAA Special Report, 436 p. http://nthmp.tsunami.gov

Nicolsky, D.J., 2012, Alaska tsunami model, *in* Proceedings and Results of the 2011 NTHMP Model Benchmarking Workshop: Boulder, CO, U.S. Department of Commerce/NOAA/NTHMP, NOAA Special Report, p. 55–87, http://nthmp.tsunami.gov

Nicolsky, D.J., Suleimani, E.N., Combellick, R.A., and Hansen, R.A., 2011a, Tsunami inundation maps of Whittier and western Passage Canal, Alaska: Alaska Division of Geological & Geophysical Surveys Report of Investigation 2011-7, 65 p. doi:10.14509/23244

Nicolsky, D.J., Suleimani, E.N., Haeussler, P.J., Ryan, H.F., Koehler, R.D., Combellick, R.A., and Hansen, R.A., 2013, Tsunami inundation maps of Port Valdez, Alaska: Alaska Division of Geological & Geophysical Surveys Report of Investigation 2013-1, 77 p., 1 sheet, scale 1:12,500. doi:10.14509/25055

Nicolsky, D.J., Suleimani, E.N., and Hansen, R.A., 2011b, Validation and verification of a numerical model for tsunami propagation and runup: Pure and Applied Geophysics, v. 168, p. 1,199–1,222. doi:10.1007/s00024-010-0231-9

Nicolsky, D.J., Suleimani, E.N., and Koehler, R.D., 2014, Tsunami inundation maps of Cordova and Tatitlek, Alaska: Alaska Division of Geological & Geophysical Surveys Report of Investigation 2014-1, 49 p. doi:10.14509/27241

Nicolsky, D.J., Wolken, G.J., Combellick, R.A., and Hansen, E., 2011c, Appendix B: Potential rockfall-generated tsunami at Whittier, Alaska, *in* Nicolsky, D.J., Suleimani, E.N., Combellick, R.A., and Hansen, R.A., Tsunami inundation maps of Whittier and western Passage Canal, Alaska: Alaska Division of Geological & Geophysical Surveys Report of Investigation 2011-7A, p. 57–65. doi:10.14509/23283

Nishenko, S.P., and Jacob, K.H., 1990, Seismic potential of the Queen Charlotte–Alaska–Aleutian seismic zone: Journal of Geophysical Research, v. 95, no. B3, p. 2,511–2,532.

Okada, Yoshimitsu, 1985, Surface deformation due to shear and tensile faults in a half-space: Bulletin of the Seismological Society of America, v. 75, no. 4, p. 1,135–1,154.

Oleskevich, D.A., Hyndman, R.D., and Wang, K., 1999, The updip and downdip limits to great subduction earthquakes—Thermal and structural models of Cascadia, south Alaska, SW Japan, and Chile: Journal of Geophysical Research, v. 104, no. B7 p. 14,965–14,991.

Pacheco, J.F., Sykes, L.R., and Scholz, C.H., 1993, Nature of seismic coupling along simple plate boundaries of the subduction type: Journal of Geophysical Research, v. 98, no. B8, p. 14,133–14,159.

Page, R.A., Biswas, N.N., Lahr, J.C., and Pulpan, Hans, 1991, Seismicity of continental Alaska, *in* Slemmons, D.B., Engdahl, E.R., Zoback, M.D., and Blackwell, D.D., eds., Neotectonics of North America: Boulder, Colorado, Geological Society of America, Decade Map v. 1, p. 47–68.

Papazachos, B.C., Scordilis, E.M., Panagiotopoulos, D.G., Papazachos, C.B., and Karakaisis, G.F., 2005, Global relations between seismic fault parameters and moment magnitude of earthquakes: Bulletin of the Geological Society of Greece, v. 36, p. 1,482–1,489.

Plafker, George, Kachadoorian, Reuben, Eckel, E.B., and Mayo, L.R., 1969, Effects of the earthquake of March 27, 1964, on various communities: U.S. Geological Survey Professional Paper 542-G, 50 p.

Priest, G.R., Goldfinger, Chris, Wang, Kelin, Witter, R.C., Zhang, Yinglong, and Baptista, A.M., 2009, Confidence levels for tsunami-inundation limits in northern Oregon inferred from a 10,000-year history of great earthquakes at the Cascadia subduction zone: Natural Hazards, v. 54, no. 1, p. 27–73. doi:10.1007/s11069-009-9453-5

Ross, S.L., Jones, L.M., Miller, Kevin, P., K.A., Wein, A., Wilson, Ri.I., Bahng, B., Barberopoulou, A., Borrero, J.C., Brosnan, D.M., Bwarie, J.T., Geist, E.L., Johnson, L.A., Kirby, S.H., Knight, W.R., Long, K., Lynett, P., Mortensen, C.E., Nicolsky, D.J., Perry, S.C., Plumlee, G.S., Real, C.R., Ryan, K., Suleimani, E., Thio, H., Titov, V.V., Whitmore, P.M. and Wood, N.J., 2013, SAFRR (Science Application for Risk Reduction) Tsunami Scenario—Chapter A, Executive Summary and Introduction, *in* Ross, S.L., and Jones, L.M., eds., The SAFRR Tsunami Scenario: U.S. Geological Survey Open-File Report 2013–1170, p. 1–17. http://pubs.usgs.gov/of/2013/1170/

Ruff, Larry, and Kanamori, Hiroo, 1983, Seismic coupling and uncoupling at subduction zones: Tectonophysics, v. 99, no. 2-4, p. 99–117.

Ryan, Holly, von Huene, Roland, Scholl, Dave, and Kirby, Steve, 2012, Tsunami hazards to U.S. coasts from giant earthquakes in Alaska: Eos Transactions, American Geophysical Union, v. 93, no. 19, p. 185–186.

Satake, Kenji, Shimazaki, Kunihiko, Tsuji, Yoshinobu, and Ueda, Kazue, 1996, Time and size of a giant earthquake in Cascadia inferred from Japanese tsunami records of January 1700: Nature, v. 379, no. 6,562, p. 246–249.

Satake, Kenji, Wang, Kelin, and Atwater, B.F., 2003, Fault slip and seismic moment of the 1700 Cascadia earthquake inferred from Japanese tsunami descriptions: Journal of Geophysical Research, v. 108, no. B11, p. 2,535–2,551. doi:10.1029/2003JB002521

Savage, J.C., 1983, A dislocation model of strain accumulation and release at a subduction zone: Journal of Geophysical Research, v. 88, no. B6, p. 4,984–4,996.

Scholz, C.H., and Campos, Jaime, 2012, The seismic coupling of subduction zones revisited: Journal of Geophysical Research—Solid Earth, v. 117, no. B5, p. 5,310. doi:10.1029/2011JB009003

Schwab, W.C., Lee, H.J., and Twichell, D.C., eds., 1993, Submarine landslides—Selected studies in the U.S. Exclusive Economic Zone: U.S. Geological Survey Bulletin 2002, 204 p.

Shao, Guangfu, Li, Xiangyu, Ji, Chen, and Maeda, Takahiro, 2011, Focal mechanism and slip history of 2011 Mw9.1 off the Pacific coast of Tohoku earthquake, constrained with teleseismic body and surface waves: Earth, Planets and Space, v. 63, no. 7, p. 559–564. doi:10.5047/eps.2011.06.028

Shao, Guangfu, Li, Xiangyu, Ji, Chen, and Maeda, Takahiro, 2011, Focal mechanism and slip history of 2011 M_W 9.1 off the Pacific coast of Tohoku earthquake, constrained with teleseismic body and surface waves: Earth Planets Space, v. 63, no. 7, p. 559–564. doi:10.5047/eps.2011.06.028

Simmons, Scott, and Nelsen, Scott, 2013, City of Unalaska hazard mitigation plan: U.S. Department of Homeland Security in cooperation with Alaska Division of Homeland

Security and Emergency Management and URS Corporation, 230 p. http://www.ci.unalaska.ak.us/planning/page/planning-department-plans-policies

Sobolev, S.V., Babeyko, A.Y., Wang, Rongjiang, Hoechner, Andreas, Galas, Roman, Rothacher, Markus, Sein, D.V., Schröter, Jens, Lauterjung, Joern, and Subarya, Cecep, 2007, Tsunami early warning using GPS-shield arrays: Journal of Geophysical Research, v. 112, no. B08, p. 415. doi:10.1029/2006JB004640

Soloviev, S.L., and Go, Ch.N., 1974, A catalogue of tsunamis on the western shore of the Pacific Ocean [dates include 1873–1968]: Moscow, Academy of Sciences of the USSR, Nauka Publishing House, 439 p. [English translation: Soloviev, S.L., and Go, Ch.N., 1984, A catalogue of tsunamis on the western shore of the Pacific Ocean: translation by Canada Institute for Scientific and Technical Information (available from Canada Institute for Scientific and Technical Information, National Research Council, Ottawa, Ontario, Canada K1A OS2), 447 p.]

Soloviev, S.L., Go, Ch.N., and Kim, Kh.S., 1992, Catalog of tsunamis in the Pacific, 1969–1982 [translated from Russian by Amerind Publishing Co. Pvt. Ltd. New Delhi, 1988]: Moscow, Academy of Sciences of the USSR, Soviet Geophysical Committee, Results of Researches on the International Geophysics Projects, p. 109–110. Available at ftp://ftp.ngdc.noaa.gov/hazards/publications/catalog_tsunamis_pacific_1969_1982.pdf

Song, Teh-Ru Alex, and Simons, Mark, 2003, Large trench-parallel gravity variations predict seismogenic behavior in subduction zones: Science, v. 301, no. 5,633, p. 630–633.

Stauder, W., 1968a, Mechanism of the Rat Island earthquake sequence of February 4, 1965, with relation to island arcs and sea floor spreading: Journal of Geophysical Research, v. 73, p. 3,847–3,858.

Stauder, W., 1968b, Tensional character of earthquake foci beneath the Aleutian Trench with relation to sea-floor spreading: Journal of Geophysical Research, v. 73, no. 24, p. 7,693–7,701. doi:10.1029/JB073i024p07693

Strasser, F.O., Arango, M.C., and Bommer, J.J., 2010, Scaling of the source dimensions of interface and intraslab subduction-zone earthquakes with moment magnitude: Seismological Research Letters, v. 81, no. 6, p. 941–950. doi:10.1785/gssrl.81.6.941

Sykes, L.R., 1971, Aftershock zones of great earthquakes, seismicity gaps, and earthquake prediction for Alaska and the Aleutians: Journal of Geophysical Research, v. 76, no. 32, p. 8,021–8,041.

Sykes, L.R., Kisslinger, J.B., House, L.S., Davies, J.N., and Jacob, K.H., 1981, Rupture zones and repeat times of great earthquakes along the Alaska–Aleutian Arc, 1784–1980, *in* Simpson, D.W., and Richards, P.G., eds., Earthquake Prediction—An international review: Washington, DC, American Geophysical Union Maurice Ewing Series, v. 4, p. 73–80.

Synolakis, C.E., Bernard, E.N., Titov, V.V., Kânoğlu, U., and González, F.I., 2007, Standards, criteria, and procedures for NOAA evaluation of tsunami numerical models: Seattle, WA, NOAA/Pacific Marine Environmental Laboratory, Technical Memorandum OAR PMEL-135, 55 p.

Tang, Liujuan, Titov, V.V., Bernard, E.N., Wei, Yong, Chamberlain, C.D., Newman, J.C., Mofjeld, H.O., Arcas, Diego, Eble, M.C., Moore, Christopher, Uslu, Burak, Pells, Clint, Spillane, Michael, Wright, Lindsey, and Gica, Edison, 2012, Direct energy estimation of the 2011 Japan tsunami using deep-ocean pressure measurements: Journal of Geophysical Research—Oceans, v. 117, no. C8, p. 8. doi:10.1029/2011JC007635

Tanioka, Yuichiro, and González, F.I., 1998, The Aleutian earthquake of June 10, 1996 (Mw7.9) ruptured parts of both the Andreanof and Delarof segments: Geophysical Research Letters, v. 25, no. 12, p. 2,245–2,248. doi:10.1029/98GL01578

Taylor, L.A., Eakins, B.W., Carignan, K.S., Warnken, R.R., Schoolcraft, D.C., Sazonova, T., and Sharman, G.F., 2008, Digital elevation model of Dutch Harbor, Alaska—Procedures, data sources, and analysis: National Oceanic and Atmospheric Administration (NOAA) Technical Memorandum NESDIS NGDC-4, 25 p.

Tichelaar, B.W., and Ruff, L.J., 1993, Depth of seismic coupling along subduction zones: Journal of Geophysical Research, v. 98, no. B2, p. 2,017–2,037. doi:10.1029/92JB02045

Titov, V.V., and Synolakis, C.E., 1995, Evolution and runup of breaking and nonbreaking waves using VTSC-2: Journal of Waterway, Port, Coastal, and Ocean Engineering, v. 121, no. 6, p. 308–316.

Titov, V.V., and Synolakis, C.E., 1997, Extreme inundation flows during the Hokkaido–Nansei–Oki Tsunami: Geophysical Research Letters, v. 24, no. 11, p. 1,315–1,318.

Uchida, Naoki, Nakajima, Junichi, Hasegawa, Akira, and Matsuzawa, Toru, 2009, What controls interplate coupling?—Evidence for abrupt change in coupling across a border between two overlaying plates in the NE Japan subduction zone: Earth and Planetary Science Letters, v. 283, no. 1-4, p. 111–121. doi:10.1016/j.epsl.2009.04.003

U.S. Geological Survey, 2015, Historic Earthquakes: Sanriku, Japan: U.S. Geological Survey, Earthquake Hazards Program website, last accessed November 30, 2015. http://earthquake.usgs.gov/earthquakes/world/events/1933_03_02.php

Uyeda, Seiya, 1982, Subduction zones—An introduction to comparative subductology: Tectonophysics, v. 81, no. 3-4, p. 133–159. doi:10.1016/0040-1951(82)90126-3

Wang, Kelin, Wells, R.E., Mazzotti, Stephane, Hyndman, R.D., and Sagiya, Takeshi, 2003, A revised dislocation model of interseismic deformation of the Cascadia subduction zone: Journal of Geophysical Research, v. 108, no. B1, p. 2,026–2,038. doi:10.1029/2001JB001227

Waythomas, C.F., Watts, Philip, Shi, Fengyan, and Kirby, J.T., 2009, Pacific Basin tsunami hazards associated with mass flows in the Aleutian Arc of Alaska: Quaternary Science Reviews, v. 28, no. 11-12, p. 1,006–1,019. doi:10.1016/j.quascirev.2009.02.019

Wei, Yong, 2008, Tsunami impact assessment for Unalaska, *in* Proceedings, Solutions to coastal disasters, 2008, Tsunamis, p. 118–131. doi:10.1061/40978(313)11

Wei, Yong, in review, PMEL Tsunami forecast series—Volume 10A, Tsunami forecast model for Unalaska, Alaska: NOAA OAR Special Report, Contribution No. 3357 from NOAA/Pacific Marine Environmental Laboratory, Contribution No. 1778 from Joint Institute for the Study of the Atmosphere and Ocean (JISAO).

Wesson, R.L., Boyd, O.S., Mueller, C.S., Bufe, C.G., Frankel, A.D., and Petersen, M.D., 2007, Revision of time-independent probabilistic seismic hazard maps for Alaska: U.S. Geological Survey Open-File Report 2007-1043, 33 p.

Wesson, R.L., Boyd, O.S., Mueller, C.S., and Frankel, A.D., 2008, Challenges in making a seismic hazard map for Alaska and the Aleutians, *in* Freymueller, J.T., Haeussler, P.J., Wesson, R., and Ekström, G., eds., Active Tectonics and Seismic Potential of Alaska: Washington, DC, American Geophysical Union, Geophysical Monograph v. 179, p. 385–397.

Witter, R.C., Briggs, R.W., Koehler, R.D., Gelfenbaum, G.R., Engelhart, S., Nelson, A., Carver, Gary, Bender, A.M., and Hemphill-Haley, E., 2014, Evidence for high tsunamis in the Fox Islands implies repeated Aleutian megathrust earthquakes in the Unalaska seismic gap [abs.]: Seismological Research Letters, v. 85, no. 2, p. 442. doi:10.1785/0220140014

Witter, R.C., Carver, G.A., Bender, A.M., Briggs, R.W., Gelfenbaum, G.R., and Koehler, R.D., 2013, Six large tsunamis in the past ~1,700 years at Stardust Bay, Sedanka Island, Alaska: Eos Transactions, AGU, Fall Meeting Supplement, Abstract and Presentation #NH44A-08.

Witter, R.C., Zhang, Y., Wang, K., Priest, G.R., Goldfinger, C., Stimely, L.L., English, J.T., and Ferro, P.A., 2011, Simulating tsunami inundation at Bandon, Coos County, Oregon, using hypothetical Cascadia and Alaska earthquake scenarios: Oregon Department of Geology and Mineral Industries Special Paper 43, 57 p.

Wu, F.T., and Kanamori, Hiroo, 1973, Source mechanism of February 4, 1965, Rat Island earthquake: Journal of Geophysical Research, v. 78, no. 26, p. 6,082–6,092.

Zweck, Chris, Freymueller, J.T., and Cohen, S.C., 2002, Three-dimensional elastic dislocation modeling of the postseismic response to the 1964 Alaska earthquake: Journal of Geophysical Research, v. 107, no. B4, p. 2,064. doi:10.1029/2001JB000409

APPENDIX A

Appendix A-1. Maps showing locations of time series points in Unalaska Bay and Captains Bay (left) and in the city of Unalaska (right). The latitude and longitude locations for time series points are listed in table A-1.

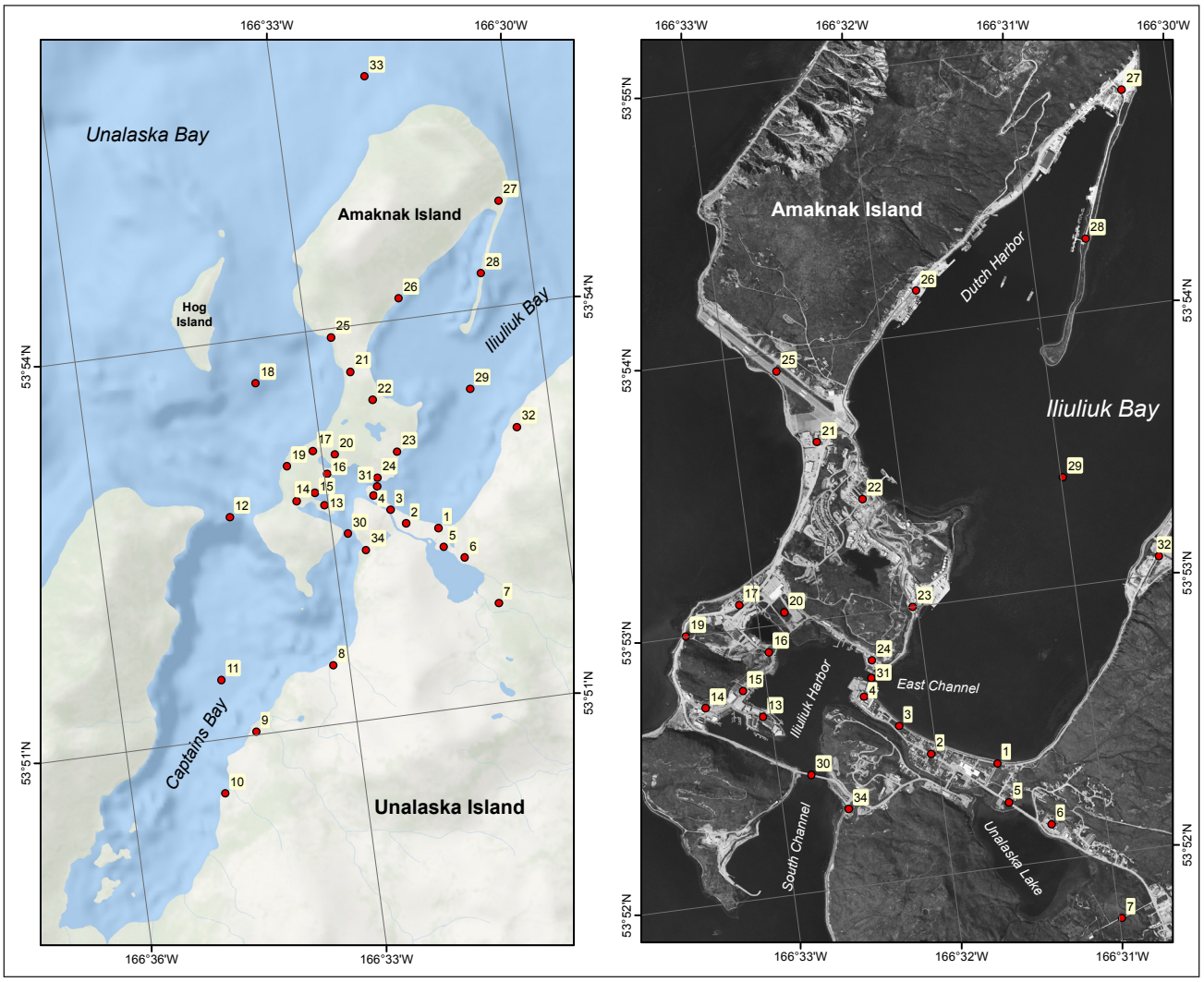

Table A-1. The longitude and latitude locations of the time series points in Unalaska/Dutch Harbor. The maximum water level above ground is provided for onshore locations, whereas the maximum water level above the pre-earthquake MHHW is provided for offshore locations. The pre-earthquake onshore (S) and offshore (O) locations are specified in the third column. The minimum elevation above the post-earthquake MHHW datum is provided for the onshore locations, while the minimum post-earthquake depth is provided for the offshore locations.

#	Label	S / O	Longitude (°W)	Latitude (°N)	Minimum Elevation/ Depth (meters)	Maximum Water Level Above Ground/Sea Level (meters)										Maximum Water Velocity (meters/second)									
						Scenario										Scenario									
						1	2	3	4	5	6	7	8	9	10	1	2	3	4	5	6	7	8	9	10
1	Bayview Ave.	S	-166.527139	53.873056	2	4.5	3.0	1.9	0.0	0.6	0.2	2.7	1.5	0.0	0.0	21.7	9.3	2.2	0.0	2.2	0	4.7	2.9	0.0	0.0
2	W. Broadway Ave.	S	-166.533889	53.874167	1.9	5.3	3.5	2.3	0.0	0.6	0.4	3.5	2.0	0.0	0.0	6.5	6.2	2.7	0.0	3.1	2.2	6.3	4.2	0.0	0.0
3	1st St.	S	-166.536806	53.876139	0.8	6.3	4.5	3.2	0.0	1.8	1.5	4.3	2.7	0.0	0.0	2.5	1.7	1.6	0.0	2.2	2.4	2.0	2.3	0.0	0.0
4	Alyeska Seafoods	S	-166.540056	53.878222	-0.3	6.2	4.3	3.1	0.0	2.0	1.8	3.8	2.8	0.0	0.0	6.2	5.7	5.1	0.0	4.4	4.0	5.5	4.8	0.0	0.0
5	E. Broadway Ave.	S	-166.526472	53.870583	-0.1	6.2	4.3	1.0	0.0	0.1	0.0	3.9	0.8	0.0	0.0	8.1	6.4	4.5	0.0	0.0	0.0	5.1	4.5	0.0	0.0
6	Unalaska City Elementary School	S	-166.522361	53.868889	4.4	2.0	0.2	0.0	0.0	0.0	0.0	0.0	0.0	0.0	0.0	2.1	0.0	0.0	0.0	0.0	0.0	0.0	0.0	0.0	0.0
7	Whittern Ln.	S	-166.516361	53.862583	1.5	5.4	3.2	0.0	0.0	0.0	0.0	3.1	0.0	0.0	0.0	14.1	9.5	0.0	0.0	0.0	0.0	4.9	0.0	0.0	0.0
8	Westward Seafoods	S	-166.553417	53.857472	2.4	3.0	1.6	0.6	0.0	0.0	0.0	0.8	0.0	0.0	0.0	0.9	0.6	0.3	0.0	0.0	0.0	0.5	0.0	0.0	0.0
9	Captains Bay Rd., B	S	-166.571639	53.850389	0.8	4.7	3.4	2.1	0.0	0.0	0.0	2.5	0.0	0.0	0.0	1.9	1.7	1.5	0.0	0.0	0.0	1.8	0.0	0.0	0.0
10	Captains Bay Rd., C	S	-166.580028	53.843139	-2.2	8.2	6.7	5.4	0.8	2.8	2.8	5.9	2.9	1.5	0.3	1.3	1.2	1.0	0.3	0.7	0.8	1.4	1.0	0.4	0.0
11	Captains Bay	O	-166.577639	53.857500	80.3	8.3	6.9	5.7	1.4	3.1	3.1	6.0	3.4	2.1	0.9	0.8	0.9	0.5	0.2	0.5	0.5	0.8	0.6	0.6	0.2
12	Strait, A	O	-166.571278	53.877889	12.7	7.2	5.9	4.9	1.2	2.7	2.4	4.9	3.0	1.7	0.6	10.9	10.7	10.2	3.7	9.9	9.6	10.2	9.8	6.5	4.3
13	Pacesetter Way	S	-166.550778	53.877806	-0.1	6.7	4.9	3.3	0.0	1.0	0.7	3.7	1.5	0.0	0.0	1.8	1.3	0.9	0.0	0.8	0.8	1.6	2.0	0.0	0.0
14	Gilman Way	S	-166.556611	53.878806	0	6.1	4.4	3.0	0.0	1.0	1.0	3.4	1.4	0.0	0.0	3.9	2.7	2.3	0.0	1.9	2.0	4.1	2.1	0.0	0.0
15	UniSea Plant	S	-166.552500	53.879556	0	6.7	4.9	3.2	0.0	1.1	0.8	3.6	1.5	0.0	0.0	2.3	1.6	1.2	0.0	1.0	1.0	2.0	1.6	0.0	0.0
16	Salmon Way	S	-166.549306	53.881722	-0.4	6.6	4.8	3.4	0.0	1.0	1.0	3.9	1.9	0.0	0.0	3.7	3.0	3.4	0.0	2.0	1.8	4.5	3.0	0.0	0.0
17	Airport Beach Rd., A	S	-166.551722	53.884833	1.5	3.9	2.4	1.3	0.0	0.0	0.0	1.7	0.1	0.0	0.0	5.3	4.2	2.3	0.0	0.0	0.0	4.2	0.0	0.0	0.0
18	Broad Bay	O	-166.562000	53.894333	20.7	8.0	6.5	5.2	1.1	2.9	3.0	6.5	4.4	1.5	0.6	2.8	2.6	2.2	0.2	1.2	1.0	1.3	1.1	0.5	0.4
19	Airport Beach Rd., B	S	-166.557694	53.883361	1.3	3.9	2.5	1.0	0.0	0.0	0.0	2.3	0.3	0.0	0.0	2.8	2.2	1.2	0.0	0.0	0.0	2.6	0.2	0.0	0.0
20	Container Storage Yard	S	-166.547139	53.884028	-0.3	6.1	4.4	3.3	0.0	1.2	1.0	3.9	1.9	0.0	0.0	2.7	2.4	1.9	0.0	1.5	1.5	2.7	2.2	0.0	0.0
21	Pen Air Terminal	S	-166.541444	53.894194	1.2	4.2	2.8	1.8	0.0	0.7	0.4	2.9	1.2	0.0	0.0	4.3	3.2	2.1	0.0	1.0	0.8	2.6	2.3	0.0	0.0
22	Delta Way	S	-166.537500	53.890333	1.2	5.4	4.1	2.6	0.0	1.7	0.8	3.5	2.2	0.0	0.0	9.0	8.1	6.3	0.0	3.6	3.1	9.0	7.9	0.0	0.0
23	E. Point Dr., A	S	-166.533778	53.883333	0.4	6.7	4.9	3.6	0.0	2.3	1.8	4.5	3.3	0.0	0.0	2.0	1.7	1.5	0.0	2.1	2.0	2.1	2.0	0.0	0.0
24	E. Point Dr., B	S	-166.538722	53.880389	-0.1	6.5	4.6	2.9	0.0	0.7	0.6	3.2	1.1	0.0	0.0	13.3	13.7	7.8	0.0	2.1	1.3	7.6	6.3	0.0	0.0
25	Unalaska Airport	S	-166.544639	53.898861	0.2	5.1	3.6	2.4	0.0	0.7	0.5	3.8	1.8	0.0	0.0	2.2	1.9	1.7	0.0	1.7	1.4	2.5	2.1	0.0	0.0
26	Ballyhoo Rd., A	S	-166.529083	53.902667	-0.1	6.3	5.1	3.8	0.0	2.6	2.0	4.2	3.1	0.0	0.0	2.1	1.6	0.7	0.0	1.6	1.1	1.3	1.6	0.0	0.0
27	Ballyhoo Rd., B	S	-166.505028	53.913306	0.2	4.7	3.6	2.7	0.0	2.0	1.7	3.0	2.6	0.0	0.0	5.1	4.5	3.7	0.0	3.1	2.8	4.1	3.8	0.0	0.0
28	Spit	S	-166.510806	53.904472	0.8	4.7	3.1	2.0	0.0	1.3	0.9	2.4	1.8	0.0	0.0	6.3	5.6	4.8	0.0	3.6	3.5	5.1	4.0	0.0	0.0
29	Iliuliuk Bay	O	-166.516417	53.890056	35.6	9.2	7.8	6.5	1.1	5.3	4.7	7.1	5.4	2.0	1.3	2.0	1.6	1.2	0.3	1.7	1.4	1.6	1.7	0.5	0.4
30	Bridge	O	-166.546556	53.873861	10.6	7.7	6.6	5.7	1.4	3.3	3.4	5.6	3.7	2.1	1.0	7.5	5.8	4.5	1.7	4.8	4.7	5.6	5.8	2.2	2.9
31	Strait, B	O	-166.539028	53.879306	11.3	9.0	6.9	5.4	1.2	3.6	3.3	5.7	4.3	2.0	1.1	9.1	8.8	8.7	3.5	7.7	7.4	8.6	7.7	3.8	3.7
32	Summer Bay Rd.	S	-166.507556	53.884444	2.5	4.1	2.5	1.2	0.0	0.4	0.0	2.1	0.7	0.0	0.0	5.0	4.4	3.7	0.0	3.1	0.0	5.2	5.8	0.0	0.0
33	Unalaska Bay	O	-166.530083	53.931222	51.8	6.3	5.3	3.8	0.6	2.1	1.9	4.7	2.5	1.1	0.5	1.1	1.0	0.8	0.2	0.8	0.7	1.0	1.1	0.3	0.2
34	Captains Bay Rd., A	S	-166.543167	53.871472	1.8	3.2	2.0	0.0	0.0	0.0	0.0	0.0	0.0	0.0	0.0	1.4	1.2	0.0	0.0	0.0	0.0	0.0	0.0	0.0	0.0

Appendix A-2. Graphs showing time series of water level (left column) and velocity (right column) for selected locations in Unalaska for scenarios 1, 2, 3, and 7. For each location, pre-earthquake and post-earthquake elevation/depth corresponding to the MHHW datum is provided for each scenario. For offshore locations, to show the height of an arriving tsunami, the vertical datum is such that zero corresponds to the pre-earthquake sea level. Dashed lines indicate the water level after the tsunami.

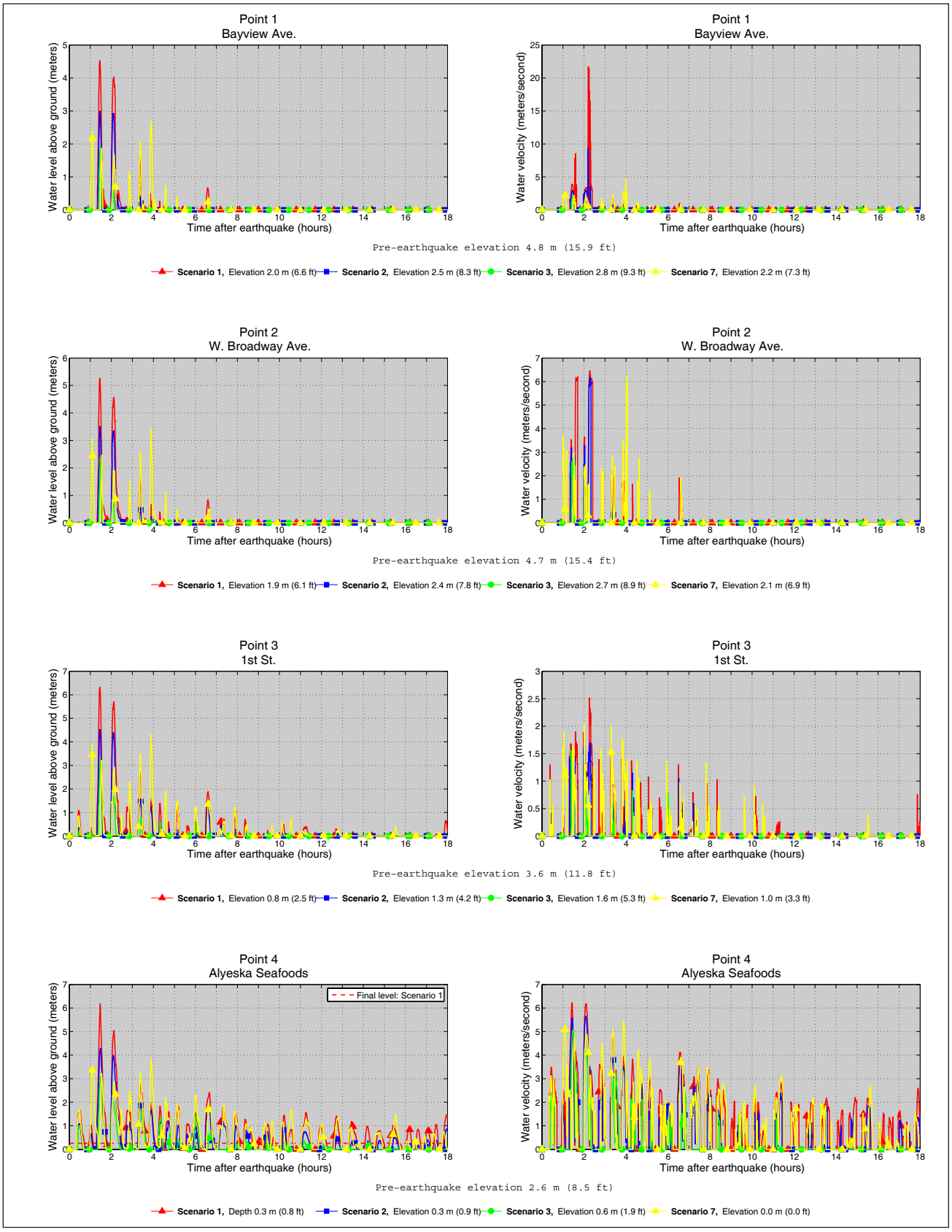

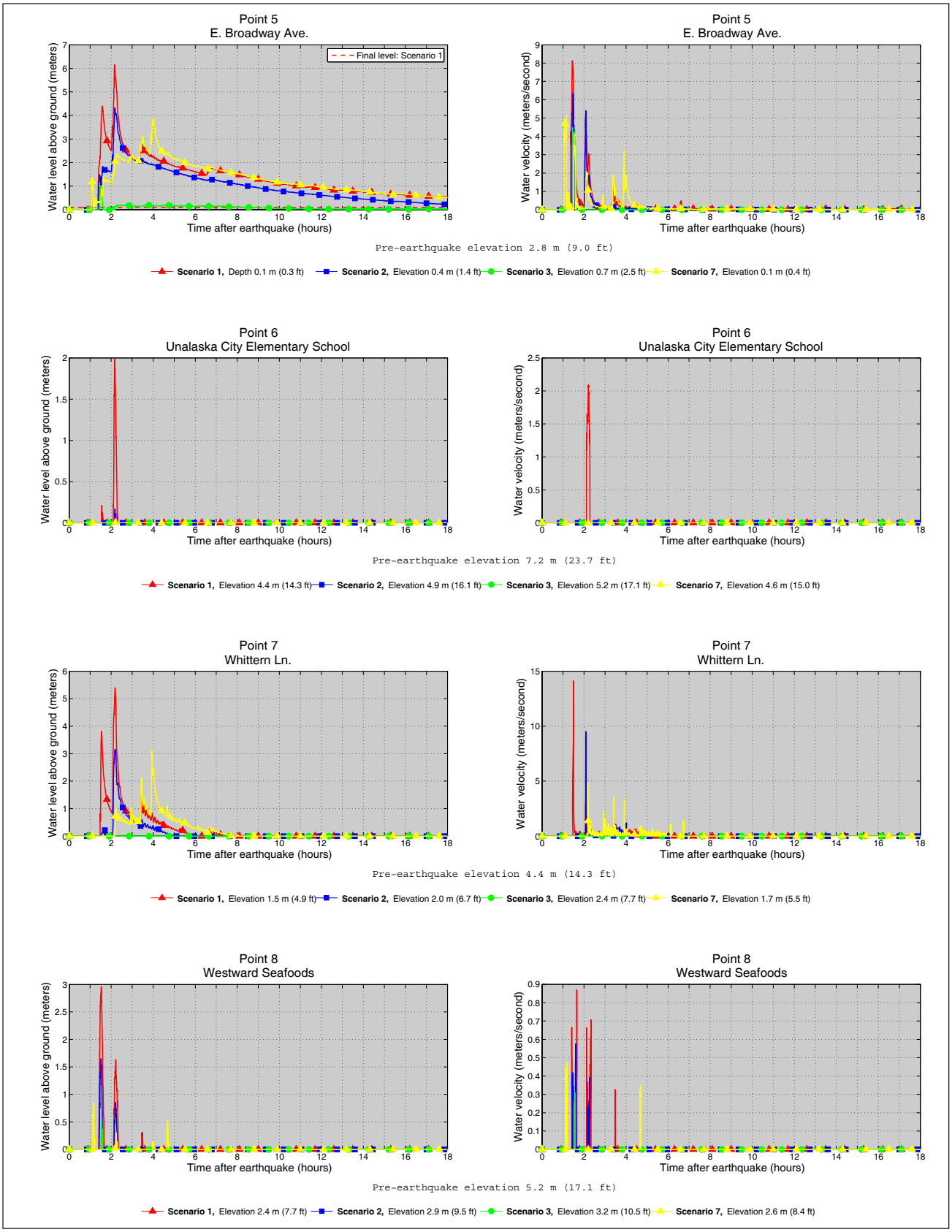
Point 5
E. Broadway Ave.
Final level: Scenario 1
Water level above ground (meters)
Time after earthquake (hours)
Point 5
E. Broadway Ave.
Water velocity (meters/second)
Time after earthquake (hours)
Pre-earthquake elevation 2.8 m (9.0 ft)
Scenario 1, Depth 0.1 m (0.3 ft)
Scenario 2, Elevation 0.4 m (1.4 ft)
Scenario 3, Elevation 0.7 m (2.5 ft)
Scenario 7, Elevation 0.1 m (0.4 ft)
Point 6
Unalaska City Elementary School
Water level above ground (meters)
Time after earthquake (hours)
Point 6
Unalaska City Elementary School
Water velocity (meters/second)
Time after earthquake (hours)
Pre-earthquake elevation 7.2 m (23.7 ft)
Scenario 1, Elevation 4.4 m (14.3 ft)
Scenario 2, Elevation 4.9 m (16.1 ft)
Scenario 3, Elevation 5.2 m (17.1 ft)
Scenario 7, Elevation 4.6 m (15.0 ft)
Point 7
Whittern Ln.
Water level above ground (meters)
Time after earthquake (hours)
Point 7
Whittern Ln.
Water velocity (meters/second)
Time after earthquake (hours)
Pre-earthquake elevation 4.4 m (14.3 ft)
Scenario 1, Elevation 1.5 m (4.9 ft)
Scenario 2, Elevation 2.0 m (6.7 ft)
Scenario 3, Elevation 2.4 m (7.7 ft)
Scenario 7, Elevation 1.7 m (5.5 ft)
Point 8
Westward Seafoods
Water level above ground (meters)
Time after earthquake (hours)
Point 8
Westward Seafoods
Water velocity (meters/second)
Time after earthquake (hours)
Pre-earthquake elevation 5.2 m (17.1 ft)
Scenario 1, Elevation 2.4 m (7.7 ft)
Scenario 2, Elevation 2.9 m (9.5 ft)
Scenario 3, Elevation 3.2 m (10.5 ft)
Scenario 7, Elevation 2.6 m (8.4 ft)

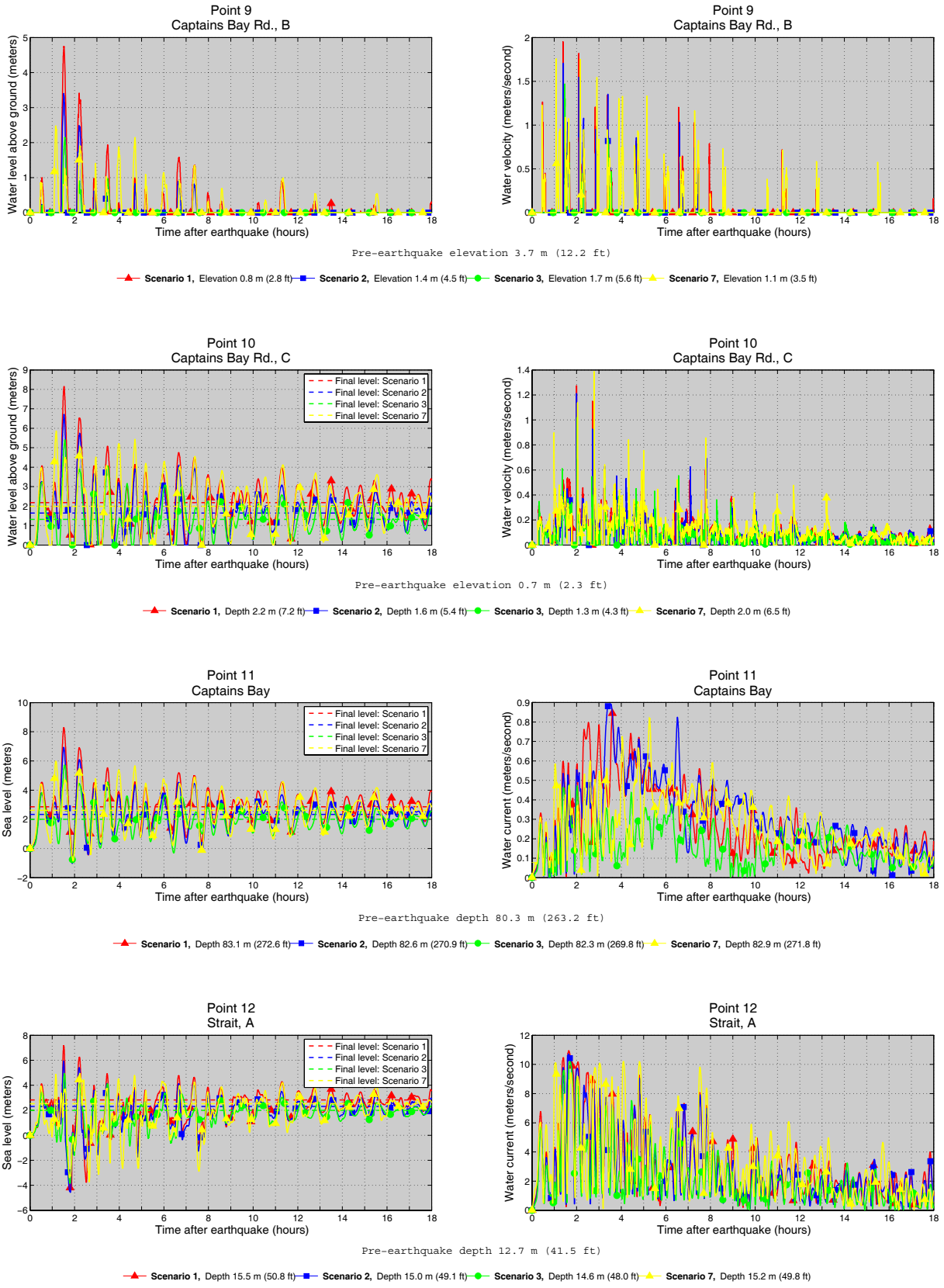
Point 9
Captains Bay Rd., B
Water level above ground (meters)
Time after earthquake (hours)
Point 9
Captains Bay Rd., B
Water velocity (meters/second)
Time after earthquake (hours)
Pre-earthquake elevation 3.7 m (12.2 ft)
Scenario 1, Elevation 0.8 m (2.8 ft) Scenario 2, Elevation 1.4 m (4.5 ft) Scenario 3, Elevation 1.7 m (5.6 ft) Scenario 7, Elevation 1.1 m (3.5 ft)
Point 10
Captains Bay Rd., C
Final level: Scenario 1
Final level: Scenario 2
Final level: Scenario 3
Final level: Scenario 7
Water level above ground (meters)
Time after earthquake (hours)
Point 10
Captains Bay Rd., C
Water velocity (meters/second)
Time after earthquake (hours)
Pre-earthquake elevation 0.7 m (2.3 ft)
Scenario 1, Depth 2.2 m (7.2 ft) Scenario 2, Depth 1.6 m (5.4 ft) Scenario 3, Depth 1.3 m (4.3 ft) Scenario 7, Depth 2.0 m (6.5 ft)
Point 11
Captains Bay
Final level: Scenario 1
Final level: Scenario 2
Final level: Scenario 3
Final level: Scenario 7
Sea level (meters)
Time after earthquake (hours)
Point 11
Captains Bay
Water current (meters/second)
Time after earthquake (hours)
Pre-earthquake depth 80.3 m (263.2 ft)
Scenario 1, Depth 83.1 m (272.6 ft) Scenario 2, Depth 82.6 m (270.9 ft) Scenario 3, Depth 82.3 m (269.8 ft) Scenario 7, Depth 82.9 m (271.8 ft)
Point 12
Strait, A
Final level: Scenario 1
Final level: Scenario 2
Final level: Scenario 3
Final level: Scenario 7
Sea level (meters)
Time after earthquake (hours)
Point 12
Strait, A
Water current (meters/second)
Time after earthquake (hours)
Pre-earthquake depth 12.7 m (41.5 ft)
Scenario 1, Depth 15.5 m (50.8 ft) Scenario 2, Depth 15.0 m (49.1 ft) Scenario 3, Depth 14.6 m (48.0 ft) Scenario 7, Depth 15.2 m (49.8 ft)

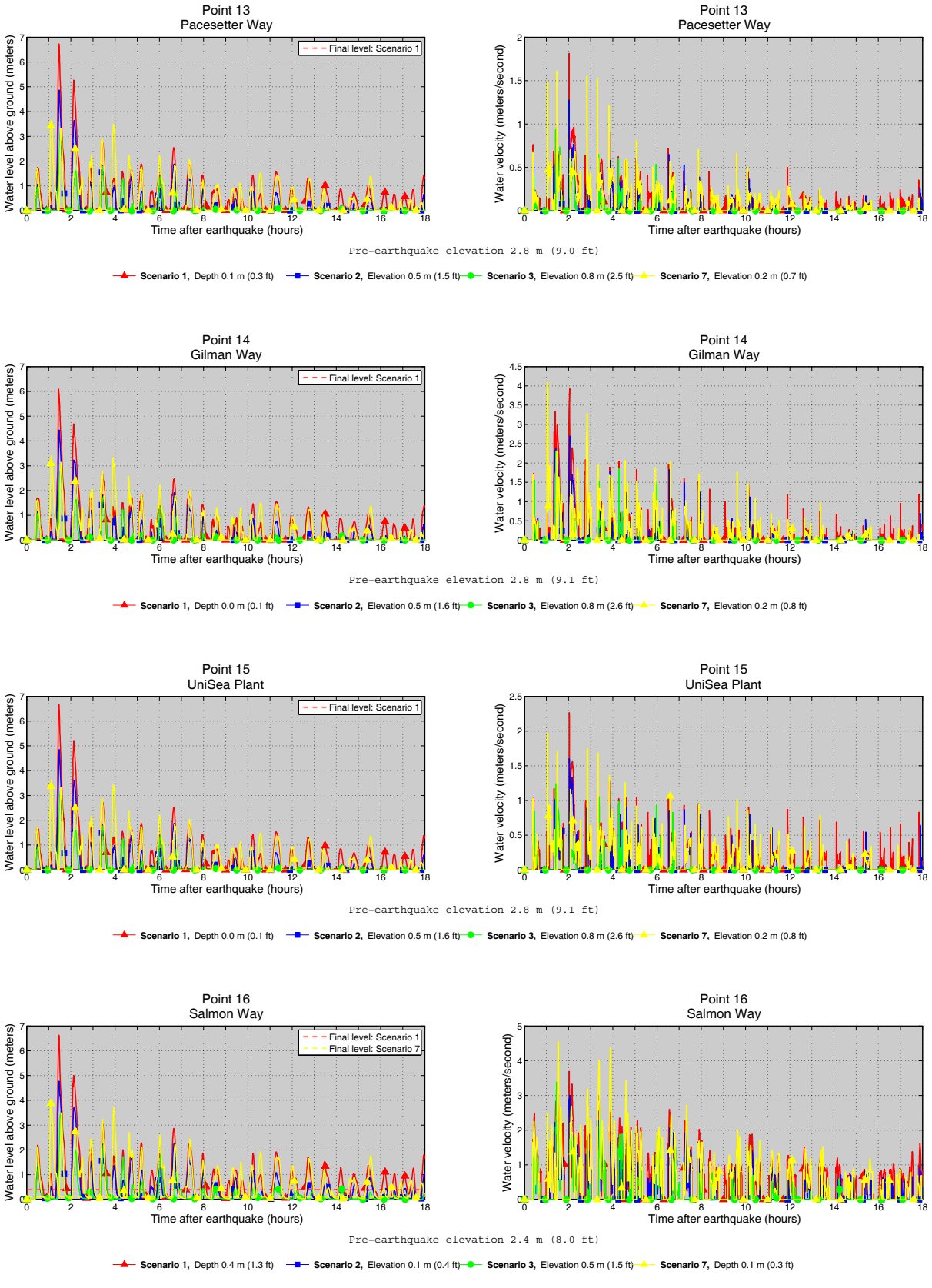
Point 13
Pacesetter Way
Water level above ground (meters)
Final level: Scenario 1
Time after earthquake (hours)
Point 13
Pacesetter Way
Water velocity (meters/second)
Time after earthquake (hours)
Pre-earthquake elevation 2.8 m (9.0 ft)
Scenario 1, Depth 0.1 m (0.3 ft)
Scenario 2, Elevation 0.5 m (1.5 ft)
Scenario 3, Elevation 0.8 m (2.5 ft)
Scenario 7, Elevation 0.2 m (0.7 ft)
Point 14
Gilman Way
Water level above ground (meters)
Final level: Scenario 1
Time after earthquake (hours)
Point 14
Gilman Way
Water velocity (meters/second)
Time after earthquake (hours)
Pre-earthquake elevation 2.8 m (9.1 ft)
Scenario 1, Depth 0.0 m (0.1 ft)
Scenario 2, Elevation 0.5 m (1.6 ft)
Scenario 3, Elevation 0.8 m (2.6 ft)
Scenario 7, Elevation 0.2 m (0.8 ft)
Point 15
UniSea Plant
Water level above ground (meters)
Final level: Scenario 1
Time after earthquake (hours)
Point 15
UniSea Plant
Water velocity (meters/second)
Time after earthquake (hours)
Pre-earthquake elevation 2.8 m (9.1 ft)
Scenario 1, Depth 0.0 m (0.1 ft)
Scenario 2, Elevation 0.5 m (1.6 ft)
Scenario 3, Elevation 0.8 m (2.6 ft)
Scenario 7, Elevation 0.2 m (0.8 ft)
Point 16
Salmon Way
Water level above ground (meters)
Final level: Scenario 1
Final level: Scenario 7
Time after earthquake (hours)
Point 16
Salmon Way
Water velocity (meters/second)
Time after earthquake (hours)
Pre-earthquake elevation 2.4 m (8.0 ft)
Scenario 1, Depth 0.4 m (1.3 ft)
Scenario 2, Elevation 0.1 m (0.4 ft)
Scenario 3, Elevation 0.5 m (1.5 ft)
Scenario 7, Depth 0.1 m (0.3 ft)

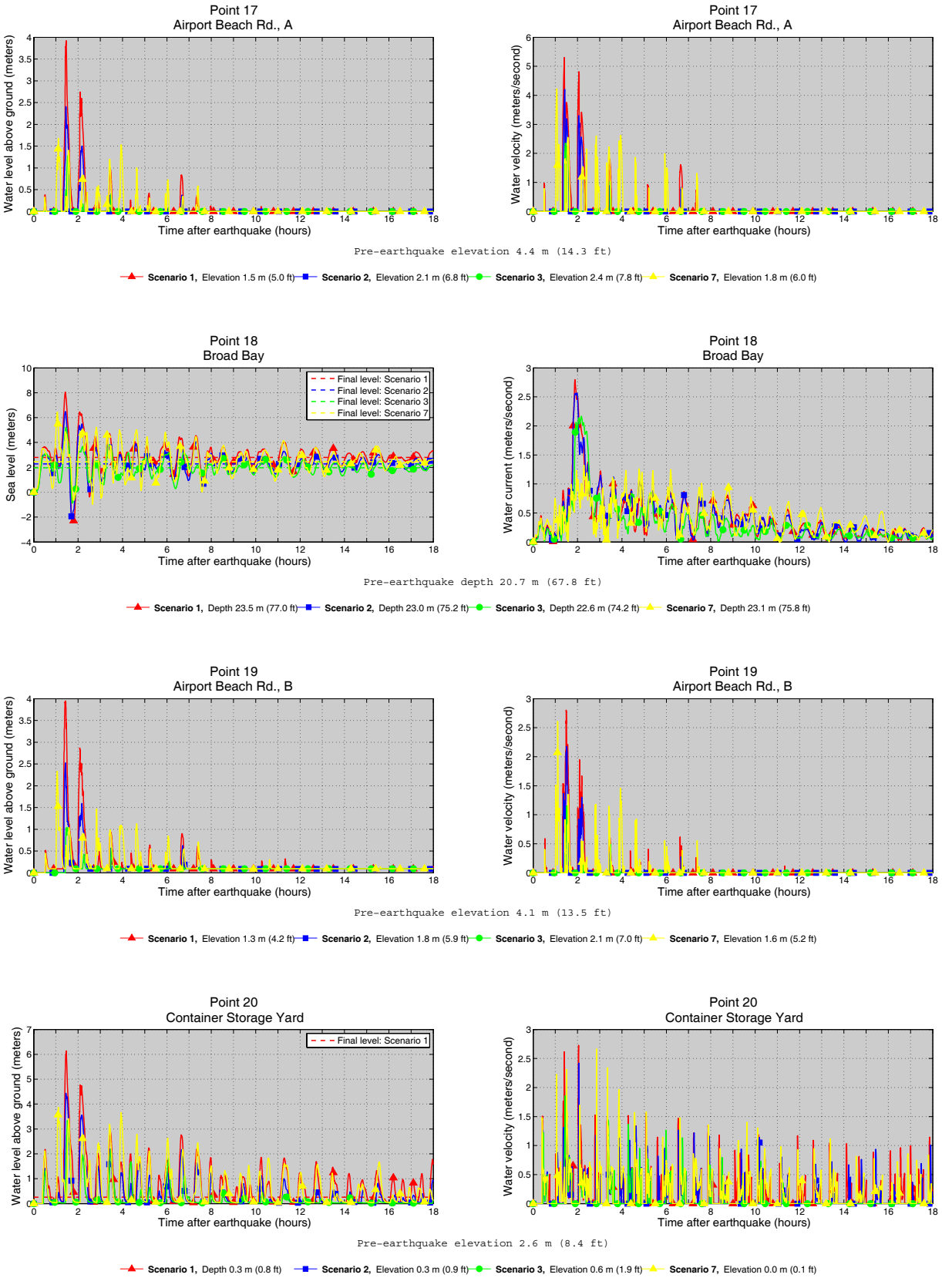
Point 17
Airport Beach Rd., A
Water level above ground (meters)
Time after earthquake (hours)
Point 17
Airport Beach Rd., A
Water velocity (meters/second)
Time after earthquake (hours)
Pre-earthquake elevation 4.4 m (14.3 ft)
Scenario 1, Elevation 1.5 m (5.0 ft) Scenario 2, Elevation 2.1 m (6.8 ft) Scenario 3, Elevation 2.4 m (7.8 ft) Scenario 7, Elevation 1.8 m (6.0 ft)
Point 18
Broad Bay
Sea level (meters)
Final level: Scenario 1
Final level: Scenario 2
Final level: Scenario 3
Final level: Scenario 7
Time after earthquake (hours)
Point 18
Broad Bay
Water current (meters/second)
Time after earthquake (hours)
Pre-earthquake depth 20.7 m (67.8 ft)
Scenario 1, Depth 23.5 m (77.0 ft) Scenario 2, Depth 23.0 m (75.2 ft) Scenario 3, Depth 22.6 m (74.2 ft) Scenario 7, Depth 23.1 m (75.8 ft)
Point 19
Airport Beach Rd., B
Water level above ground (meters)
Time after earthquake (hours)
Point 19
Airport Beach Rd., B
Water velocity (meters/second)
Time after earthquake (hours)
Pre-earthquake elevation 4.1 m (13.5 ft)
Scenario 1, Elevation 1.3 m (4.2 ft) Scenario 2, Elevation 1.8 m (5.9 ft) Scenario 3, Elevation 2.1 m (7.0 ft) Scenario 7, Elevation 1.6 m (5.2 ft)
Point 20
Container Storage Yard
Water level above ground (meters)
Final level: Scenario 1
Time after earthquake (hours)
Point 20
Container Storage Yard
Water velocity (meters/second)
Time after earthquake (hours)
Pre-earthquake elevation 2.6 m (8.4 ft)
Scenario 1, Depth 0.3 m (0.8 ft) Scenario 2, Elevation 0.3 m (0.9 ft) Scenario 3, Elevation 0.6 m (1.9 ft) Scenario 7, Elevation 0.0 m (0.1 ft)

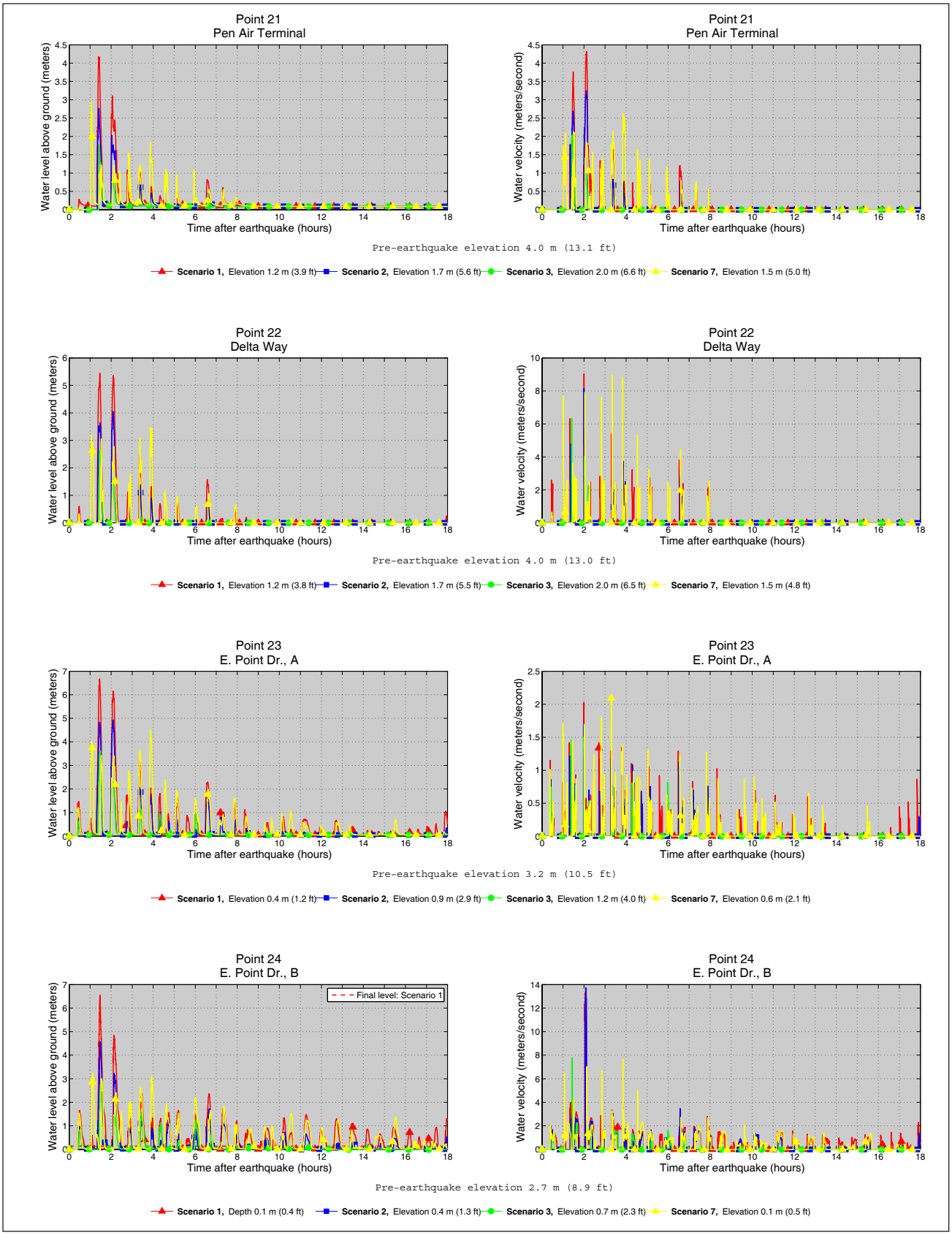
Point 21
Pen Air Terminal
Water level above ground (meters)
Time after earthquake (hours)
Point 21
Pen Air Terminal
Water velocity (meters/second)
Time after earthquake (hours)
Pre-earthquake elevation 4.0 m (13.1 ft)
Scenario 1, Elevation 1.2 m (3.9 ft)
Scenario 2, Elevation 1.7 m (5.6 ft)
Scenario 3, Elevation 2.0 m (6.6 ft)
Scenario 7, Elevation 1.5 m (5.0 ft)
Point 22
Delta Way
Water level above ground (meters)
Time after earthquake (hours)
Point 22
Delta Way
Water velocity (meters/second)
Time after earthquake (hours)
Pre-earthquake elevation 4.0 m (13.0 ft)
Scenario 1, Elevation 1.2 m (3.8 ft)
Scenario 2, Elevation 1.7 m (5.5 ft)
Scenario 3, Elevation 2.0 m (6.5 ft)
Scenario 7, Elevation 1.5 m (4.8 ft)
Point 23
E. Point Dr., A
Water level above ground (meters)
Time after earthquake (hours)
Point 23
E. Point Dr., A
Water velocity (meters/second)
Time after earthquake (hours)
Pre-earthquake elevation 3.2 m (10.5 ft)
Scenario 1, Elevation 0.4 m (1.2 ft)
Scenario 2, Elevation 0.9 m (2.9 ft)
Scenario 3, Elevation 1.2 m (4.0 ft)
Scenario 7, Elevation 0.6 m (2.1 ft)
Point 24
E. Point Dr., B
Final level: Scenario 1
Water level above ground (meters)
Time after earthquake (hours)
Point 24
E. Point Dr., B
Water velocity (meters/second)
Time after earthquake (hours)
Pre-earthquake elevation 2.7 m (8.9 ft)
Scenario 1, Depth 0.1 m (0.4 ft)
Scenario 2, Elevation 0.4 m (1.3 ft)
Scenario 3, Elevation 0.7 m (2.3 ft)
Scenario 7, Elevation 0.1 m (0.5 ft)

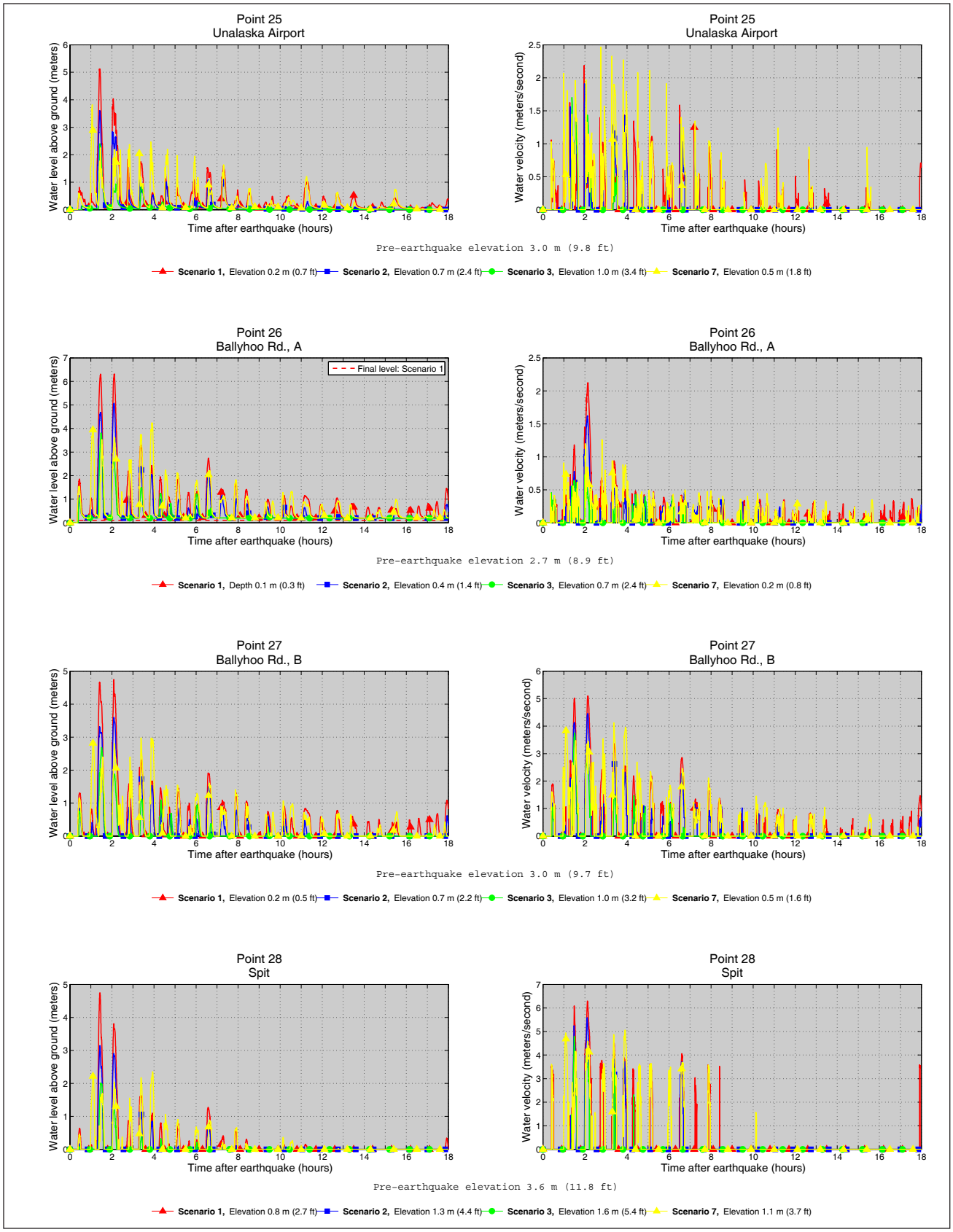
Point 25
Unalaska Airport
Water level above ground (meters)
Time after earthquake (hours)
Point 25
Unalaska Airport
Water velocity (meters/second)
Time after earthquake (hours)
Pre-earthquake elevation 3.0 m (9.8 ft)
Scenario 1, Elevation 0.2 m (0.7 ft) Scenario 2, Elevation 0.7 m (2.4 ft) Scenario 3, Elevation 1.0 m (3.4 ft) Scenario 7, Elevation 0.5 m (1.8 ft)
Point 26
Ballyhoo Rd., A
Final level: Scenario 1
Water level above ground (meters)
Time after earthquake (hours)
Point 26
Ballyhoo Rd., A
Water velocity (meters/second)
Time after earthquake (hours)
Pre-earthquake elevation 2.7 m (8.9 ft)
Scenario 1, Depth 0.1 m (0.3 ft) Scenario 2, Elevation 0.4 m (1.4 ft) Scenario 3, Elevation 0.7 m (2.4 ft) Scenario 7, Elevation 0.2 m (0.8 ft)
Point 27
Ballyhoo Rd., B
Water level above ground (meters)
Time after earthquake (hours)
Point 27
Ballyhoo Rd., B
Water velocity (meters/second)
Time after earthquake (hours)
Pre-earthquake elevation 3.0 m (9.7 ft)
Scenario 1, Elevation 0.2 m (0.5 ft) Scenario 2, Elevation 0.7 m (2.2 ft) Scenario 3, Elevation 1.0 m (3.2 ft) Scenario 7, Elevation 0.5 m (1.6 ft)
Point 28
Spit
Water level above ground (meters)
Time after earthquake (hours)
Point 28
Spit
Water velocity (meters/second)
Time after earthquake (hours)
Pre-earthquake elevation 3.6 m (11.8 ft)
Scenario 1, Elevation 0.8 m (2.7 ft) Scenario 2, Elevation 1.3 m (4.4 ft) Scenario 3, Elevation 1.6 m (5.4 ft) Scenario 7, Elevation 1.1 m (3.7 ft)

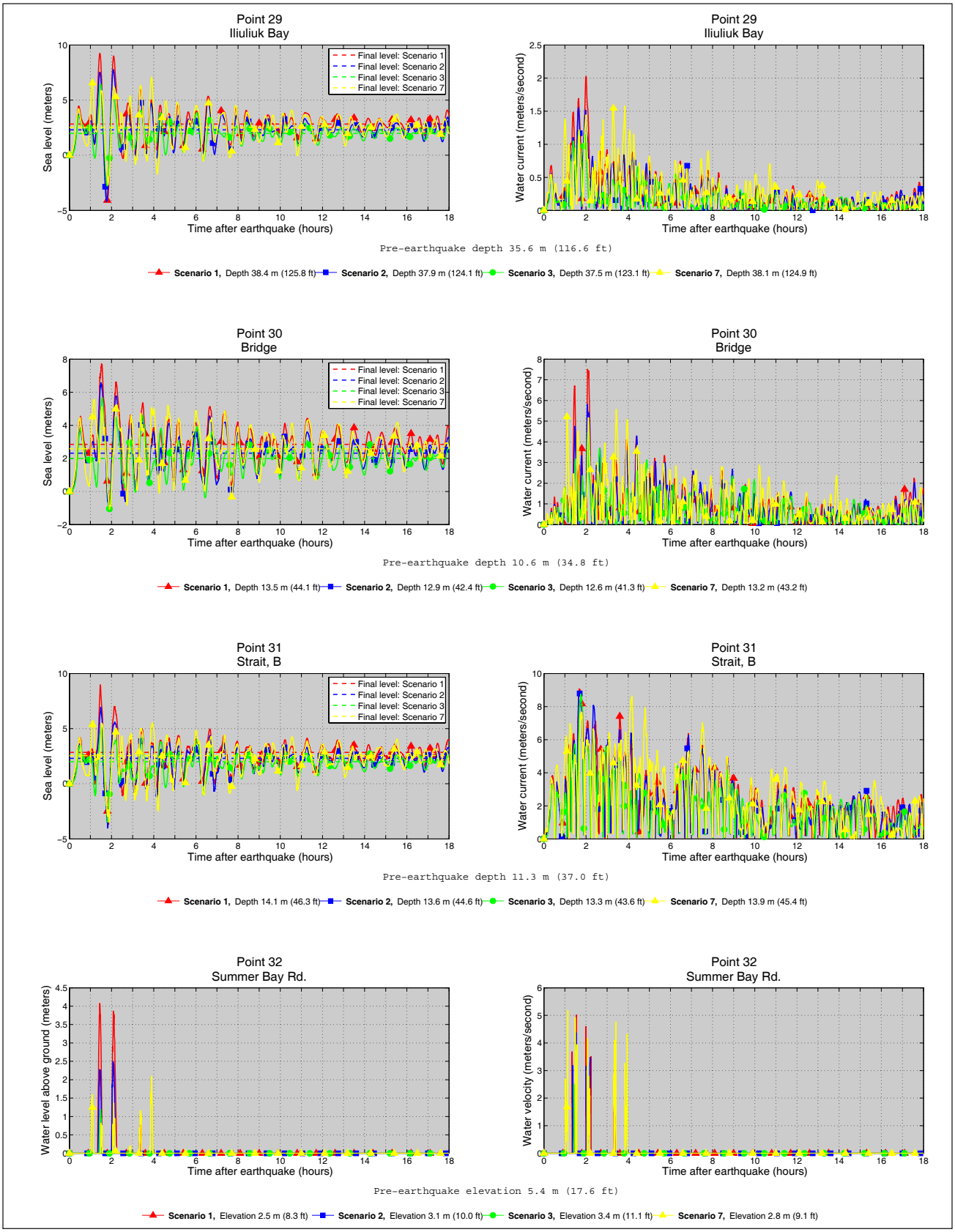
Point 29
Iliuliuk Bay
Sea level (meters)
Time after earthquake (hours)
Final level: Scenario 1
Final level: Scenario 2
Final level: Scenario 3
Final level: Scenario 7
Point 29
Iliuliuk Bay
Water current (meters/second)
Time after earthquake (hours)
Pre-earthquake depth 35.6 m (116.6 ft)
Scenario 1, Depth 38.4 m (125.8 ft)
Scenario 2, Depth 37.9 m (124.1 ft)
Scenario 3, Depth 37.5 m (123.1 ft)
Scenario 7, Depth 38.1 m (124.9 ft)
Point 30
Bridge
Sea level (meters)
Time after earthquake (hours)
Final level: Scenario 1
Final level: Scenario 2
Final level: Scenario 3
Final level: Scenario 7
Point 30
Bridge
Water current (meters/second)
Time after earthquake (hours)
Pre-earthquake depth 10.6 m (34.8 ft)
Scenario 1, Depth 13.5 m (44.1 ft)
Scenario 2, Depth 12.9 m (42.4 ft)
Scenario 3, Depth 12.6 m (41.3 ft)
Scenario 7, Depth 13.2 m (43.2 ft)
Point 31
Strait, B
Sea level (meters)
Time after earthquake (hours)
Final level: Scenario 1
Final level: Scenario 2
Final level: Scenario 3
Final level: Scenario 7
Point 31
Strait, B
Water current (meters/second)
Time after earthquake (hours)
Pre-earthquake depth 11.3 m (37.0 ft)
Scenario 1, Depth 14.1 m (46.3 ft)
Scenario 2, Depth 13.6 m (44.6 ft)
Scenario 3, Depth 13.3 m (43.6 ft)
Scenario 7, Depth 13.9 m (45.4 ft)
Point 32
Summer Bay Rd.
Water level above ground (meters)
Time after earthquake (hours)
Point 32
Summer Bay Rd.
Water velocity (meters/second)
Time after earthquake (hours)
Pre-earthquake elevation 5.4 m (17.6 ft)
Scenario 1, Elevation 2.5 m (8.3 ft)
Scenario 2, Elevation 3.1 m (10.0 ft)
Scenario 3, Elevation 3.4 m (11.1 ft)
Scenario 7, Elevation 2.8 m (9.1 ft)

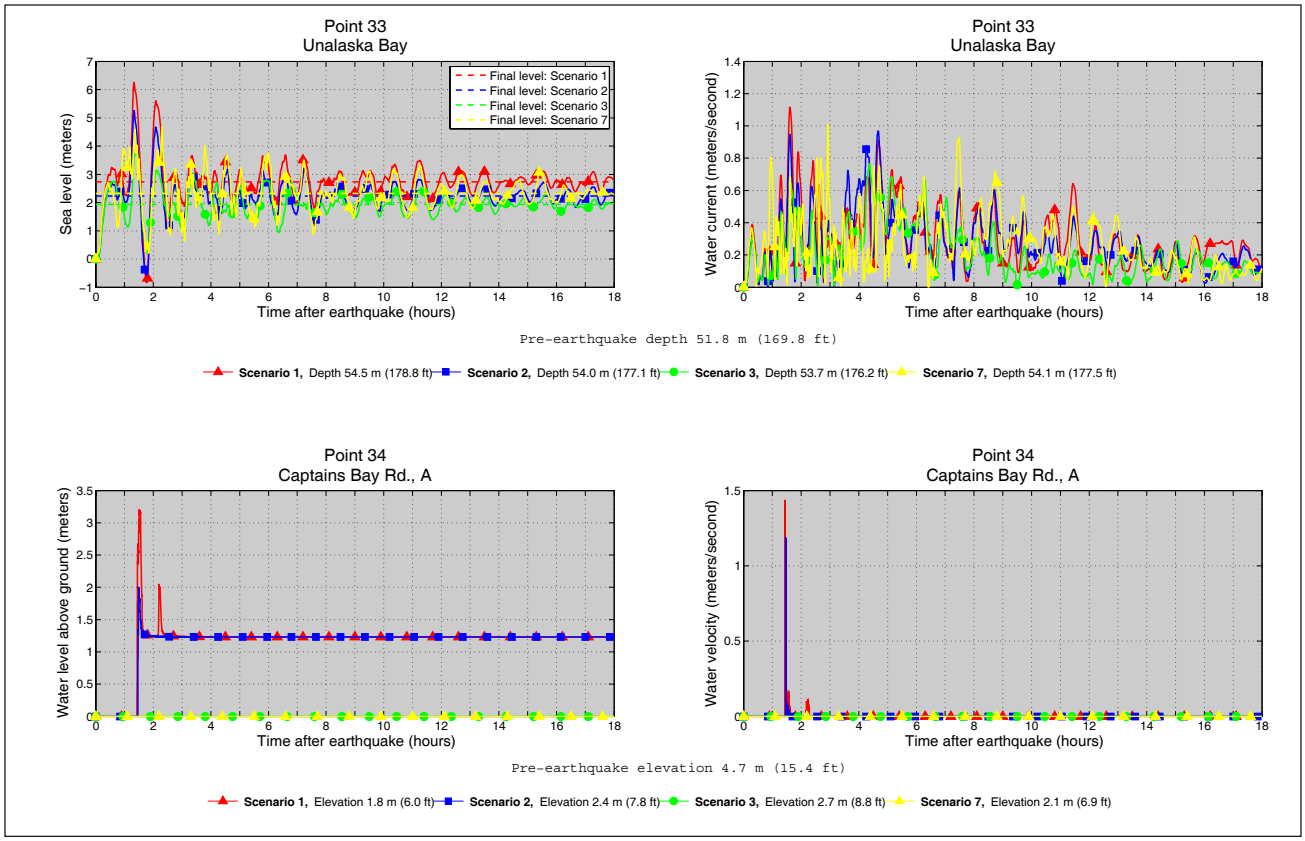
Point 33
Unalaska Bay
Final level: Scenario 1
Final level: Scenario 2
Final level: Scenario 3
Final level: Scenario 7
Sea level (meters)
Time after earthquake (hours)
Point 33
Unalaska Bay
Water current (meters/second)
Time after earthquake (hours)
Pre-earthquake depth 51.8 m (169.8 ft)
Scenario 1, Depth 54.5 m (178.8 ft)
Scenario 2, Depth 54.0 m (177.1 ft)
Scenario 3, Depth 53.7 m (176.2 ft)
Scenario 7, Depth 54.1 m (177.5 ft)
Point 34
Captains Bay Rd., A
Water level above ground (meters)
Time after earthquake (hours)
Point 34
Captains Bay Rd., A
Water velocity (meters/second)
Time after earthquake (hours)
Pre-earthquake elevation 4.7 m (15.4 ft)
Scenario 1, Elevation 1.8 m (6.0 ft)
Scenario 2, Elevation 2.4 m (7.8 ft)
Scenario 3, Elevation 2.7 m (8.8 ft)
Scenario 7, Elevation 2.1 m (6.9 ft)

Appendix A-3. Graphs showing time series of water level (left column) and velocity (right column) for selected offshore locations in Unalaska for scenarios 4, 9, and 10. For each location, pre-earthquake and post-earthquake depth corresponding to the MHHW is provided for each scenario. For offshore locations, to show the height of an arriving tsunami, the vertical datum is such that zero corresponds to the pre-earthquake sea level. Dashed lines show the water level after the tsunami.

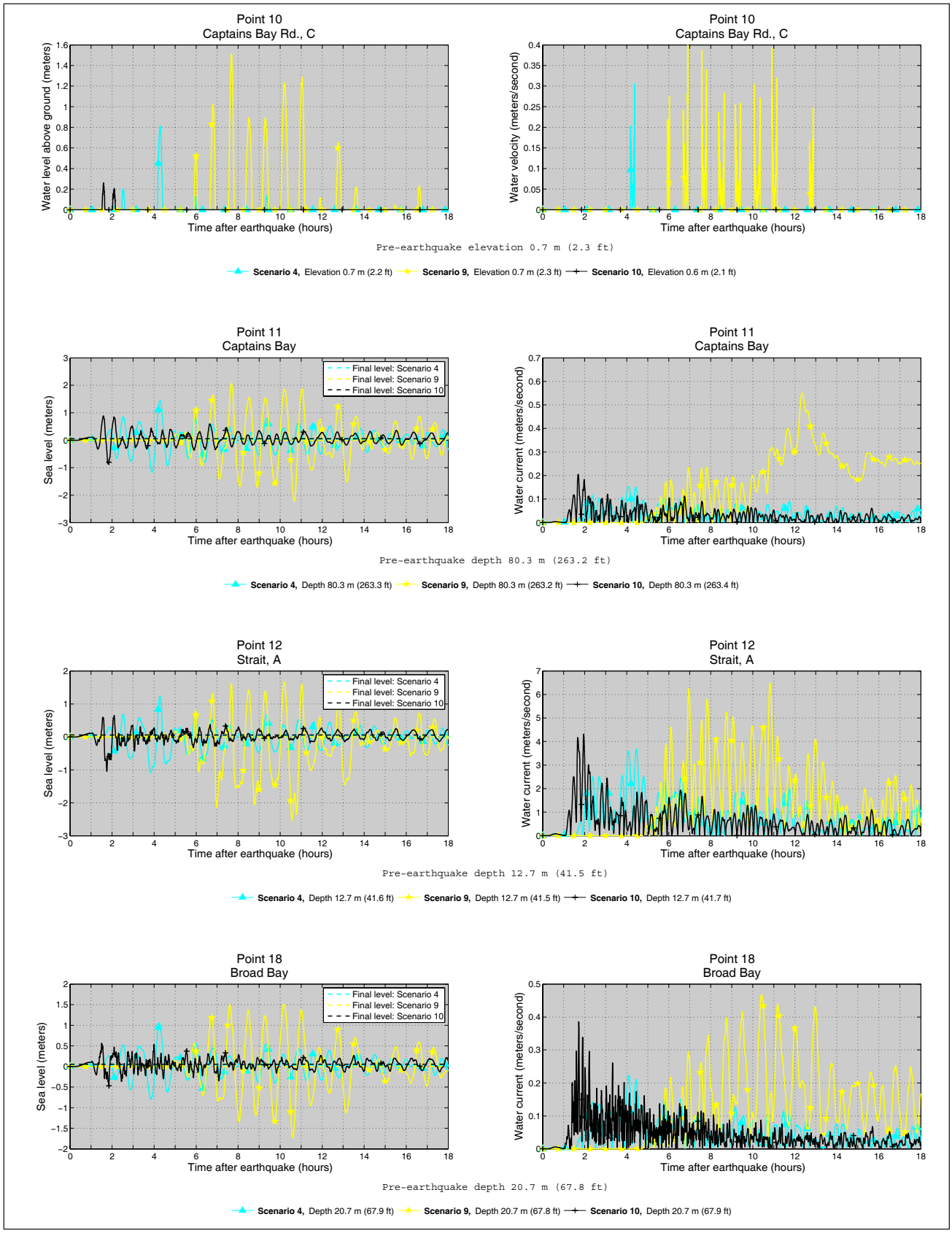

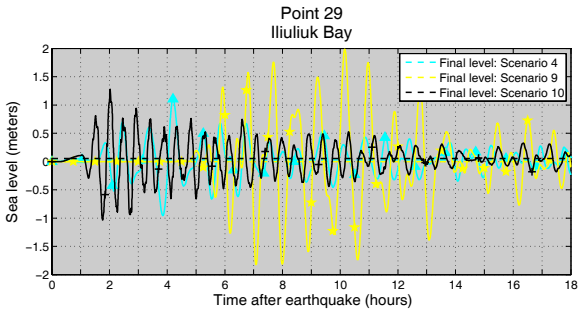

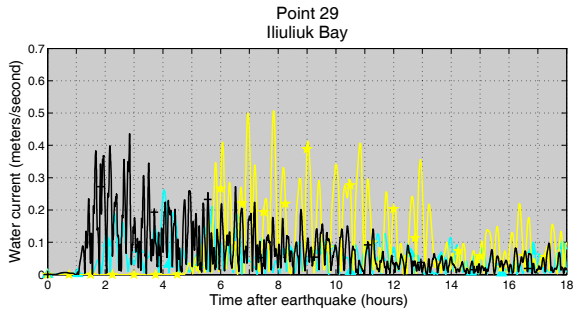

Pre-earthquake depth 35.6 m (116.6 ft)

Scenario 4, Depth 35.6 m (116.7 ft) **Scenario 9,** Depth 35.6 m (116.6 ft) **Scenario 10,** Depth 35.6 m (116.8 ft)

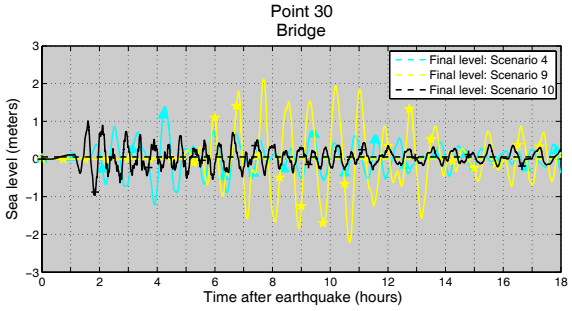

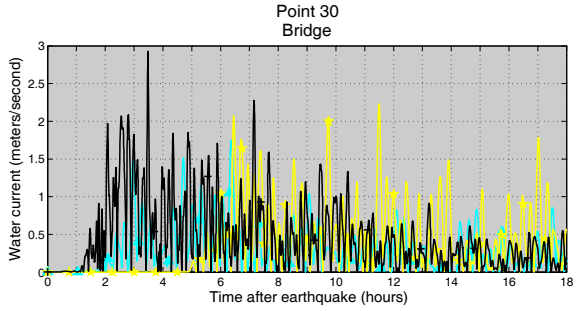

Pre-earthquake depth 10.6 m (34.8 ft)

Scenario 4, Depth 10.6 m (34.9 ft) **Scenario 9,** Depth 10.6 m (34.8 ft) **Scenario 10,** Depth 10.7 m (35.0 ft)

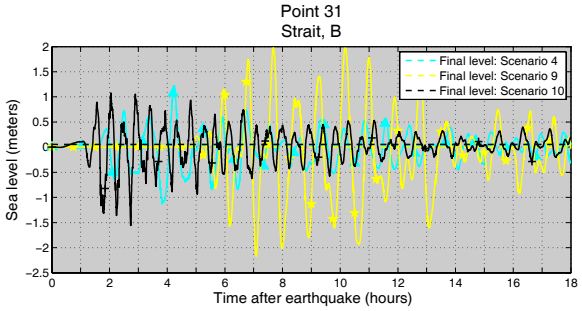

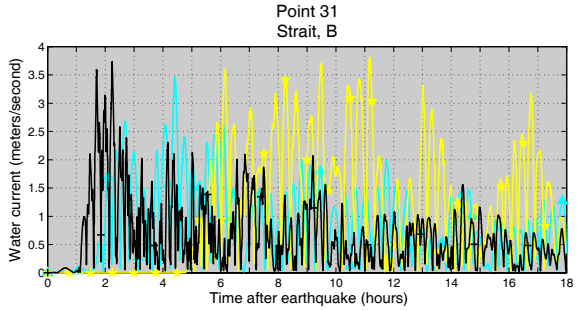

Pre-earthquake depth 11.3 m (37.0 ft)

Scenario 4, Depth 11.3 m (37.1 ft) **Scenario 9,** Depth 11.3 m (37.0 ft) **Scenario 10,** Depth 11.3 m (37.2 ft)

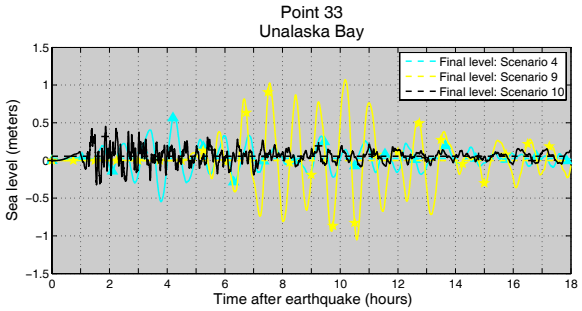

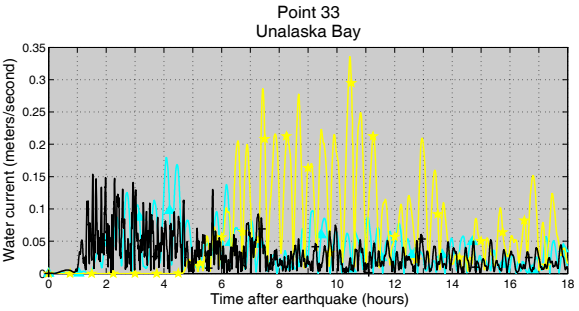

Pre-earthquake depth 51.8 m (169.8 ft)

Scenario 4, Depth 51.8 m (169.9 ft) **Scenario 9,** Depth 51.8 m (169.8 ft) **Scenario 10,** Depth 51.9 m (170.0 ft)

APPENDIX B

Appendix B-1. Maps showing locations of time series points in Akutan Bay (top) and in the community of Akutan (bottom). The latitude and longitude locations for time series points are listed in table B-1.

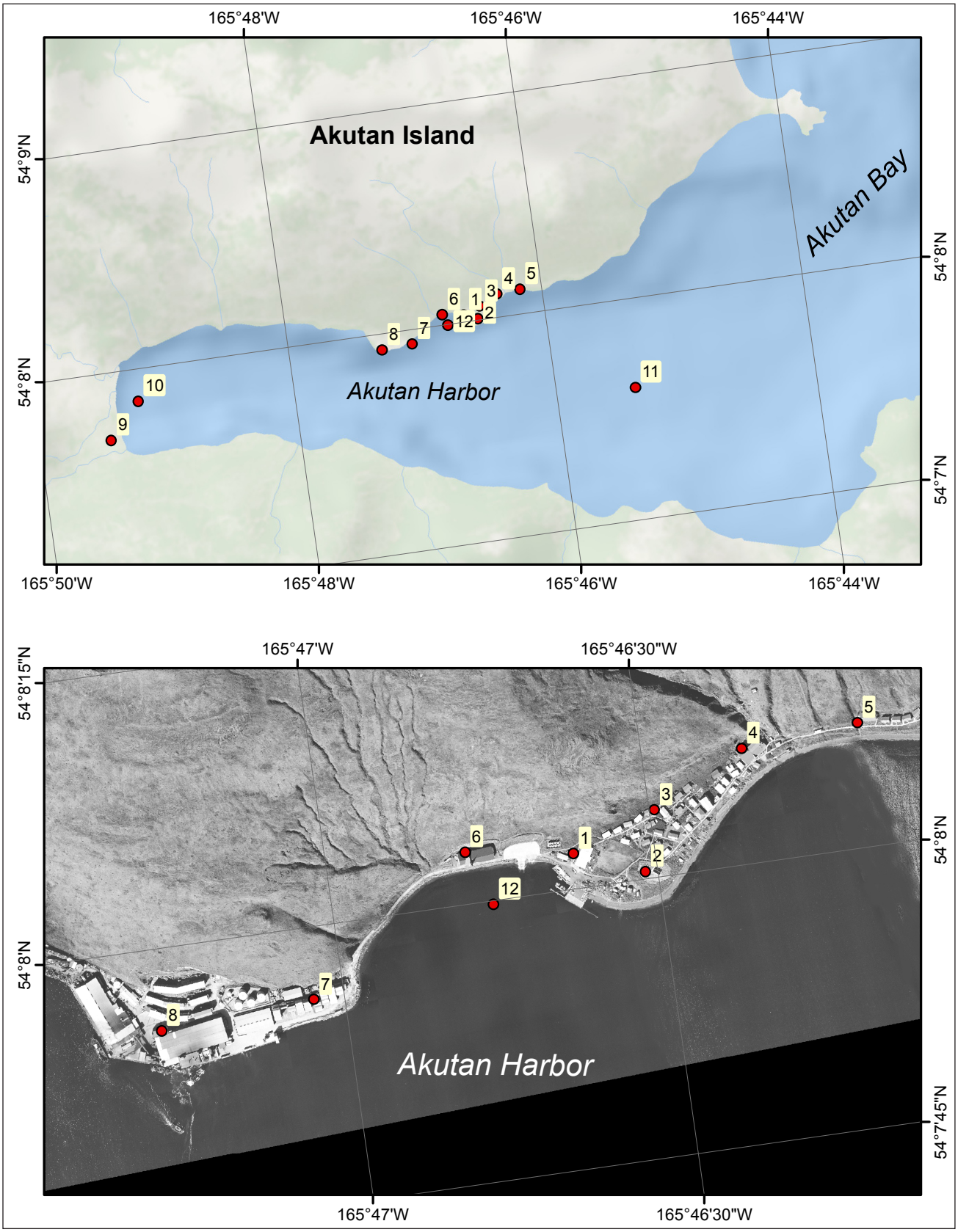

Table B-1. The longitude and latitude locations of the time series points in Akutan. The maximum water level above ground is provided for on-shore locations, whereas the maximum water level above the pre-earthquake MHHW is provided for offshore locations. The pre-earthquake onshore (S) and offshore (O) locations are specified in the third column. The minimum elevation above the post-earthquake MHHW datum is provided for the onshore locations, while the minimum post-earthquake depth is provided for the offshore locations

#	Label	S / O	Longitude (°W)	Latitude (°N)	Minimum Elevation/ Depth (meters)	Maximum Water Level Above Ground/Sea Level (meters)										Maximum Water Velocity (meters/second)									
						Scenario										Scenario									
						1	2	3	4	5	6	7	8	9	10	1	2	3	4	5	6	7	8	9	10
1	Post Office	S	-165.77706	54.13386	-0.4	5.6	4.0	2.9	0.0	2.7	2.8	8.5	3.5	0.0	0.0	1.5	1.3	1.2	0.0	2.7	2.8	3.4	3.5	0.0	0.0
2	St. Alexander Nevski	S	-165.77531	54.13344	-0.1	5.1	3.6	2.5	0.0	2.5	2.6	8.0	3.3	0.0	0.0	2.6	2.2	1.4	0.0	3.8	3.8	4.0	4.4	0.0	0.0
3	Salmonberry Inn	S	-165.77486	54.13433	-0.2	5.2	3.7	2.7	0.0	2.6	2.8	8.3	3.4	0.0	0.0	1.9	1.6	1.0	0.0	2.8	2.8	3.0	3.4	0.0	0.0
4	School	S	-165.77244	54.13506	2.5	2.5	1.0	0.0	0.0	0.0	0.0	5.5	0.9	0.0	0.0	0.5	0.9	0.0	0.0	0.0	0.0	1.5	0.6	0.0	0.0
5	Library	S	-165.76944	54.13519	3.9	1.0	0.0	0.0	0.0	0.0	0.0	3.9	0.0	0.0	0.0	1.5	0.0	0.0	0.0	0.0	0.0	3.0	0.0	0.0	0.0
6	Akutan Bay, near church	O	-165.77978	54.13411	0.5	7.9	6.3	5.1	0.9	4.9	4.8	10.8	5.6	1.3	1.1	0.6	0.5	0.4	0.1	1.2	1.1	1.2	1.1	0.2	0.3
7	Container Yard	S	-165.78411	54.13225	-0.7	6.0	4.4	3.0	0.0	2.9	2.9	9.0	3.4	0.0	0.0	2.1	1.7	1.7	0.0	2.1	1.8	4.1	3.1	0.0	0.0
8	Trident Seafoods	S	-165.78806	54.13211	-1.1	6.5	5.0	3.3	0.0	3.6	3.2	9.5	3.7	0.0	0.0	2.7	2.6	2.3	0.0	3.4	3.4	4.6	4.4	0.0	0.0
9	Akutan Harbor Parking	S	-165.82414	54.12825	4.4	2.0	0.7	0.0	0.0	2.6	2.6	7.0	3.6	0.0	0.0	1.6	1.1	0.0	0.0	3.8	3.7	2.7	4.4	0.0	0.0
10	Akutan Bay, west	O	-165.82000	54.13089	26.5	8.9	7.5	5.6	0.9	7.8	7.7	13.6	8.9	1.6	2.4	1.4	1.1	1.1	0.1	2.0	2.0	2.7	2.1	0.3	0.4
11	Akutan Bay, east	O	-165.75656	54.12661	54	7.1	5.7	5.0	0.8	4.7	4.7	9.2	5.6	1.1	0.9	1.1	0.9	0.8	0.1	1.2	1.2	2.0	1.6	0.3	0.4
12	Akutan Seaplane Base	O	-165.77925	54.13328	15.4	7.8	6.2	5.1	0.8	4.9	4.8	10.7	5.5	1.3	1.1	0.7	0.5	0.5	0.1	1.1	1.1	1.3	1.2	0.2	0.4

Appendix B-2. Graphs showing time series of water level (left column) and velocity (right column) for selected locations in Akutan for scenarios 1, 2, 3, and 7. For each location, pre-earthquake and post-earthquake elevation/depth corresponding to the MHHW datum is provided for each scenario. For offshore locations, to show the height of an arriving tsunami, the vertical datum is such that zero corresponds to the pre-earthquake sea level. Dashed lines show the water level after the tsunami.

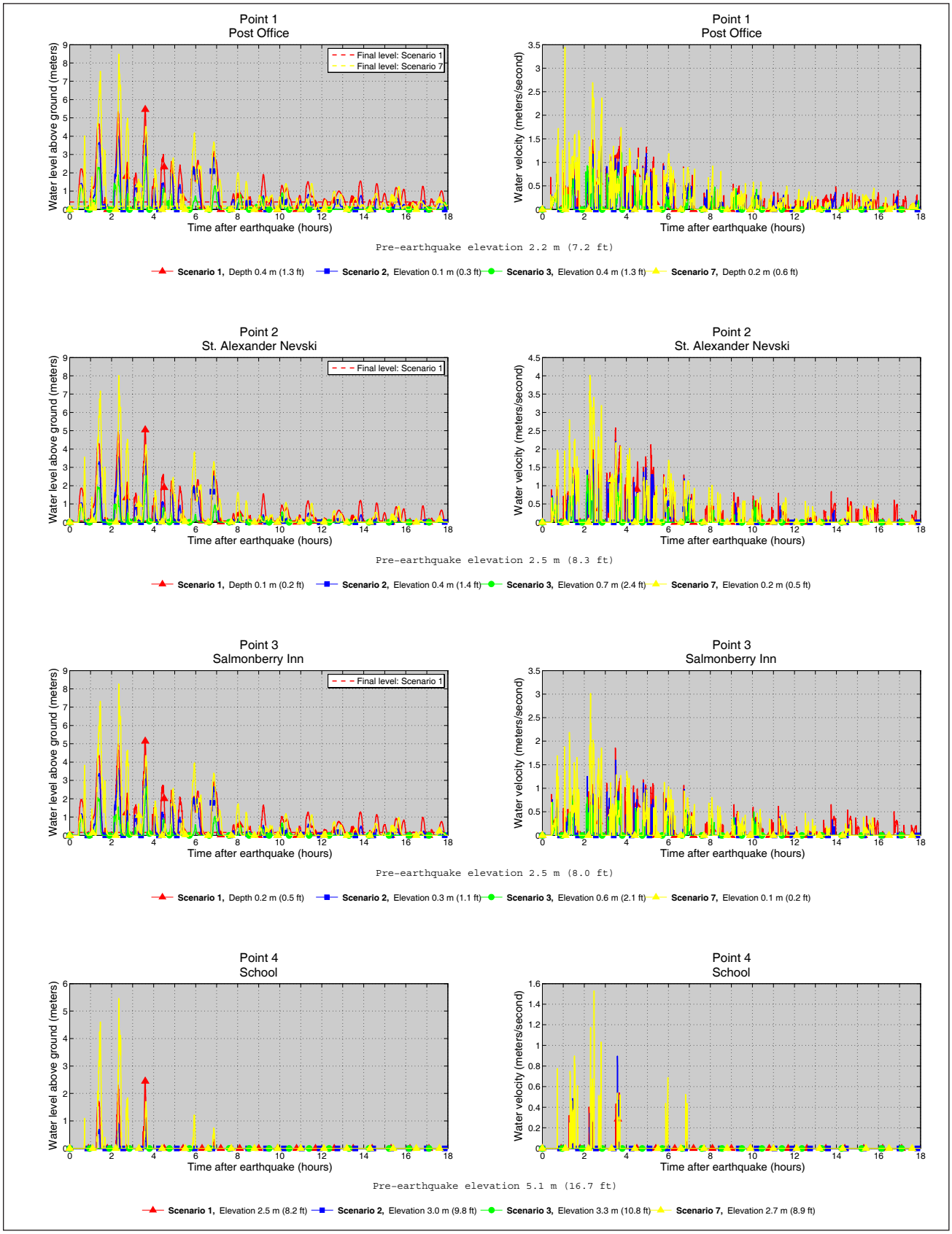

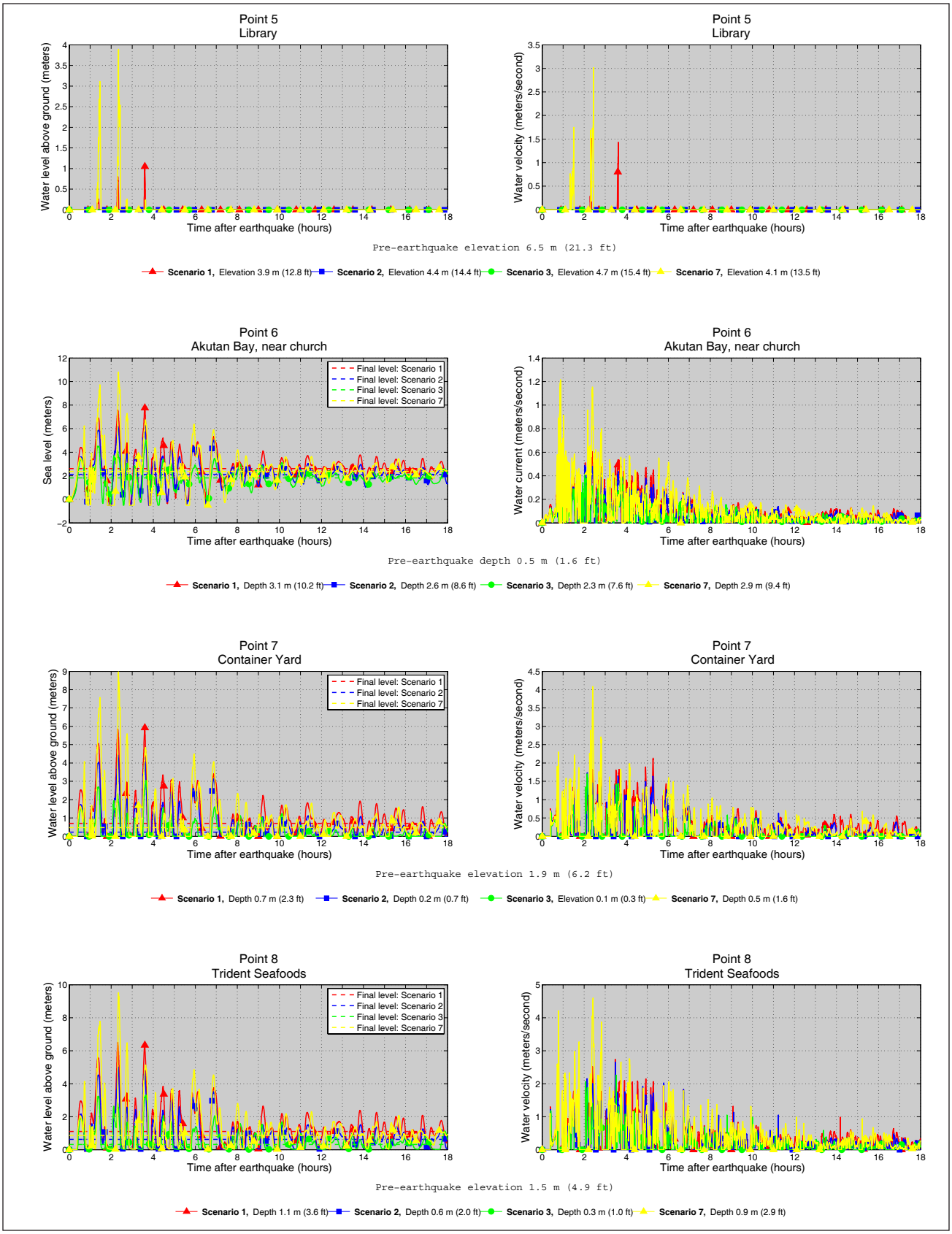
Point 5
Library
Water level above ground (meters)
Time after earthquake (hours)
Point 5
Library
Water velocity (meters/second)
Time after earthquake (hours)
Pre-earthquake elevation 6.5 m (21.3 ft)
Scenario 1, Elevation 3.9 m (12.8 ft) Scenario 2, Elevation 4.4 m (14.4 ft) Scenario 3, Elevation 4.7 m (15.4 ft) Scenario 7, Elevation 4.1 m (13.5 ft)
Point 6
Akutan Bay, near church
Sea level (meters)
Final level: Scenario 1
Final level: Scenario 2
Final level: Scenario 3
Final level: Scenario 7
Time after earthquake (hours)
Point 6
Akutan Bay, near church
Water current (meters/second)
Time after earthquake (hours)
Pre-earthquake depth 0.5 m (1.6 ft)
Scenario 1, Depth 3.1 m (10.2 ft) Scenario 2, Depth 2.6 m (8.6 ft) Scenario 3, Depth 2.3 m (7.6 ft) Scenario 7, Depth 2.9 m (9.4 ft)
Point 7
Container Yard
Water level above ground (meters)
Final level: Scenario 1
Final level: Scenario 2
Final level: Scenario 7
Time after earthquake (hours)
Point 7
Container Yard
Water velocity (meters/second)
Time after earthquake (hours)
Pre-earthquake elevation 1.9 m (6.2 ft)
Scenario 1, Depth 0.7 m (2.3 ft) Scenario 2, Depth 0.2 m (0.7 ft) Scenario 3, Elevation 0.1 m (0.3 ft) Scenario 7, Depth 0.5 m (1.6 ft)
Point 8
Trident Seafoods
Water level above ground (meters)
Final level: Scenario 1
Final level: Scenario 2
Final level: Scenario 3
Final level: Scenario 7
Time after earthquake (hours)
Point 8
Trident Seafoods
Water velocity (meters/second)
Time after earthquake (hours)
Pre-earthquake elevation 1.5 m (4.9 ft)
Scenario 1, Depth 1.1 m (3.6 ft) Scenario 2, Depth 0.6 m (2.0 ft) Scenario 3, Depth 0.3 m (1.0 ft) Scenario 7, Depth 0.9 m (2.9 ft)

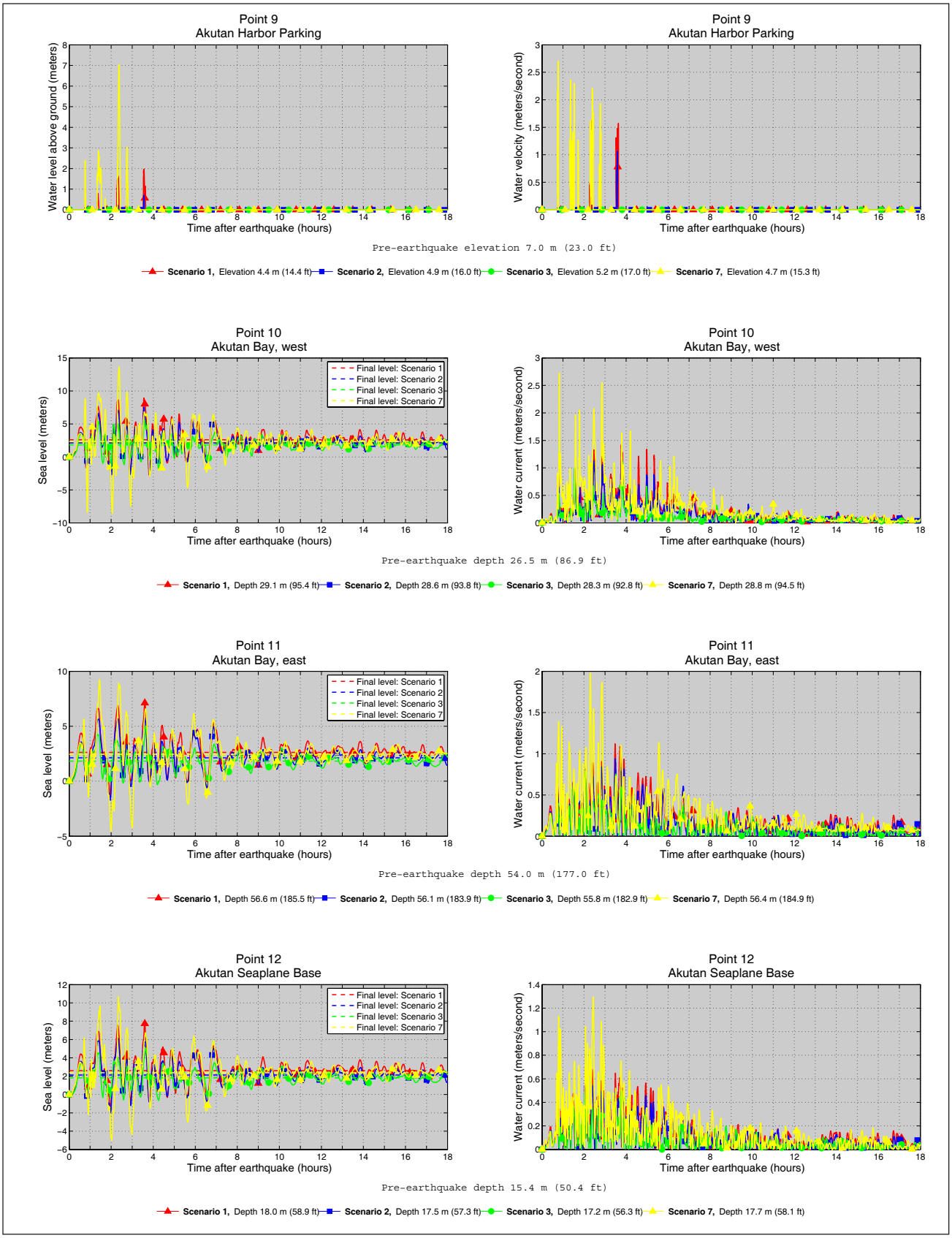
Point 9
Akutan Harbor Parking
Water level above ground (meters)
Time after earthquake (hours)
Point 9
Akutan Harbor Parking
Water velocity (meters/second)
Time after earthquake (hours)
Pre-earthquake elevation 7.0 m (23.0 ft)
Scenario 1, Elevation 4.4 m (14.4 ft)
Scenario 2, Elevation 4.9 m (16.0 ft)
Scenario 3, Elevation 5.2 m (17.0 ft)
Scenario 7, Elevation 4.7 m (15.3 ft)
Point 10
Akutan Bay, west
Sea level (meters)
Final level: Scenario 1
Final level: Scenario 2
Final level: Scenario 3
Final level: Scenario 7
Time after earthquake (hours)
Point 10
Akutan Bay, west
Water current (meters/second)
Time after earthquake (hours)
Pre-earthquake depth 26.5 m (86.9 ft)
Scenario 1, Depth 29.1 m (95.4 ft)
Scenario 2, Depth 28.6 m (93.8 ft)
Scenario 3, Depth 28.3 m (92.8 ft)
Scenario 7, Depth 28.8 m (94.5 ft)
Point 11
Akutan Bay, east
Sea level (meters)
Final level: Scenario 1
Final level: Scenario 2
Final level: Scenario 3
Final level: Scenario 7
Time after earthquake (hours)
Point 11
Akutan Bay, east
Water current (meters/second)
Time after earthquake (hours)
Pre-earthquake depth 54.0 m (177.0 ft)
Scenario 1, Depth 56.6 m (185.5 ft)
Scenario 2, Depth 56.1 m (183.9 ft)
Scenario 3, Depth 55.8 m (182.9 ft)
Scenario 7, Depth 56.4 m (184.9 ft)
Point 12
Akutan Seaplane Base
Sea level (meters)
Final level: Scenario 1
Final level: Scenario 2
Final level: Scenario 3
Final level: Scenario 7
Time after earthquake (hours)
Point 12
Akutan Seaplane Base
Water current (meters/second)
Time after earthquake (hours)
Pre-earthquake depth 15.4 m (50.4 ft)
Scenario 1, Depth 18.0 m (58.9 ft)
Scenario 2, Depth 17.5 m (57.3 ft)
Scenario 3, Depth 17.2 m (56.3 ft)
Scenario 7, Depth 17.7 m (58.1 ft)

Appendix B-3. Graphs showing time series of water level (left column) and velocity (right column) for selected offshore locations in Akutan for scenarios 4, 9, and 10. For each location, pre-earthquake and post-earthquake depth corresponding to the MHHW is provided for each scenario. For offshore locations, to show the height of an arriving tsunami, the vertical datum is such that zero corresponds to the pre-earthquake sea level. Dashed lines show the water level after the tsunami.

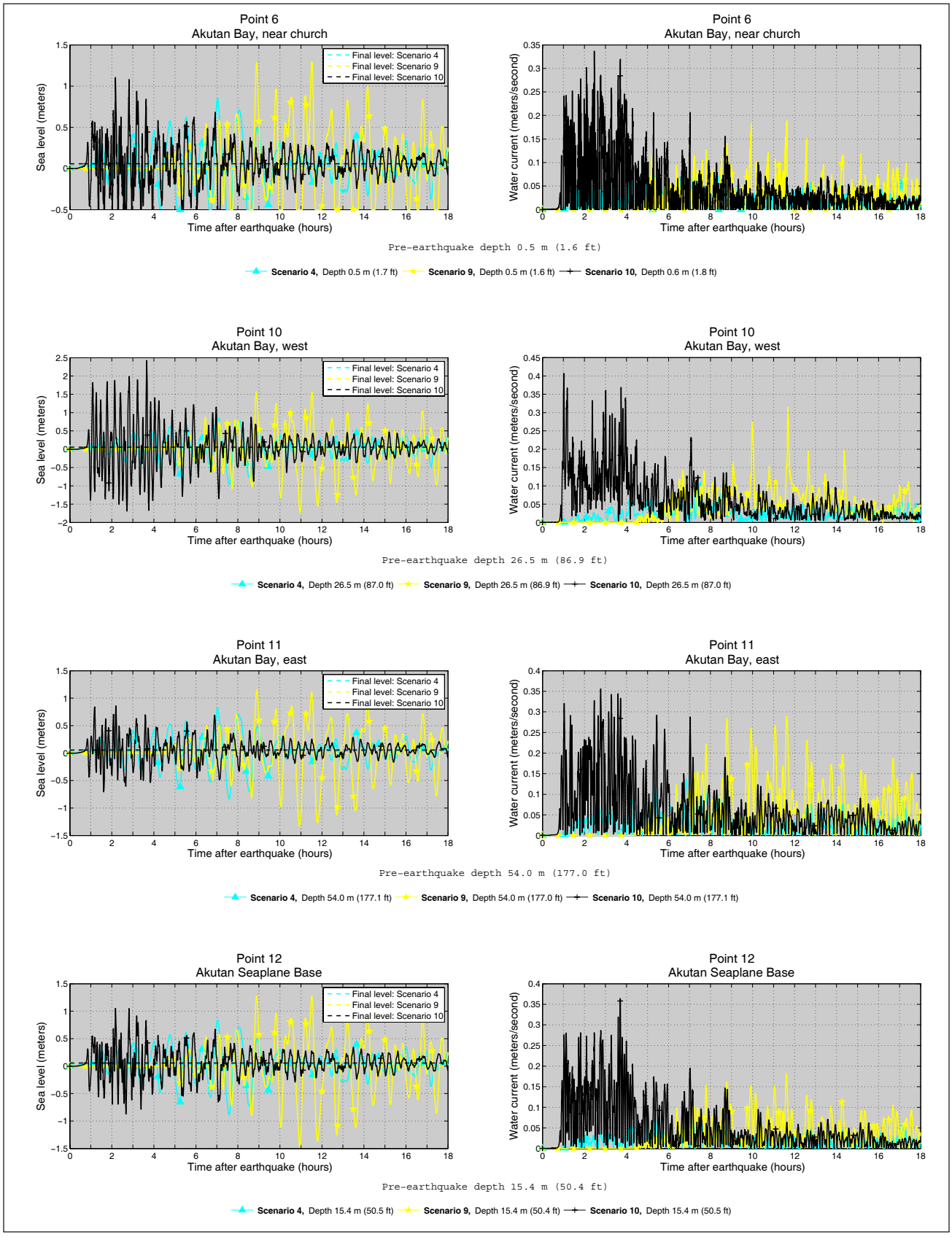

APPENDIX C

Appendix C-1. Map showing potential maximum permanent flooding in Unalaska. Values of the subsidence according to each scenario are listed in table 2.

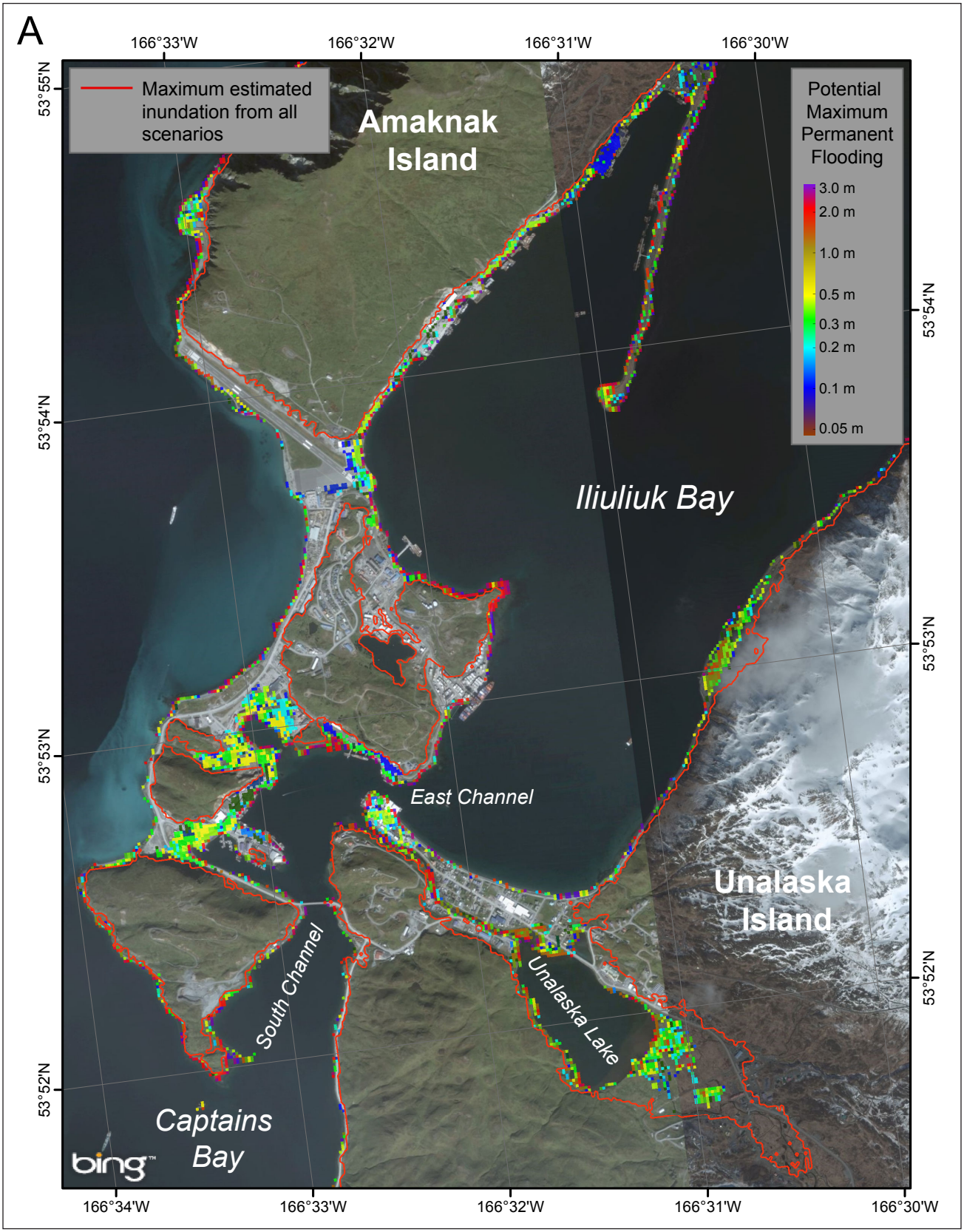

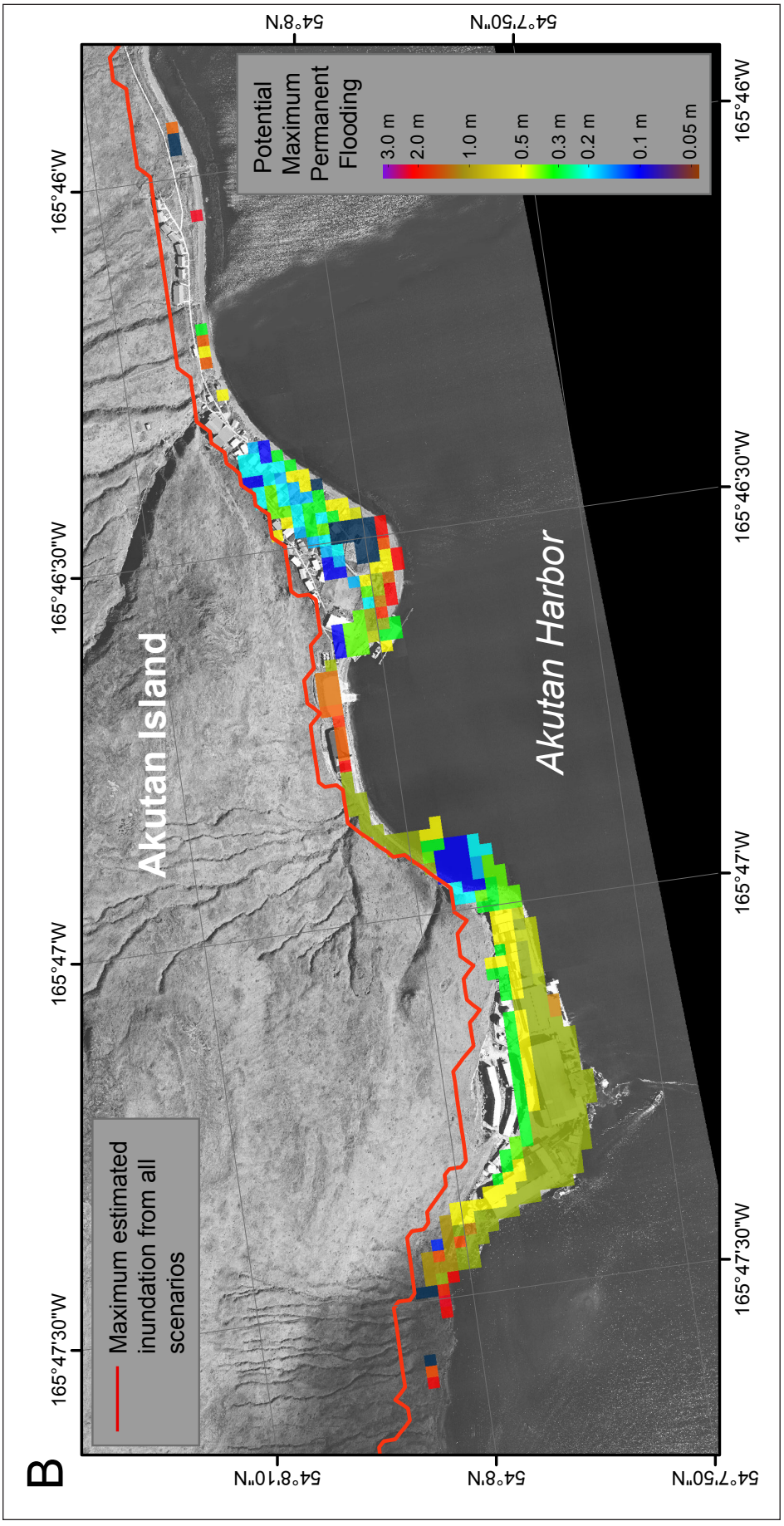

Appendix C-2. Map showing potential maximum permanent flooding in Akutan. Values of the subsidence according to each scenario are listed in table 2.